NTNU – Trondheim
Norwegian University of
Science and Technology

Analysis and Design of Columns in Offshore Structures subjected to Supply Vessel Beam Collisions

Kjetil Hatlestad Qvale

Marine Technology (2 year)
Submission date: June 2012
Supervisor: Jørgen Amdahl, IMT

Norwegian University of Science and Technology
Department of Marine Technology

Master Thesis 2012

For

Stud. Techn. Kjetil Hatlestad Qvale

Analysis and Design of Columns in Offshore Structures subjected to Supply Vessel Beam Collisions

Supply vessels, passing merchant vessels and shuttle tankers are regarded a major threat for offshore structures and platforms are often designed intentionally to resist collisions. In Norwegian sector of the North Sea the standard design event is a supply vessel of 5000 tons displacement sailing into a platform with a speed of 2m/s. For design purposes standard force-deformation curves for bow, side and stern impacts have been defined in NORSOK N-004 Appendix A for bow, sideways and stern impact.

With respect to the distribution of strain energy dissipation there may be distinguished between three design principles, namely *strength design, ductility design* and *shared-energy design* depending upon the relative strength the ship and the platform:

Strength design implies that the platform is strong enough to resist the collision force with minor deformation, so that the striking ship is forced to deform and dissipate the major part of the collision energy. *Ductility design* implies that the platform undergoes large, plastic deformations and dissipates the major part of the collision energy.

Shared energy design implies that both the platform and the striking ship contribute significantly to the energy dissipation.

From a calculation point of view, strength design or ductility design is favourable. In strength design, it is only necessary to verify that the struck ship is capable of resisting the total collision force and the local high pressure intensities during the deformation process. In ductility design, the shape of the deformation is highly dominated by the geometry of the striking ship structure and the energy dissipation can be analyzed by means of plastic methods. In shared energy design, both the magnitude and the distribution of the collision force depend upon the deformation of both ships. This interaction makes the analysis more complex and calls for nonlinear finite element analysis. In most cases ductility or shared energy design is used or assumed. However, strength design may in some cases be achieved with small changes in structural configuration or material improvement.

Force intensities to apply for strength design are only given for stern collisions in Norsok-N004. Recently, considerable work has been on supply vessel, but no recommendations exist for strength design against supply vessel beam impacts.

The purpose of this work is to investigate the integrated response o unstiffened and stiffened columns/towers of offshore structures subjected to impacts form supply vessels and to

establish guidelines for analysis and design. The starting point for the work is the Master thesis of Reny Watan. Reference is also made to the Master thesis of Henrik Raaholt.

The following topics should be addressed:

1. Perform analysis of ship side impacts against an unstiffened platform leg. The analysis model used by Revy Watan shall be reviewed, notably with respect to modelling of boundary conditions, and improved to the extent needed. Parametric variations shall be performed, where the diameter and thickness of the platform leg are varied. Evaluate the resistance to local indentation and compare with the simplified model in NORSOK N-004. Investigate whether a simplified model may be developed that takes into account the gradual increase of the contact area. Investigate the validity of a simplified collapse mechanism where the capacity of the impacted section is reduced.

2. In the analysis in pt 1, the ship is assumed to translate sideways only. On the basis of a simple model for rigid body motions of the ship, check whether roll motions should be taken into account during impact. If this is necessary, propose a simple model to account for the influence of ship rolling on the development of contact area.

3. Perform analysis of stern impact against unstiffened columns. The stern section model shall be based upon a previously developed finite element model. The validity of the simplified approach – refer pt. 1 - shall be investigated.

4. Perform parametric studies of bow, side and stern impacts against stiffened columns. A previously developed bow model shall be used. Among others, the ring stiffener and longitudinal stiffener spacing and dimensions shall be varied. Determine the force and energy dissipation versus indentation for both the ship and the platform column. Describe the development of damage in the structures and discuss whether the impact can be classified as a strength, ductile or shared energy event. Identify the force intensities *strength type* impacts and use this information to propose requirement to plates and stiffeners for *strength design*. (*The exact scope of work for pt.4 will have to be decided in the course of the thesis work*)

5. Conclusions and recommendation for further work

References:

Reny Watan: Analysis and Design of Columns in Offshore Structures subjected to Supply Vessel Collisions, Master thesis, 2011

Henrik Raaholt: Analysis and Design of Columns in Offshore Structures subjected to Supply Vessel Beam Collisions, Master thesis, 2009

Literature studies of specific topics relevant to the thesis work may be included.

The work scope may prove to be larger than initially anticipated. Subject to approval from the supervisor, topics may be deleted from the list above or reduced in extent.

In the thesis the candidate shall present his personal contribution to the resolution of problems within the scope of the thesis work.

Theories and conclusions should be based on mathematical derivations and/or logic reasoning identifying the various steps in the deduction.

The candidate should utilise the existing possibilities for obtaining relevant literature.

The thesis should be organised in a rational manner to give a clear exposition of results, assessments, and conclusions. The text should be brief and to the point, with a clear language. Telegraphic language should be avoided.

The thesis shall contain the following elements: A text defining the scope, preface, list of contents, summary, main body of thesis, conclusions with recommendations for further work, list of symbols and acronyms, references and (optional) appendices. All figures, tables and equations shall be numerated.

The supervisor may require that the candidate, in an early stage of the work, presents a written plan for the completion of the work. The plan should include a budget for the use of computer and laboratory resources which will be charged to the department. Overruns shall be reported to the supervisor.

The original contribution of the candidate and material taken from other sources shall be clearly defined. Work from other sources shall be properly referenced using an acknowledged referencing system.

Deadline:, June 10, 2012

Trondheim, January 13, 2012

Jørgen Amdahl

Summary

During this Master Thesis, leg-segments of jacket platforms subjected to supply vessel impacts have been considered. Finite element analyses (FEA) have been conducted using the explicit solver LS DYNA. The FEA results have been discussed and compared against simplified calculation methods and basic theory.

In order to investigate the effect of the surrounding structure, two sets of boundary conditions have been considered for the columns:

- Perfectly clamed boundary conditions
- Axial flexible boundary conditions.

The results have shown that the effect of the surrounding structure should be included. The effect is most important of the strength of the column is small relative to the striking ship.

Parameter studies of the column-design with respect to column diameter and thickness have been performed. Three column diameters have been considered, namely 1.0 m, 1.5 m and 2.0 m. The thickness has been varied from 30 mm – 70 mm. Force-deformation relationships for the different columns have been compared and discussed. Based on the available amount of impact-energy, the different column-designs have been categorised as strength-designed, ductile-designed or shared-energy designed. The parameter study shows that if strength-design is aimed for, a column thickness of 70 mm in the case where the diameter = 1.5 m is required. If the column diameter is 2.0 m, strength design is achieved with a column thickness of 60 mm. Strength design was not achieved for the column with diameter = 1.0 m. However, based on the results, strength design of the 1.0 m column would probably require a thickness above 70 mm.

The resistance against local indentation for the different columns have been considered and compared against resistance curves recommended by NORSOK N-004. The NORSOK-curves give a reasonable estimation of the strength for the weakest columns but becomes quite conservative compared to the strongest columns. An empirical design curve which takes the gradual increasing contact area into account was suggested based on the results. The resistance against global deformations have been compared against a simplified collapse mechanism. The results show that the accuracy of the simplified model is very dependent on the load definition and whether or not effects of reduced capacity due to local indentations are included.

Two impact-scenarios have been considered: beam impacts and stern impacts. The beam impacts scenario proved to be the critical case in most cases.

Finally, the effect of ring stiffeners applied in the collision-zone of the platform leg has been considered. 4 different designs have been evaluated. However, it was found that the effect on the column strength is larger if the column thickness is increased.

Preface

This Master Thesis is a continuation of the author's Project Thesis that was conducted during the fall-semester of 2011. The master was assigned by the Institute for Marine Technology, NTNU. The problem text was formulated by Professor Jørgen Amdahl.

During the master thesis, a comprehensive understanding of the theory and practical calculation-methods regarding ship-platform collision has been obtained. The thesis has been both challenging and interesting. The most challenging part has been to explain the FEA-results using basic theory. However, this has also been the most interesting part.

A total number of 28 finite element analyses (FEA) have been performed with an estimated total clock-time of 150-200 hours. The total CPU-time is considerably larger as an external server with 8 CPUs has been used to perform the analyses.

I would especially like to thank the following persons for their help and contribution to this Master Thesis:

- Master Thesis Supervisor Professor Jørgen Amdahl for guidance and motivation.

- PhD Candidate Martin Storheim for help with the LS DYNA analysis.

Trondheim, June 10. 2012

Kjetil H. Qvale

Table of Contents

List of Figures

List of Figures in Appendix

List of Tables

Nomenclature

Variable	Unit	Description
$\boldsymbol{a}^n$	-	Nodal Acceleration Vector
A	m^2	Cross Sectional Area
As	m^2	Shell Element Area
a_s		Ship added mass
a_p		Added mass of installation
b	m	Collision-width
$\boldsymbol{C}$	Kg/s	Damping Matrix
C	-	Strain Rate Parameters
c	m/s	Acoustic Wave Speed
C_1	-	Coefficient
C_2	-	Coefficient
D	m	Column Diameter
Deff	m	Effective Column Diameter
d	m	Column Diameter
δ	m	Force Work Distance
E_T	J	Total Energy
E_s	J	Strain Energy
E	Pa	Young's Modulus
$E_{external}$	Nm	External Work
$E_{internal}$	Nm	Internal Work
e	m	Elongation
ε_{yp}	-	Elastic Strain to yield
$\bar{\varepsilon}^p$	-	Effective plastic strain
$\dot{\boldsymbol{\varepsilon}}$	-	Strain Rate
$\varepsilon^{effective}$	-	Effective Strain
ε_{ij}	-	engineering strain-tensor components
$\mathbf{F}^n$	N	Stress Divergence Vector
$\boldsymbol{H}^n$	N	Hourglass Resistance vector
K	N/m	Spring Stiffness
k	Pa	Strength Coefficient in the Power-law
$\boldsymbol{K}$	N/m	Stiffness Matrix

Variable	Unit	Description
l	m	Column Length
L_s	m	Element Length
$\boldsymbol{\lambda}$	-	Proportionality Constant
m_s	kg	Ship Mass
m_p	kg	Mass of installation
$\boldsymbol{M}$	kg	Mass Matrix
M	Nm	Moment
M_p	Nm	Plastic Moment Capacity
M_{red}	Pa	Reduced Plastic Moment Capacity
N	N	Axial Force
N_p	N	Plastic Tension Capacity
μ	-	Poisson's Ratio
n	-	Hardening Parameter for Power-law
$\mathbf{P}^n$	N	External and Body Force Loads
P	N	External Load
p	-	Strain Rate Parameter
Pcrit	N	Critical Load
ρ	kg/m^3	Density
$\boldsymbol{Q}(t)$	N	Time-dependent External Loading
q(x)	N	Distributed Load
$\boldsymbol{R}_{internal}$	N	Internal Forces
$\boldsymbol{R}_{external}$	N	External Forces
R_c	N	Characteristic Strength Factor
R_s	N	Impact force on ship
R_i	N	Impact force on installation
R	N	Impact Force
$d\boldsymbol{r}$	m	Displacement Increment
$d\boldsymbol{R}$	N	Force Increment Vector
$\boldsymbol{r}$	m	Displacement Vector
$\dot{\boldsymbol{r}}$	m/s	Velocity Vector
$\ddot{\boldsymbol{r}}$	m/s^2	Acceleration Vector

Variable	Unit	Description
$\boldsymbol{S}^i$	N	Element Force Vector
σ_y	Pa	Yield Strength
t	m	Thickness
t_n	s	Time step n
u	m/s	Global Nodal Velocity
v	m	Displacement Vector
Δt	s	Length of Time Step
θ	rad	Plastic rotation
v_p	m/s	Speed of installation
v_s	m/s	Ship impact speed
v_c	m/s	Speed of installation and ship after impact
w	m	Lateral displacement
w_d	m	Indentation length
Wp	m^3	Plastic Section Modulus
W	m^3	Elastic Section Modulus
$\boldsymbol{x}^n$	-	Nodal Coordinate Vector
ω_{max}	Hz	Largest Natural Frequency

‘

1. Introduction

Due to increasing ship traffic and offshore operations, impacts from passing merchant vessels, shuttle tankers or supply vessels on offshore installations are becoming an increased threat. Usually, there is a safety zone around the installations where the passing ships may not enter. However, since an offshore installation is dependent on supply vessels which have to operate within the safety zone of the installation, it is important to include impact-analyses in the design of offshore structures. Impacts from drifting ships may also be of importance.

Ship collisions with offshore structures may be critical with respect to the ship, installation or both. Accurate analyses are therefore important to ensure that the installation can withstand a high-energy ship impact. Both local and global analyses should be carried out to ensure that the main safety functions of the installation are not impaired by the impact.

Standardised design-curves and calculation procedures are commonly used in order to predict the resistance and capacity of the installations. Many of the standardised design-methods are based on simplifications of the real problem. Thus, the methods may have severe limitations in its use. The simplified methods may produce reasonable strength estimations of structures that may be classified as strength- or ductile-designed structures. However, the methods may fail to predict the strength when the problems are more complex. Accurate nonlinear finite element analyses are therefore crucial in order to verify that the design meets the strength requirements.

Agreed Scope of Work

Throughout the Master Thesis, the scope of work has been discussed with the project supervisor, Professor Jørgen Amdahl. The following modifications regarding the scope of work have been agreed:

Topic 2 – Effects of roll motion
This topic has been dropped.
This was done mainly because of shifting focus and partly because this would require information about the reference ship that was not available.

Topic 4 – Stiffened Columns
This topic has been briefly addressed.
The effect of ring stiffeners on a jacket leg-segment with column diameter = 1.5 m and thickness 50 mm has been evaluated. This topic was reduced in extent because the work scope of the other topics proved to be larger than initially anticipated

2. Ship Collisions – Design Principles

2.1 General

Ship collisions are classified as accidental loads which can be defined in the following way:

> "Accidental actions are actions caused by abnormal operation or technical failure. They include for instance fires and explosions, impacts from ships, dropped objects, helicopter crash and change of intended pressure difference." [3]

The overall goal when designing against accidental actions is to achieve a system with the necessary strength to resist abnormal accidental actions without impairing the main safety functions of the structure [4]:

- Usability of escapeways
- Integrity of shelter areas
- Global load bearing capacity

2.2 Design Values

In the case of a supply vessel impact on an offshore installation, NORSOK [3] gives the following design values:

- The ship mass should normally not be considered less than 5000 tons.
- Ship speed should not be considered below 2 m/s for the ALS design check.
- Hydrodynamic (added) mass can be assumed to be 40% of the ship mass for sideways impacts and 10% for bow and stern impacts. .

2.3 Energy Perspective

A ship – installation impact scenario is characterised by the available kinetic energy. The kinetic energy is governed by the mass, including hydrodynamic added mass, and speed of the ship and installation at the moment of impact. Depending on the impact conditions, a portion of the kinetic energy may remain as kinetic energy after the impact. The remaining energy is dissipated mainly as strain energy in the installation and/or the striking ship.

NORSOK distinguishes between three different design categories for energy dissipation [4]:

- *Strength design.*
  The installation is strong enough to resist the collision-force with minor deformation. This means that the ship is forced to deform and dissipate most of the collision energy.

- *Ductility design.*
  The installation undergoes large plastic deformations and absorbs most of the collision energy. In this case, the striking ship will be strong and undergo minor deformations.

- *Shared-energy design.*
  This implies that both the installation and ship contribute significantly to the dissipation of energy.

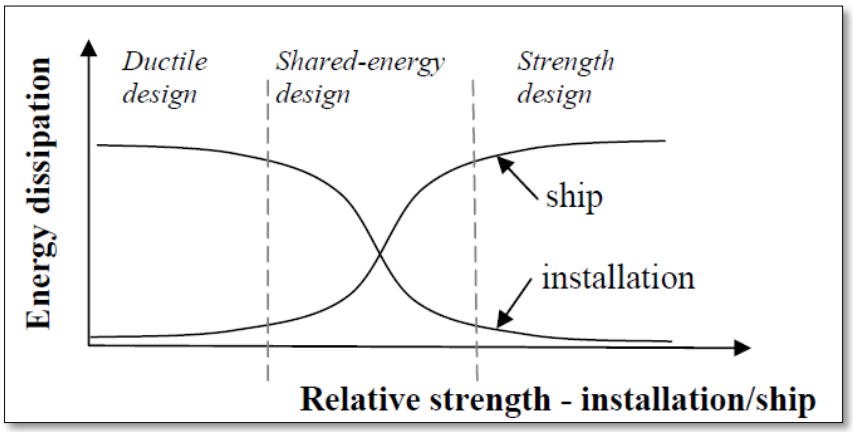

Figure 2-1 – Design Categories [4]

Strength design or ductility design is favourable seen from a calculation point of view because one of the two colliding structures will dissipate most of the impact energy. This implies that the structural response of the "soft" structure may be calculated based on simple considerations of the geometry of the stronger structure. Hence, simple calculation methods may be used. The problem is much more complex if the colliding structures are located within the shared-energy region. In this case, both the collision force and the contact area depend on the deformation of both structures. Thus, time consuming nonlinear finite element analyses is needed to estimate response accurately.

Ductility design is the most common case. However, strength design may in some cases be achievable with small changes of the structural configuration (e.g. by adding stiffeners, increasing the steel thickness etc). A strength designed construction must be able to withstand the total collision as well as local concentrations of the collision force.

By assuming conservation of energy and momentum, the part of the kinetic energy that is to be dissipated as strain energy may be calculated:

Conservation of momentum:

$$m_s v_s + m_p v_p = (m_s + m_i) v_c \rightarrow v_c = \frac{m_s v_s + m_i v_p}{m_s + m_i} \qquad \text{Eq. 2-1}$$

Conservation of energy:

$$E_T = E_s + E_i = \frac{1}{2} m_s v_s^2 + \frac{1}{2} m_i v_i^2 - \frac{1}{2} (m_s + m_i) v_c^2 \qquad \text{Eq. 2-2}$$

From these expressions, the strain energy may be calculated as:

Compliant installations:

Eq. 2-3

$$E_s = \frac{1}{2}(m_s + a_s)v_s^2 \frac{\left(1 - \frac{v_i}{v_s}\right)^2}{1 + \frac{m_s + a_s}{m_i + a_i}}$$

Fixed installations:

Eq. 2-4

$$E_s = \frac{1}{2}(m_s + a_s)v_s^2$$

$E_i = Kinetic\ Energy\ of\ the\ Installation$
$E_s = Kinetic\ Energy\ of\ Ship$
$E_T = Total\ Kinetic\ Energy$
$E_s = Strain\ Energy$
$m_s = Ship\ mass$
$a_s = Ship\ added\ mass$
$v_s = Ship\ speed$
$m_i = Mass\ of\ the\ installation$
$a_i = Added\ mass\ of\ the\ installation$
$v_s = Speed\ of\ the\ installation$

A structure is considered compliant if the impact duration is short compared to the fundamental period of vibration of the installation, and fixed if the impact duration is long compared with the fundamental period of vibration. Jacket platforms are usually considered fixed while floating platforms (semi subs, TLP, etc) are usually considered compliant [4].

2.3.1 Force – Deformation Relationships

The structural response of two colliding structures may be expressed with so called force-deformation relationships. These curves express the impact force as a function of the structural deformation.

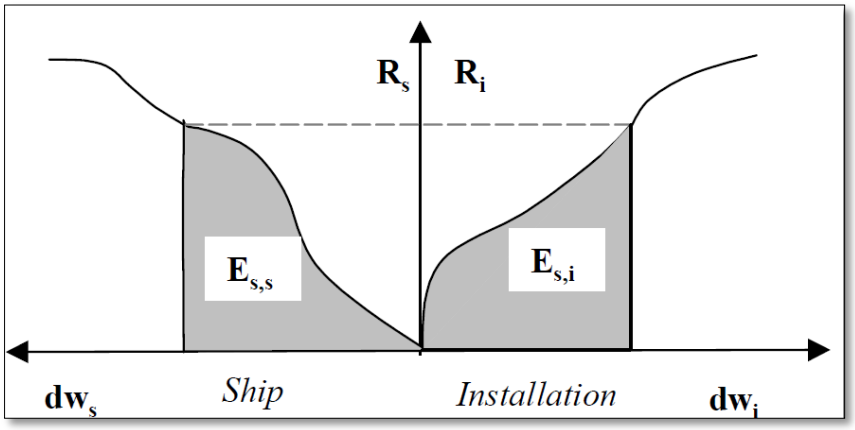

Figure 2-2 – Force-Deformation Relationship [4]

The strain energy dissipated in the collision is equal to the total area under both curves:

$$E_s = E_{s,s} + E_{s,i} = \int_0^{w_{s.max}} R_s dw_s + \int_0^{w_{i.max}} R_i dw_i \qquad \text{Eq. 2-5}$$

By calculating the strain energy as described above, the deformation may be estimated by an incremental procedure from the force-deformation curves until the available strain energy is dissipated. However, force-deformation curves are often established independently of each other under the assumption that the other structure is infinitely rigid. As a consequence, this method may have some limitations:

- Both structures will dissipate some energy regardless of the relative strength.

- The method tends to overestimate the response of the stronger of the two structures and underestimate the response of the softer structure. The reason for this is that when the softer structure deforms, the contact force will be distributed over a larger contact area. Hence, the resistance of the stronger structure will increase.

NORSOK N-004 recommended force-deformation curves for a 5000 ton supply vessel with stern roller are presented in figure 2-3 [4]. The figure includes broad side, bow, stern-end and stern-corner impacts against a circular cylinder with varying diameter.

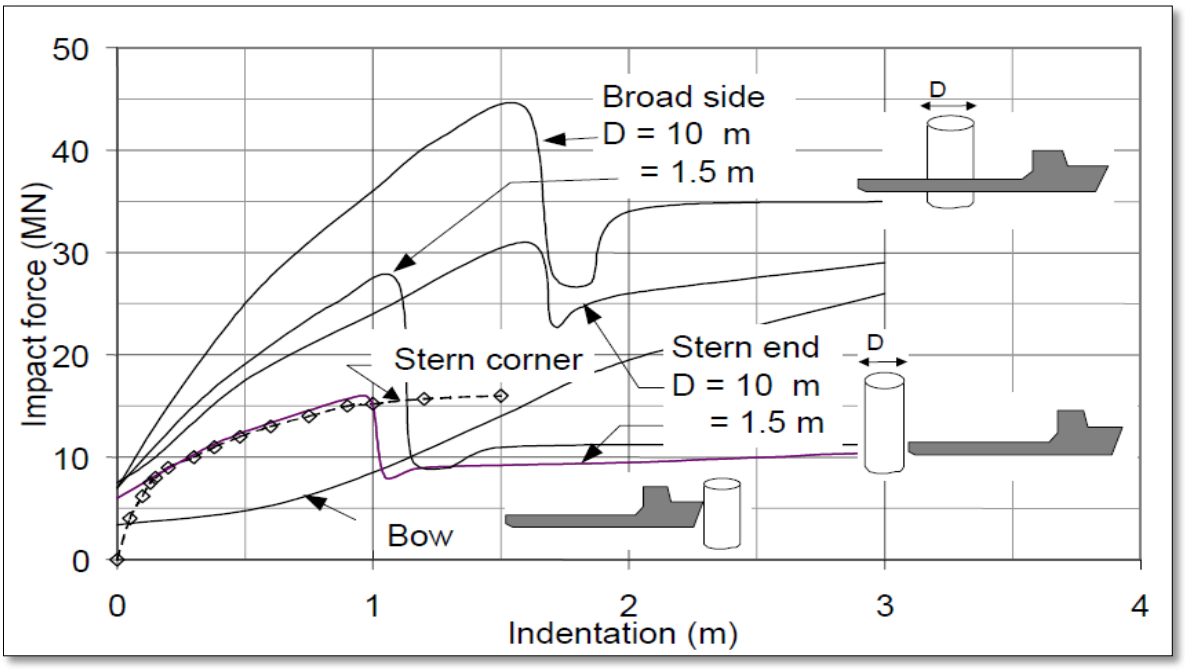

Figure 2-3 – Recommended Force-Deformation Relationships [4]

The calculation of these curves is based on penetration of an infinitely rigid vertical column. Thus, the curves are based on strength design (i.e. small deformations to the offshore installation) and may be used to determine the force that a structure needs to resist in order to achieve strength design. In cases where strength design cannot be assumed, NORSOK [4]

recommends that all the strain energy has to be assumed dissipated by the installation (unless more accurate nonlinear FEM analysis is used).

3. Simple Calculation methods

3.1 General

A ship impact generally involves large plastic strains and significant structural damage to either the installation or the ship, or both. Several methods are used for calculations of impacts between ship and offshore installations:

- Simple calculation methods
  - Empirical/semi-empirical methods
  - Energy methods combined with simple elastic-plastic methods
- Experimental methods
- Nonlinear Finite Element Methods (NFEM)

Which method that is to be used depends on the complexity of the specific problem. The time cost of a Nonlinear Finite Element Analysis (NFEA) is large. Thus, if the problem is fairly simple, simplified methods may be better. For complex problems (e.g. collisions where both structures will dissipate a major part of the strain energy) NFEA must be used in order to capture the true complexity of the problem.

In this chapter, simple calculation methods used to determine the structural response of an impacted jacket leg are considered. The structural response of the ship can also be determined by simple methods (e.g. Minorsky's method, Gerard's method, Amdahl's method), but, since the focus of this thesis is on the impacted jacket leg, these methods will not be discussed. A review of some of the simple calculation methods used to estimate the response of a ship is included in the authors Project Thesis [13].

3.2 Deformation modes

During a ship-impact on a jacket structure, the different deformation modes that may contribute to the energy dissipation are [5]:

- Local deformation of bracing/leg at impact point (local denting)
- Global deformation of bracing and leg element
- Overall deformation of the platform (not considered in this thesis)

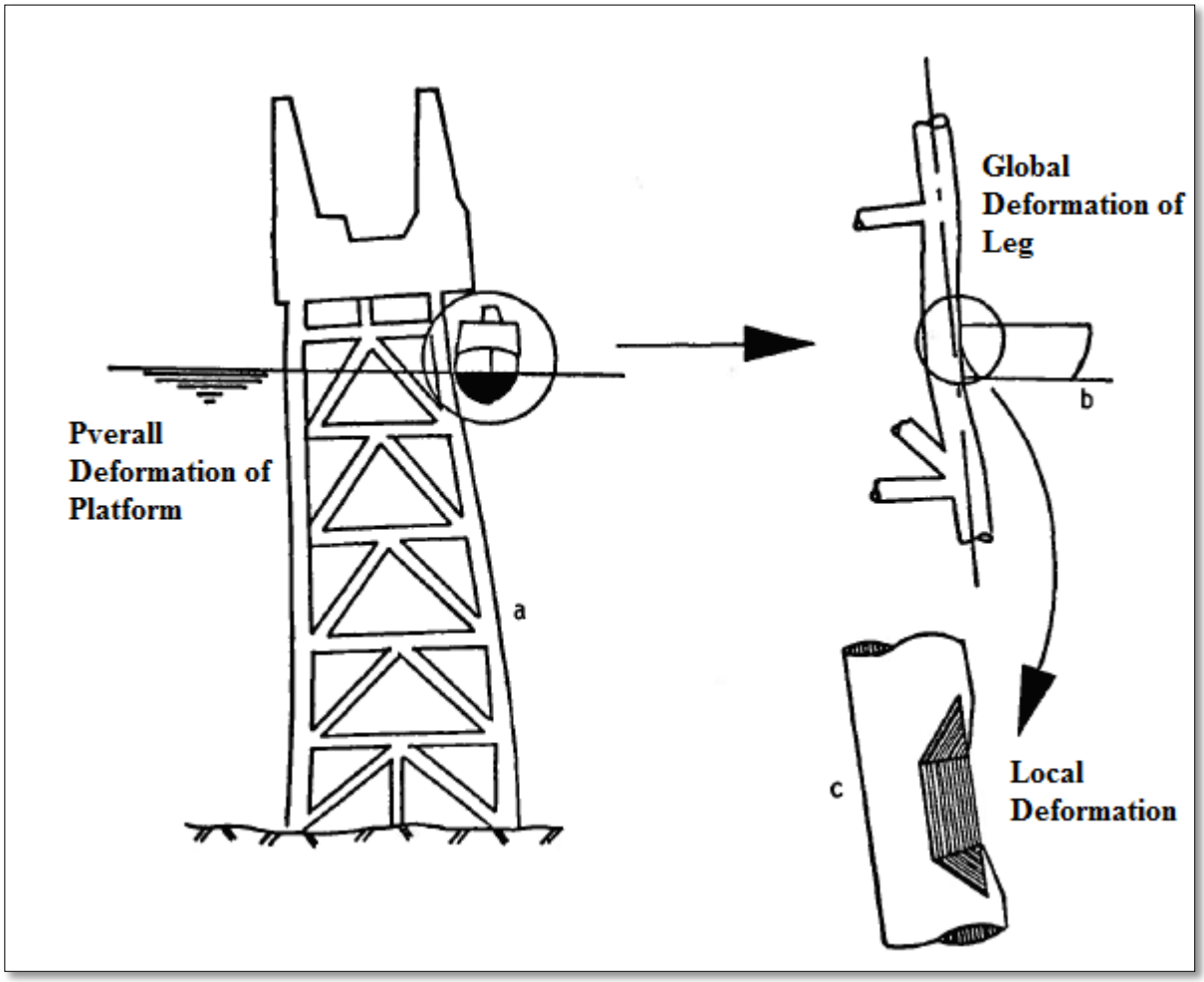

Figure 3-1 – Deformation modes [5]

3.3 Mechanism Method

When analysing collisions involving fairly small diameter columns such as jacket legs/bracings, the mechanism method is a good approach in order to find the critical loads. In this method, a perfect elastic-plastic relationship is assumed, i.e. any section of the beam behaves elastically until the fully plastic moment, Mp, is reached. Any extra increase in the structural strength caused by strain hardening processes is also neglected. This behaviour is shown in figure 3-2.

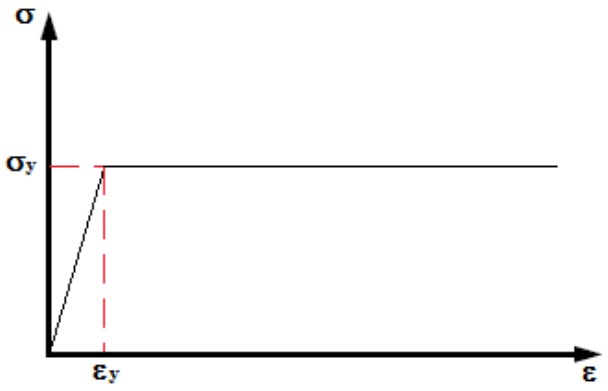

Figure 3-2 – Idealised Stress-Strain Relationships

The mechanism method is based on the kinematic (upper bound) theorem and the uniqueness theorem:

- Kinematic (upper bound) theorem:
  "This theorem states that the collapse load or load factor obtained for a structure that satisfies all the conditions of yield and collapse mechanism is either greater than or equal to the true collapse load" [6]
- Uniqueness theorem:
  "The uniqueness theorem states that a true collapse load is obtained when the structure is under a distribution of bending moments that are in static equilibrium with the applied forces and no plastic moment capacity is exceeded at any cross section when a collapse mechanism is formed" [6]

This means that in order to find the critical collapse load, all the plastic collapse mechanisms must be identified and the internal and external virtual work for each mechanism must be established. The collapse load for each mechanism can then be found by setting the total virtual external work, expressed as a sum of the products of the externally applied loads multiplied with the corresponding distances, equal to the virtual internal work expressed as a sum of the product of the plastic moment multiplied with the corresponding plastic rotation:

$$E_{internal} = E_{external} \quad \text{Eq. 3-1}$$

$$\sum_i (M_p * \theta)_i = \sum_j (P\delta)_j \quad \text{Eq. 3-2}$$

The true collapse load will then be the minimum value of all the possible collapse loads. According to the uniqueness theorem, it is required that the moments in the structure are smaller than or equal to the plastic moment capacity.

The drawback of this method is that it might be difficult to find the proper collapse mechanisms for the structure.

Point load on an axially fixed beam

This beam problem is highly relevant to this thesis. The results derived here are used later in the thesis as a comparison with the FEA results. Therefore, the problem is discussed in detail.

The beam is subjected to a point load at the middle of the beam as shown in figure 3-3.

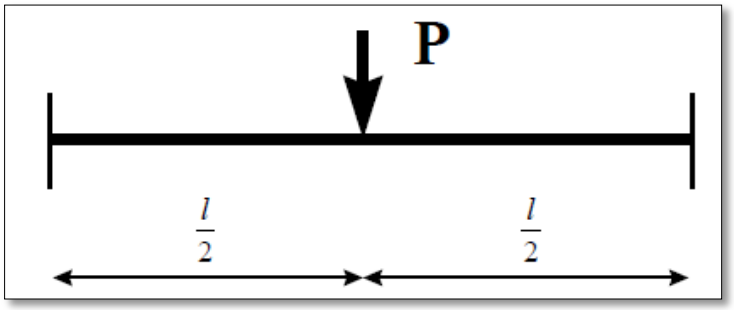

Figure 3-3 – Fixed Beam with Point load

This simple beam configuration has only one collapse mechanism. The mechanism is a three hinge mechanism as shown in figure 3-4.

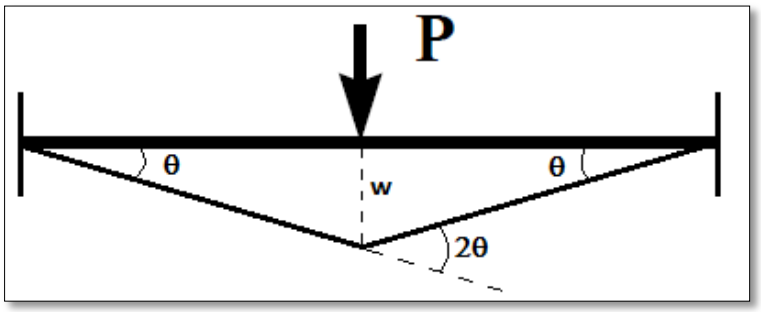

Figure 3-4 – Three Hinge Collapse Mechanism

In order to check that the mechanism satisfies the uniqueness theorem, one needs to consider the beam's moment diagram. The moment diagram is shown in figure 3-5 and it shows that when the plastic moment capacity is reached at the ends and at the middle, no other moments exceeds this value. Hence, the uniqueness requirement is satisfied.

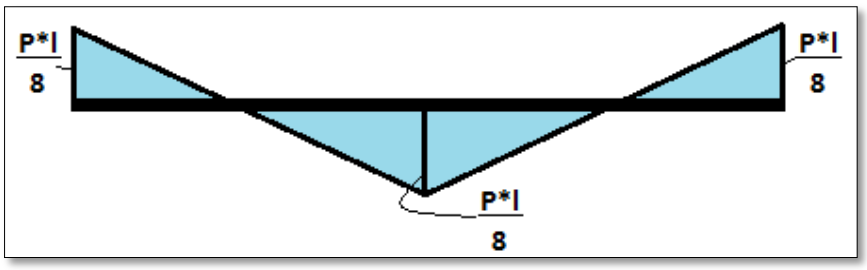

Figure 3-5 – Moment Diagram – Beam Example 1

The ideal rigid collapse load for pure bending can now be found according to the mechanism method:

$$E_{internal} = 2 * M_p * \theta + 2 * M_p * \theta \quad \text{Eq. 3-3}$$

$$E_{external} = P * w = P * \frac{l}{2} * \theta \quad \text{Eq. 3-4}$$

$$E_{internal} = E_{external} \Rightarrow P_{crit} = 8\frac{M_p}{l} \quad \text{Eq. 3-5}$$

Where $E_{internal}$ is the internal work, $E_{external}$ is the external work, M_p is the plastic moment capacity, θ is the plastic rotation, l is the beam length, P is the external applied load, w is the beam deformation at the middle and P_{crit} is the critical load for the mechanism.

The next step is to calculate the plastic moment capacity for the beam. The plastic moment capacity is reached when the stress level over the entire cross section is equal to the yield stress and a plastic hinge is formed. Thus, the plastic moment capacity can be calculated from equation 3-6.

$$M_p = \sigma_y * W_p \qquad \text{Eq. 3-6}$$

Where σ_y is the yield stress and W_p is the plastic section modulus.

Assuming that the beam has a cylindrical cross-section as shown in figure 3-6, the plastic section modulus can be calculated from equation 3-7 [4].

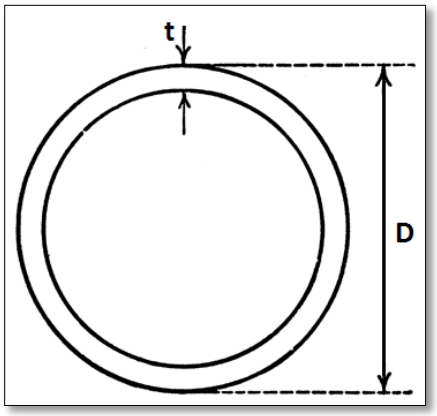

Figure 3-6 – Cylindrical Cross-section

$$W_p = \frac{1}{6}[D^3 - (D - 2t)^3] \qquad \text{Eq. 3-7}$$

The critical load, P_{crit}, may not correspond very well compared to the true behaviour obtained from experiments or finite element analyses. P_{crit} is an ideal rigid plastic collapse load that assumes that the external load is carried by bending only. In reality, local damage, local buckling and the development of membrane forces for axially fixed beams will have a significant effect on the load history. Figure 3-7 shows what might be the true behaviour of the example beam when local buckling effects are neglected. The idealised critical load is also sketched in the figure.

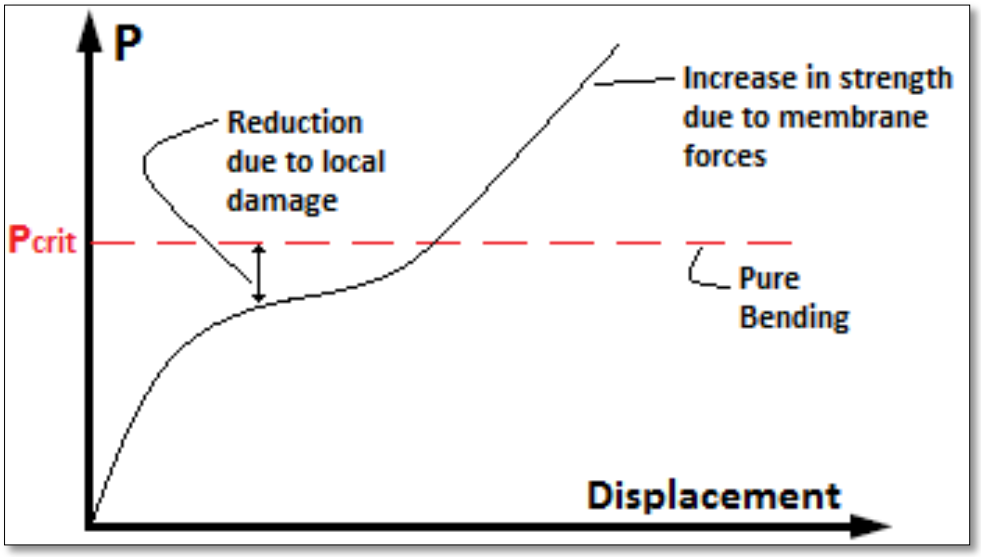

Figure 3-7 – True Behaviour versus Ideal Critical Load

It is also possible to derive an expression for the ideal force-deformation relationship that take into account the increased strength due to the development of membrane forces. Figure 3-8 shows how the membrane forces would develop in the beam.

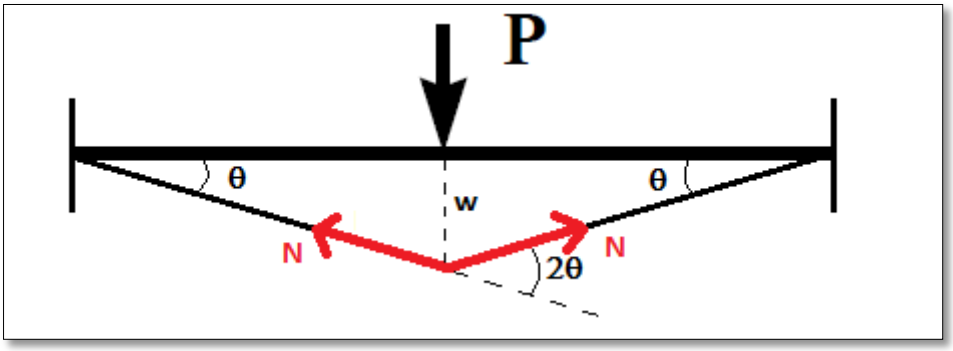

Figure 3-8 – Membrane Forces in Beam Example 1

The external force is now balanced by the moment and membrane forces in the beam. Equilibrium gives:

$$P = 8\frac{M}{l} + 2N * sin(\theta) = 8\frac{M}{l} + 2N\frac{\frac{w}{l}}{2} = 8\frac{M}{l} + 4N\frac{w}{l} \qquad \text{Eq. 3-8}$$

The beam must satisfy the plastic interaction function at the hinges. This function is given in equation 3-10 for a cylindrical cross-section [15]:

$$F = \frac{M}{M_p} - cos\left[\frac{\pi}{2}\frac{N}{N_p}\right] \leq 0 \Rightarrow M = M_p * cos\left[\frac{\pi}{2}\frac{N}{N_p}\right] \qquad \text{Eq. 3-9}$$

Where M_p is the plastic moment capacity and N_p is the plastic tension capacity of the beam.

$$M_p = \sigma_y W_p = \sigma_y d^2 t \quad , \quad N_p = \sigma_y A = \sigma_y \pi d t \qquad \text{Eq. 3-10}$$

Simplified expressions for the plastic section modulus and cross sectional area which are valid for thin walled tubes are used to simplify the expressions. Combining equations 3-9 and 3-10 gives:

$$P = 8\frac{M_p}{l} * cos\left[\frac{\pi}{2}\frac{N}{N_p}\right] + 4N\frac{w}{l} \qquad \text{Eq. 3-11}$$

The next step is to find an expression for the membrane force, N, that is dependent on the lateral displacement, i.e. N=N(w). In order to do this, the Drucker's postulate (or the normality rule) is used. This states that there exist an incremental plastic displacement vector which components are the incremental plastic rotation and incremental plastic elongation of the beam. The vector is a normal to the yield surface defined by the plastic interaction function, F (Eq. 3-10). Mathematically, the incremental plastic displacement vector is expressed as:

$$\delta \boldsymbol{v}_p = \begin{bmatrix}\delta\theta \\ \delta e\end{bmatrix} = \delta\lambda \begin{bmatrix}\frac{\partial F}{\partial M} \\ \frac{\partial F}{\partial N}\end{bmatrix} \qquad \text{Eq. 3-12}$$

Where λ is a proportionality constant. Thus:

$$\delta\theta = \delta\lambda \frac{1}{M_p} \qquad \text{Eq. 3-13}$$

$$\delta e = \delta\lambda \frac{\pi}{2}\frac{1}{N_p} * sin\left[\frac{\pi}{2}\frac{N}{N_p}\right] \qquad \text{Eq. 3-14}$$

Eliminating $\delta\lambda$ gives:

$$M_p \delta\theta = \frac{2}{\pi} N_p \frac{\delta e}{sin\left[\frac{\pi}{2}\frac{N}{N_p}\right]} \qquad \text{Eq. 3-15}$$

A geometric relationship between the plastic rotation and plastic elongation can be established based on figure 3-9. The elongation is expressed in equation 3-17.

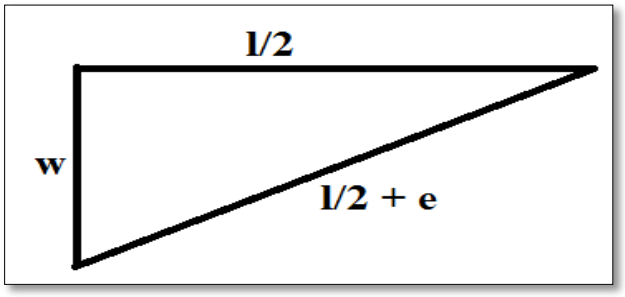

Figure 3-9 – Beam Elongation

$$e = \sqrt{\left(\frac{l}{2}\right)^2 + w^2} - \frac{l}{2} = \frac{l}{2}\left(\sqrt{1 + \frac{4w^2}{l^2}} - 1\right) = \frac{l}{2}\left(1 + \frac{2w^2}{l^2} - 1\right) \cong \frac{w^2}{l} \qquad \text{Eq. 3-16}$$

Differentiating the elongation with respect to the displacement gives:

$$\frac{\delta e}{\delta w} = \frac{2w}{l} \Rightarrow \delta e = \frac{2w\delta w}{l} = w\delta\theta \quad using:\ \delta\theta = \frac{\delta w}{\frac{l}{2}} \qquad \text{Eq. 3-17}$$

Equation 3-16 can now be written as:

$$M_p = \frac{N_p}{\pi}\frac{w}{sin\left[\frac{\pi}{2}\frac{N}{N_p}\right]} \qquad \text{Eq. 3-18}$$

Inserting for M_p and N_p gives:

$$sin\left[\frac{\pi}{2}\frac{N}{N_p}\right] = \frac{w}{d} \quad , \quad \frac{w}{d} \leq 1 \qquad \text{Eq. 3-19}$$

$$\Rightarrow \frac{N}{N_p} = \frac{2}{\pi}\sin^{-1}\left[\frac{w}{d}\right] \qquad \text{Eq. 3-20}$$

Combining equation 3-12 and equation 3-20:

$$P = 8\frac{M_p}{l} * cos\left[\frac{\pi}{2}\frac{2}{\pi}\sin^{-1}\left[\frac{w}{d}\right]\right] + \frac{8}{\pi}N_p\sin^{-1}\left[\frac{w}{d}\right]\frac{w}{l} \qquad \text{Eq. 3-21}$$

$$\Rightarrow P = 8\frac{M_p}{l} * cos\left[\sin^{-1}\left[\frac{w}{d}\right]\right] + \frac{8}{\pi}\frac{N_p}{M_p}M_p\sin^{-1}\left[\frac{w}{d}\right]\frac{w}{l} \qquad \text{Eq. 3-22}$$

Inserting for M_p and N_p and using:

$$cos[\sin^{-1}[x]] = \sqrt{1-x^2} \qquad \text{Eq. 3-23}$$

gives:

$$P = 8\frac{M_p}{l}\sqrt{1-\left(\frac{w}{d}\right)^2} + \frac{8}{\pi}\frac{\pi}{d}M_p\frac{w}{l}\sin^{-1}\left[\frac{w}{d}\right] \qquad \text{Eq. 3-24}$$

$$\Rightarrow P = 8\frac{M_p}{l}\sqrt{1-\left(\frac{w}{d}\right)^2} + 8\frac{M_p}{l}\frac{w}{d}\sin^{-1}\left[\frac{w}{d}\right] \qquad \text{Eq. 3-25}$$

Normalising equation 3-26 by equation 3-5 gives the normalised force-deformation relationship:

$$\Rightarrow \frac{P}{P_{crit}} = \sqrt{1-\left(\frac{w}{d}\right)^2} + \frac{w}{d}\sin^{-1}\left[\frac{w}{d}\right] \quad , \quad \frac{w}{d} \leq 1 \qquad \text{Eq. 3-26}$$

When $\frac{w}{d} > 1$, the membrane force becomes fully plastic ($N=N_p$) and the contribution from bending vanishes. Thus, the equilibrium equation (Eq. 3-9) becomes:

$$P = 2N_p * sin(\theta) = 2N_p\frac{\frac{w}{l}}{2} = 4N_p\frac{w}{l} \qquad \text{Eq. 3-27}$$

$$\Rightarrow P = 4\frac{N_p}{M_p}M_p\frac{w}{l} \qquad \text{Eq. 3-28}$$

Inserting for M_p and N_p:

$$\Rightarrow P = 4\frac{\pi}{d}M_p\frac{w}{l} = 8\frac{M_p}{l}\frac{\pi}{2}\frac{w}{d} \qquad \text{Eq. 3-29}$$

Thus:

$$\frac{P}{P_{crit}} = \frac{\pi}{2}\frac{w}{d} \quad , \quad \frac{w}{d} > 1 \qquad \text{Eq. 3-30}$$

3.4 Local Denting of Tubular Members

The strength of tubular members exposed to impact loads may be significantly reduced due to local denting of the member, i.e. local deformation of the cross section. According to Skallerud & Amdahl [7], the denting effect is two-fold:

- Impact energy is dissipated in the denting process.
- The local denting reduces the effective bending capacity if the section and causes an additional bending moment from the axial force through the eccentricity created in the damaged section.

The contribution from local denting to energy dissipation is normally only of significance when one consider jacket legs. Thus, the energy dissipated in local denting of platform braces may be neglected.

The resistance to the denting process can be calculated by means of the virtual work principle where the model for the dented region is an idealized yield line model as shown in figure 3-10.

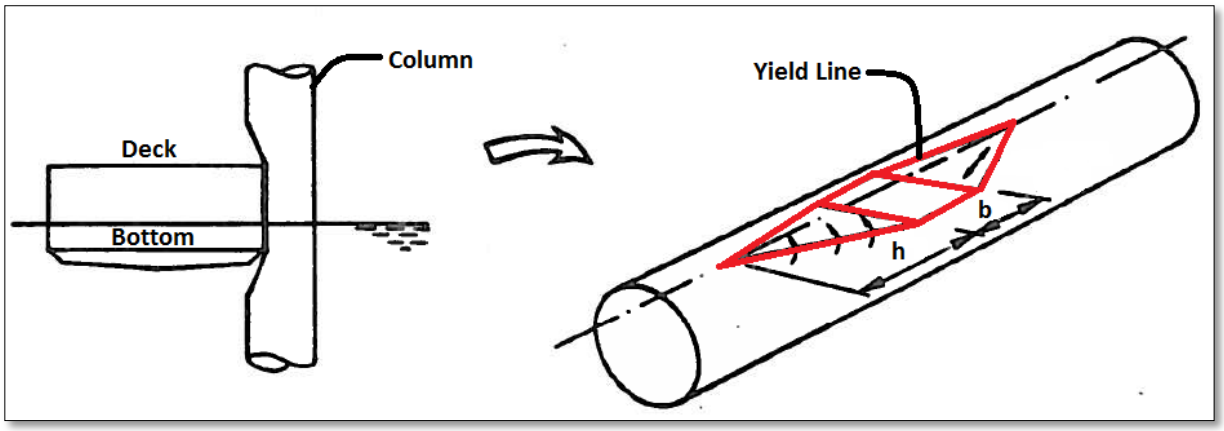

Figure 3-10 –Local Denting Model [15]

The calculation model is based on a perfectly right ship and includes three major sources of energy dissipation [7]:

- Rotation along yield lines
- Plastic change of curvature in circumferential direction
- Plastic work associated with membrane forces

According to NORSOK [4], the resistance to local denting of unstiffened tubular members may be taken from figure 3-11 or alternatively from equations 3-31 to 3-34.

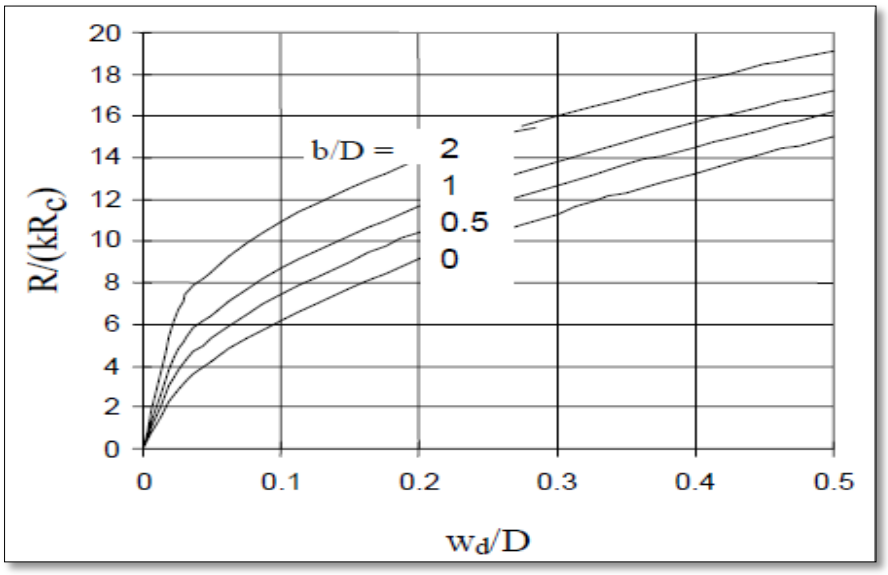

Figure 3-11 – Local Denting Resistance [4]

$$\frac{R}{R_C} = kc_1\left(\frac{w_d}{D}\right)^{c_2} \quad \text{Eq. 3-31}$$

$$R_C = f_y\frac{t^2}{4}\sqrt{\frac{D}{t}} \quad \text{Eq. 3-32}$$

$$c_1 = 22 + 1.2 * \frac{b}{D} \quad \text{Eq. 3-33}$$

$$c_2 = \frac{1.925}{3.5 + \frac{b}{D}} \quad \text{Eq. 3-34}$$

Where R is the resistance to the denting process, R_C is the characteristic strength factor, D is the diameter of the member, t is the thickness of the member, and b is the width of the collision contact zone. The dent dept, w_d, is defined as the original diameter minus the effective diameter after denting, $D-D_{eff}$.

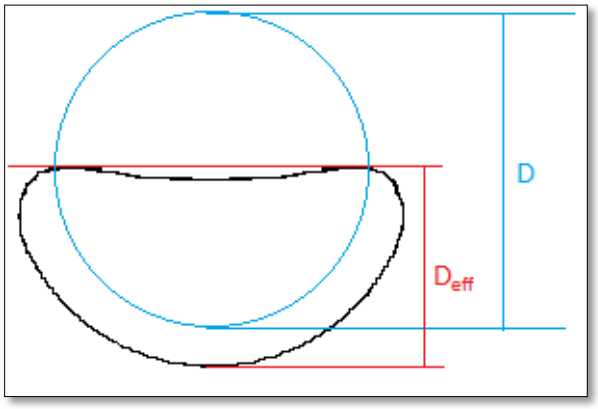

Figure 3-12 – Definition of the Effective Diameter

NORSOK [4] specifies that the curves in figure 3-11 are inaccurate for small indentation and should not be used to verify a design where the dent damage is required to be less than $\frac{w_d}{D} < 0.05$.

The reduction of the bending capacity of the dented member may, according to NORSOK [4], be taken from figure 3-13 or alternatively from equations 3-35 – 3-37.

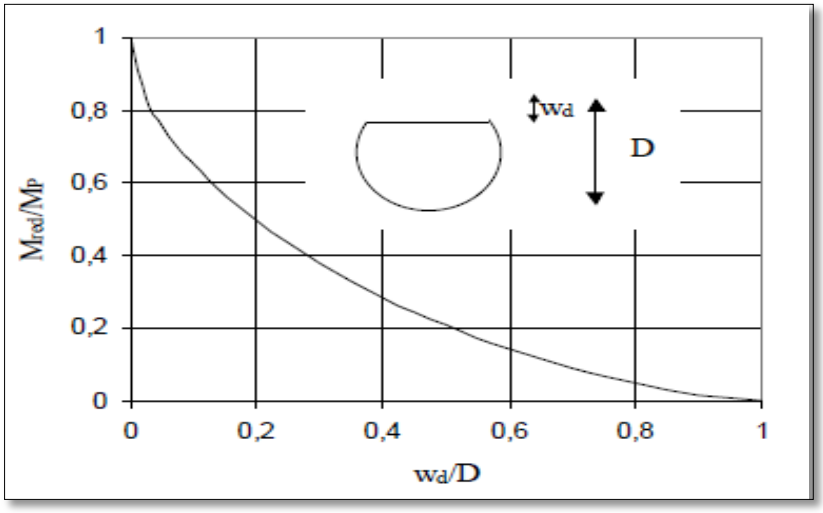

Figure 3-13 – Reduction of Bending Capacity due to Local Denting [4]

$$\frac{M_{red}}{M_p} = cos\left(\frac{\theta}{2}\right) - \frac{1}{2}sin(\theta) \qquad \text{Eq. 3-35}$$

$$M_p = f_y D^2 t \qquad \text{Eq. 3-36}$$

$$\theta = arccos\left(1 - \frac{2w_d}{D}\right) \qquad \text{Eq. 3-37}$$

4. Nonlinear FEA using LS DYNA

In connections with ship impact analyses, large structural deformations are expected and the stress state of the material will normally exceed the linear elastic range. The boundary of the problem will be changing throughout the analysis since as the impact develops. Thus, the problem will be highly nonlinear.

A review of the principles of Nonlinear Finite Element Analysis (NFEA) was performed during the author's project thesis [13] and will not be repeated in here. This chapter deals with NFEA using the simulation software LS-DYNA with emphasis on the keywords used in this thesis.

4.1 Ls-Dyna in General

LS-DYNA is a general-purpose finite element program developed by the Livermore Software Technology Corporation (LSTC). The development started in the 70's with military applications. LS-DYNA is still being developed today with many application regions. Some of these are:

- Crashworthiness analyses (Automotive, train, ship and aerospace)
- Dropped object simulations
- Explosive detonation simulations
- Seismic safety simulations
- Biomechanics simulations

LSTC lists LS-DYNA's capabilities as (among others):

- Nonlinear dynamics
- Rigid body dynamics
- Quasi-static simulations
- Linear statics
- Thermal analysis

For post- and pre-processing purposes, LSTC has developed LS-PrePost. This program has been used during this thesis to prepare analyses and for post-processing of the results.

4.2 Solution Method

In LS-DYNA, the dynamic equilibrium equation (eq. 4-1) is solved using time integration techniques.

$$\boldsymbol{M\ddot{r} + C\dot{r} + Kr = Q}(t) \qquad \text{Eq. 4-1}$$

The main solution methodology in LS-DYNA is based on an explicit time integration technique. The method is called explicit because the displacements at a new time step are only

a function of the accelerations, velocities and displacements at the previous steps, as shown in equation 4-2.

$$\boldsymbol{r_{i+1}} = f(\boldsymbol{r}_i, \ddot{\boldsymbol{r}}_i, \dot{\boldsymbol{r}}_i, \boldsymbol{r}_{i-1}, \ddot{\boldsymbol{r}}_{i-1}, \dot{\boldsymbol{r}}_{i-1}, \dots) \quad \text{Eq. 4-2}$$

There is also an implicit solution method in LS-DYNA. In the implicit method, the displacements at a new step are a function of the accelerations and velocities at the new step as well as the accelerations, velocities and displacements at the previous steps as shown in equation 4-3. Thus, an iterative solution method is required.

$$\boldsymbol{r_{i+1}} = f(\ddot{\boldsymbol{r}}_{i+1}, \dot{\boldsymbol{r}}_{i+1}, \boldsymbol{r}_i, \ddot{\boldsymbol{r}}_i, \dot{\boldsymbol{r}}_i, \boldsymbol{r}_{i-1}, \ddot{\boldsymbol{r}}_{i-1}, \dot{\boldsymbol{r}}_{i-1}, \dots) \quad \text{Eq. 4-3}$$

The implicit method is not used in this thesis because it has somewhat limited capabilities with regard to structural analyses and contact problems [14].

The explicit method used in LS-DYNA is a modified Central Difference method. A short review of the central difference method is included below, details about this method can be found in the LS-Dyna user's manual.

The discretization of one time step is shown in figure 4-1:

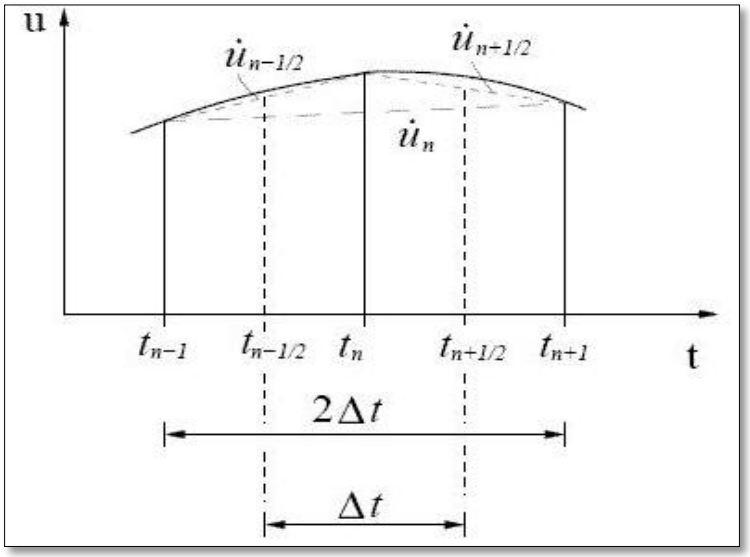

Figure 4-1 – Discretization in the central difference technique [18]

The semi-discrete equations of motion at time n are:

$$\boldsymbol{M}\boldsymbol{a}^n = \boldsymbol{P}^n - \boldsymbol{F}^n + \boldsymbol{H}^n \quad \text{Eq. 4-4}$$

Where **M** is the diagonal mass matrix, $\mathbf{P}^n$ accounts for external and body force loads, $\mathbf{F}^n$ is the stress divergence vector, and $\mathbf{H}^n$ is the hourglass resistance. To advance to time t^{n+1}, the central difference time integration is used:

$$\boldsymbol{a}^n = \boldsymbol{M}^{-1} * (\boldsymbol{P}^n - \boldsymbol{F}^n + \boldsymbol{H}^n) \quad \text{Eq. 4-5}$$

$$\boldsymbol{v}^{n+1/2} = \boldsymbol{v}^{n-1/2} + \boldsymbol{a}^n \Delta t^n \quad \text{Eq. 4-6}$$

$$\boldsymbol{u}^{n+1} = \boldsymbol{u}^n + \boldsymbol{v}^{n+1/2} \Delta t^{n+1/2} \quad \text{Eq. 4-7}$$

$$\Delta t^{n+1/2} = \frac{\Delta t^n + \Delta t^{n+1}}{2} \quad \text{Eq. 4-8}$$

u and **v** are global nodal velocity and displacement vectors. Finally, the geometry is updated by adding the displacement increments to the initial geometry:

$$\boldsymbol{x}^{n+1} = \boldsymbol{x}^0 + \boldsymbol{u}^{n+1} \quad \text{Eq. 4-9}$$

The time integration process performed by LS-DYNA can be presented in the following time integration loop:

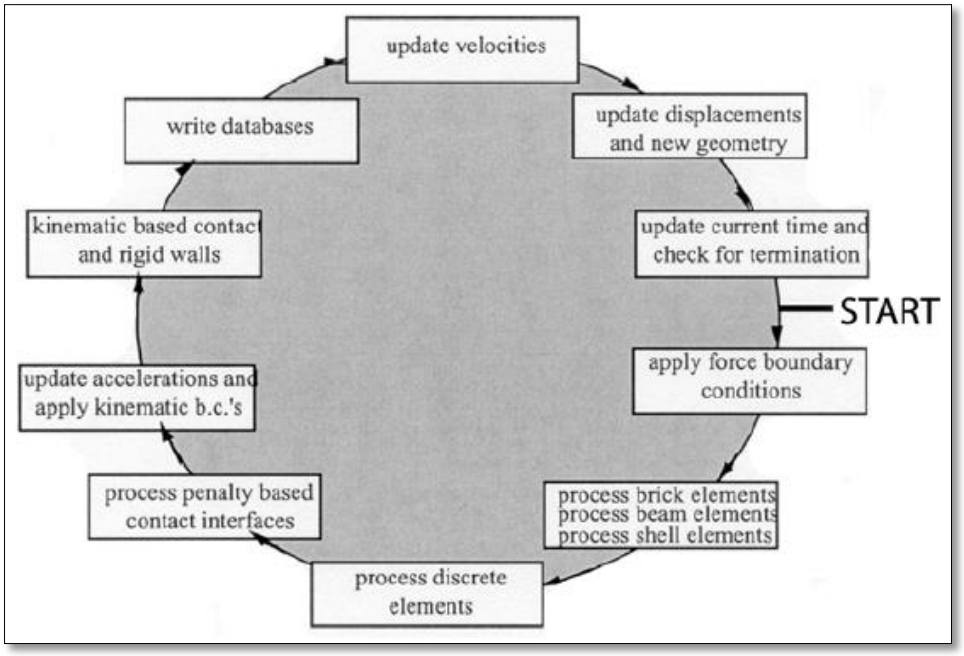

Figure 4-2 – Time integration loop [14]

4.2.1 Stability and Time step

While some implicit time integration techniques may be unconditionally stable with regard to the size of the time step, Δt, the explicit methods are conditionally stable. This often results in very small time steps in the scale of 1E-6 s and thus time consuming analyses.

The stability of the central difference method is governed by the largest natural frequency of the structure, which, in turn, is bounded by the highest frequency of any individual element in the finite element mesh. The critical time step is expressed by equation 4-10 [11]

$$\Delta t = \frac{2}{\omega_{max}} \quad \text{Eq. 4-10}$$

For shell elements, the time step, Δt, must be short enough that a pressure wave does not propagate across more than one element per time step. This means that the maximum allowed time step is limited by the characteristic element length, L_s, and the acoustic wave speed, c, as shown in equation 4-11.

$$\Delta t = \frac{L_s}{c} \quad \text{Eq. 4-11}$$

$$c = \sqrt{\frac{E}{\rho(1-\nu^2)}} \quad \text{Eq. 4-12}$$

Three options for calculating the characteristic element length is included in LS DYNA. In the default option, the characteristic length is calculated as:

$$L_s = \frac{(1+\beta)A_s}{max[L_1, L_2, L_3, (1-\beta)L_4]} \quad \text{Eq. 4-13}$$

where $\beta = 0$ for quadrilateral shell elements and 1 for triangular shell elements, A_s is the shell element area, and L_i (i = 1...4) is the length of the element sides.

4.3 Shell Elements

There exist several element types in LS DYNA. The default shell element type in LS-DYNA is the Belytschko-Lin-Tsay shell element. This element is used throughout this Master thesis as it is a computational efficient and robust element.

The Belytschko-Lin-Tsay shell element is based on a combined co-rotational and velocity-strain formulation. In a co-rotational formulation, the rigid body deformations are separated from the strain producing deformations. This is achieved by comparing the current configuration with the reference configuration. The current configuration is a complete description of the deformed body in its current spatial location and orientation. The reference configuration can either be the initial configuration or the configuration at some other time. An incremental description of the deformation process is obtained by choosing the reference configuration as the previous configuration at time $t^n = t^{n+1} - \Delta t$.

The element was implemented into LS-DYNA as a computationally more efficient alternative to the Hughes-Liu shell element. According to the LS-DYNA user manual [14], a Hughes-Liu shell element with five through-thickness integration points requires 4050 mathematical operations while a Belytschko-Lin-Tsay element only requires 725 operations. A Detailed description of this element is included in the LS DYNA theory manual [14].

4.4 Material Models

4.4.1 Power Law Isotropic Material

This material model provides elastoplastic behaviour with isotropic hardening as defined in figure 4-3. The model is referred to as material model 18 – "MAT_POWER_LAW_PLASTICITY" in LS-DYNA. This material model is used for all deformable structures in this thesis.

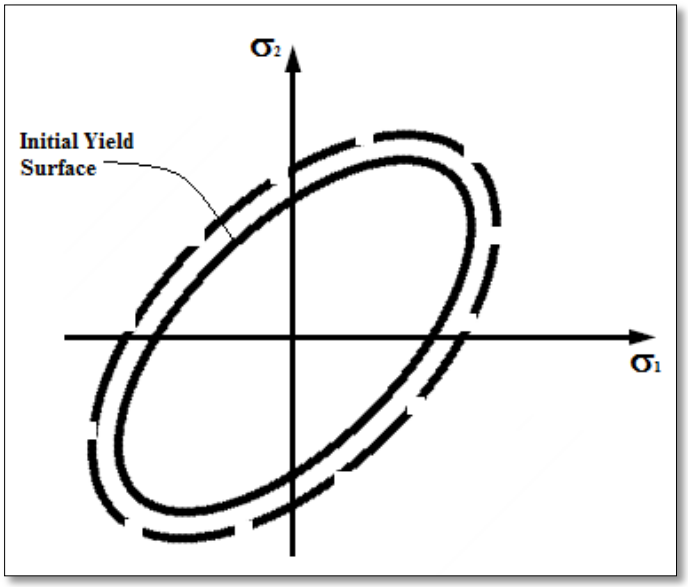

Figure 4-3 – Isotropic Hardening

In this model, the yield stress is a function of plastic strain as equation 4-14 shows:

$$\sigma_y = k\varepsilon^n = k\left(\varepsilon_{yp} + \bar{\varepsilon}^p\right)^n \qquad \text{Eq. 4-14}$$

Where ε_{yp} is the elastic strain to yield, $\bar{\varepsilon}^p$ is the effective plastic strain (logarithmic), k is the strength coefficient and n is the hardening parameter. The initial yield stress can either be defined by the user or LS DYNA can calculate it by solving for the intersection of the linearly elastic loading equation with the strain hardening equation. If the initial yield stress is user defined, equation 4-15 gives the elastic strain to yield:

$$\varepsilon_{yp} = \left(\frac{\sigma_y}{k}\right)^{\frac{1}{n}} \qquad \text{Eq. 4-15}$$

If the initial yield stress is not defined, the elastic strain to yield is given by equation 4-16:

$$\varepsilon_{yp} = \left(\frac{E}{k}\right)^{\frac{1}{n-1}} \qquad \text{Eq. 4-16}$$

The strain rate (rate of deformation) is very important to a structure's response. Tensile tests show that a higher strain rate will increase the stress level at which a specimen yields. However, the tests also show that higher strain rates will make the specimen more brittle. The strain rate effect is accounted for using the Cowper-Symonds model which scales the yield stress by a factor of:

$$1 + \left(\frac{\dot{\varepsilon}}{C}\right)^{\frac{1}{p}} \qquad \text{Eq. 4-17}$$

Where $\dot{\varepsilon}$ is the strain rate, C and p are strain rate parameters.

4.4.2 Rigid Material

This material is referred to as material model 20 – "MAT_RIGID" in LS DYNA. The material turns the elements into a rigid body, i.e. no deformations.

The material requires some input parameters such as Young's modulus, Poisson's ratio and density. These parameters are for instance used for determining sliding interface parameters for contact problems and should therefore be realistic values.

The user also has the opportunity to specify constraints in all 6 degrees of freedom which can be applied either in the global coordinate system or a user-defined local coordinate system. The constraints will apply to the parts that are defined using this material.

4.4.3 Elastic Spring material

This material is applied to the elastic springs and defines the spring stiffness. The model is referred to as material model S01 – "MAT_SPRING_ELASTIC" in LS DYNA.

4.5 Contact Modelling in LS DYNA

This section deals with how a contact works and how it is defined in LS DYNA. The section is based on the LS DYNA theory manual [14] and the LS DYNA support web-pages [18].

The contact is defined by identifying locations that are to be checked for potential penetration. This is done by defining segments of slave elements and master elements. A search for penetrations is made every time step. When a penetration is found, a force proportional to the penetration depth is applied to eliminate the penetration.

There are several types of contact definitions in LS DYNA. The LS DYNA support recommends the automatic contact types as these are non-oriented, i.e. they can detect penetration coming from either side of a shell element. For shell elements, the automatic contact type determines the contact surfaces by projecting normally from the shell mid-plane a distance equal to one-half the 'contact thickness'. Further, at the exterior edge of a shell surface, the contact surface wraps around the shell edge with a radius equal to one-half the

contact thickness thus forming a continuous contact surface. The contact thickness is equal to the shell thickness if nothing else is specified.

The recommended contact type for two-way contact treatment (two-way meaning that both slave segment and master segment are checked for penetration) is the contact type referred to as “CONTACT_AUTOMATIC_SURFACE_TO_SURFACE” in LS DYNA. This contact type is used in all analyses in this thesis and checks for external contact between ship and platform. For contact within the ship or platform (self contact during large deformations), the contact type “CONTACT_AUTOMATIC_SINGLE_SURFACE” is used. This contact type is recommended for crash analysis.

In LS DYNA, the contact is internally represented by linear springs between the master segments and slave segments. The spring stiffness determines the force that is applied to the master and slave nodes. In this thesis, the default way of calculating this stiffness is used. The default method is the so called Penalty-based approach [14]. The method is dependent on the material constants and the size of the segments. In order to work efficiently, the method requires that the material stiffness parameters between the contacting surfaces are of the same order of magnitude. This requirement is fulfilled in this thesis since the ship and column material is steel with parameters of approximately the same order of magnitude.

5. FEA Models

5.1 Side Ship Model

The finite element model of the ship-side used in the LS_DYNA analyses in this thesis was created by Henrik Raaholt during his master thesis of 2009. The reference model, Northern Wave, is a supply vessel designed by Ulstein and built by Havyard shipyard in 2002. The vessel is designed to operate in areas with platforms and is therefore an appropriate reference model for this thesis.

Figure 5-1 – Reference Model [1]

Length O.A	90.90 [m]
Length P.P	78.80 [m]
Breadth, moulded	18.80 [m]
Depth, moulded	7.60 [m]
Draught scantling	6.20 [m]
Docking load app	4600 [tons]
Displacement	6878 [tons]

Table 5-1 – Main Dimensions [1]

The FEM model consists of 24 frames in the middle of the cargo deck as shown in figure 5-2. This was considered enough to get good results in impact analyses involving relatively small diameter columns because side collision energy is relatively small compared with front collision energy.

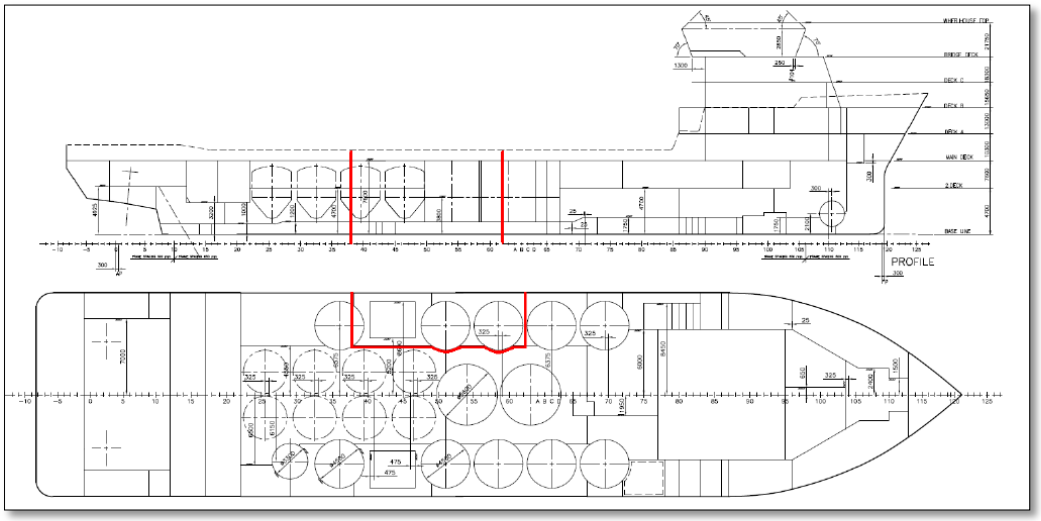

Figure 5-2 – FEA Model Section [1]

The geometry was simplified in the modelling process: circular cut-outs where modelled as square cut-outs with approximately the same area, small details (e.g. brackets) where neglected and bulbous stiffeners where modelled as L-stiffeners with the same height, thickness and area. This was done in order to reduce modelling and computational time. Figure 5-3 and 5-4 shows this simplification.

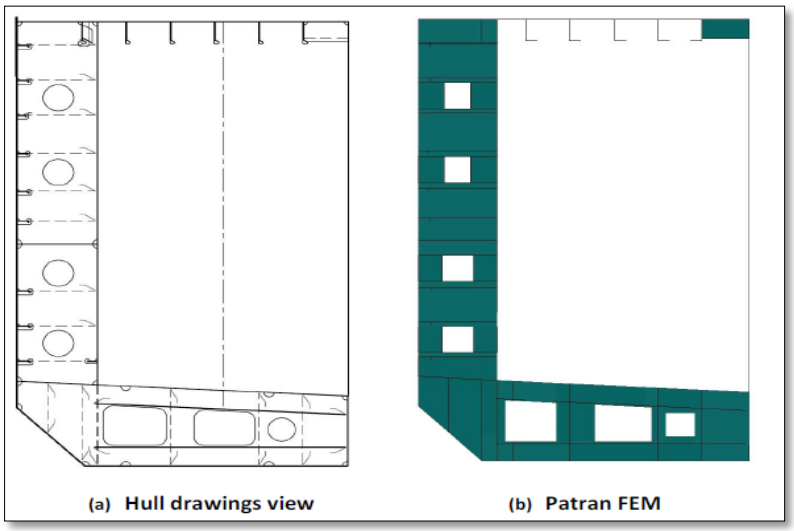

Figure 5-3 – Simplification of hull details [1]

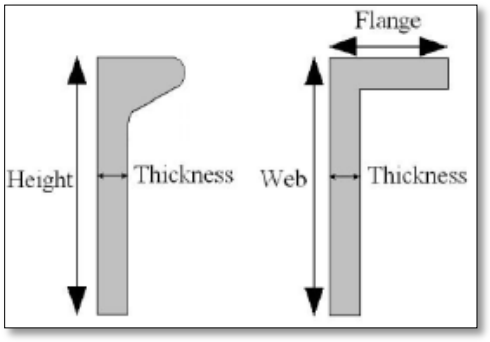

Figure 5-4 – Simplification of Stiffeners [1]

The model dimensions are presented in table 5-2 and the finished model in figure 5-6.

Length	15.60 [m]
Breadth	4.20 [m]
Height	7.60 [m]
Frame spacing	0.65 [m]
Double bottom height	1.20 – 1.45 [m]
Bottom plating thickness	13 [mm]
Side stiffeners	HP 180x8 HP200x9

Table 5-2 – Model Dimensions [1]

5.1.1 Model Verification

It is always important to verify the finite element model before starting an analysis. The most important verification is to verify that there are no duplicate nodes. When parts are created separately as in this case, it is important to verify that the parts are connected. For example: if two plates are supposed to be connected at one edge but are created separately, both plates will have nodes at the common edge. The nodes need to be merged in order to connect the plates. The model was verified and did not have any duplicate nodes.

5.1.2 Mesh and Elements

Raaholt [1] used 4-noded quadratic shell elements for the entire model. He argues that, even though triangular 3-noded elements will in general provide a better representation of complex geometry, the model is simplified in such a manner that 4-noded quadratic shell elements will represent the geometry sufficiently. Also, the 4-noded quadratic shell element will provide more accurate results than the 3-noded triangular element. Raaholt found, based on similar analysis, that an element size of 5 to 10 times the plate thickness would give a good representation of the physical effects, including shell-folding effects. This gave a total of 100.000 elements.

Raaholt used Hughes-Liu shell elements for the entire model. However, as discussed in section 4-3, the Belytschko-Lin-Tsay shell element is more efficient. Therefore, this element type is used for the entire model in this thesis.

5.1.3 Boundary Conditions

Two types of boundary conditions have been applied to the ship-model:

- The transverse edges are considered fixed in all rotational degrees of freedom and all translational degrees of freedom except in the direction of motion against the column (global y-direction). The longitudinal edges are not given any constraints. This is considered to be an conservative approach since it implies that the forces in the transverse direction must be transferred as shear forces in the plates instead of membrane forces [1]

- The longitudinal edge on the model's back-side was given a prescribed displacement of 2 m in the global y-direction in a time interval of 1 s. Hence, giving the ship an impact-velocity of 2 $^{m}/_{s}$.

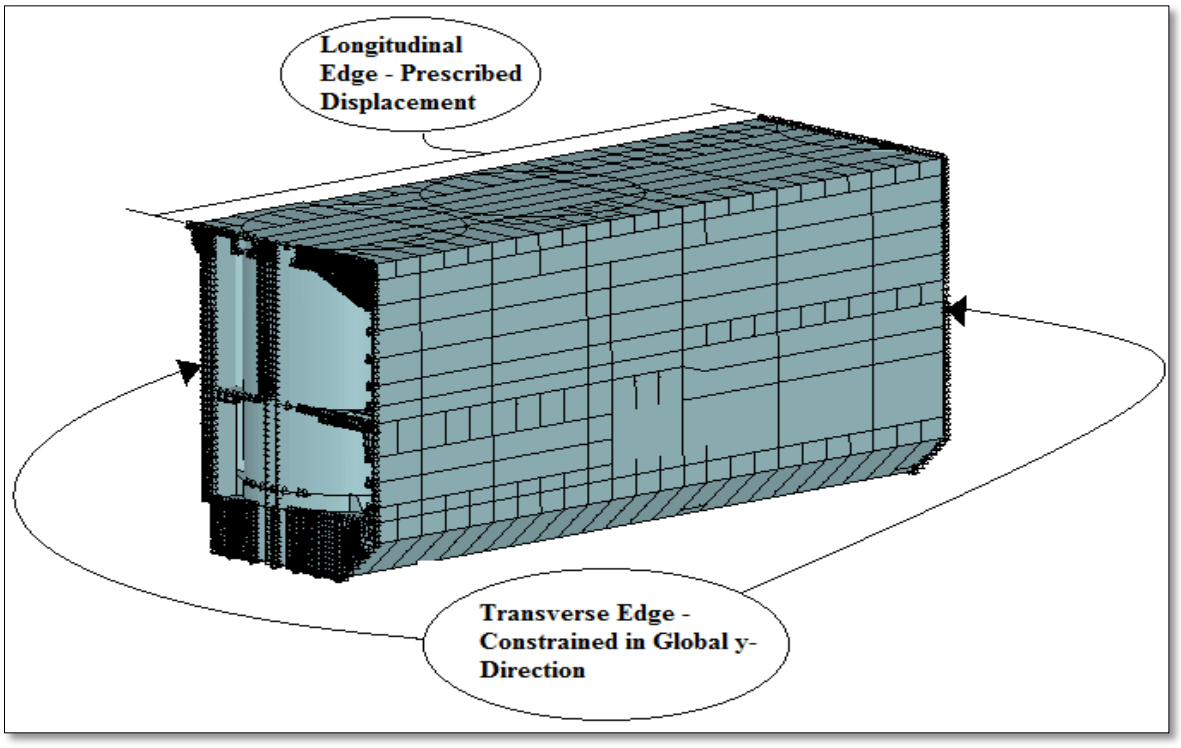

Figure 5-5 – Boundary Conditions – Ship

5.1.4 Material properties

For the purpose of this thesis, the ship is modelled using two different material models. A power law material with isotropic hardening, as described in section 4.4.1, is used in analyses where the ship is allowed to deform and dissipate impact energy. The material properties used for this model is presented in table 5-3.

Young's module	E	210	[GPa]
Yield strength	σ_y	275	[MPa]
Density	ρ	7850	[kg/m^3]
Poisson's ratio	μ	0.30	[-]
Strength coefficient	k	740	[MPa]
Hardening parameter	n	0.24	[-]

Table 5-3 – Material Properties for the Shipside Model [1]

A Rigid material model, as described in section 4.4.2, is used in analyses where the ship is not allowed to deform or dissipate impact energy. The material properties are the same as for the power law material except that the strength coefficient and hardening parameter is not defined in this case.

5.2 Stern Model

The stern model was developed by Mohammed Taghi Tavakoli, a former PhD candidate at the Department of Marine Technology at NTNU.

The model was originally created as a stern-corner model using [mm] as units. The model was mirrored using LS-PrePost in order to obtain a full stern model and converted to [m] using PATRAN. The finished model and its dimensions are presented in figure 5-6.

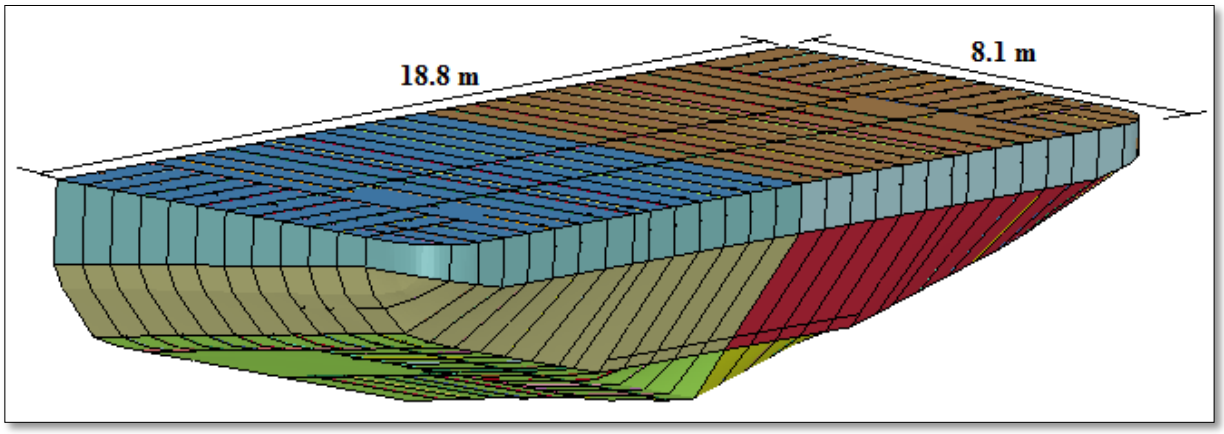

Figure 5-6 – Stern Model

5.2.1 Model Verification

When the model was mirrored in order to create a complete stern, LS-PrePost created duplicate nodes in the middle where the mirrored model is connected to the original model. These nodes were merged using LS-PrePost, completing the stern model.

5.2.2 Mesh and Elements

The general size of the elements of the stern model is 100 mm, giving $4 < L_e/t < 12$ (L_e = element length). Tavakoli meshed the model in this way to capture important structural deformation characteristics based on previously performed convergence studies [19].

The Belytschko-Lin-Tsay shell element is used for all elements.

5.2.3 Boundary Conditions

The stern model is given two sets of boundary conditions (same as for the side-model):

- The model is restricted to motion only in the global y-direction. Hence insuring that the model hits the column in a desired way.

- A prescribed displacement of 2 m in a time interval of 1 s is given to achieve a constant impact velocity of 2 $^{m}/_{s}$. The prescribed motion is in the direction of the global y axis.

5.2.4 Material properties

The material model used by Tavakoli is a user-defined material model that accounts for element failure due to a material failure criterion. In this thesis, the effects of element failure have not been a topic. Therefore, the same material model that was used for the side-ship model is used for the stern model. This has been done since it will give a better basis of comparison with respect to the results obtained using the side-ship model, and since the material parameters are approximately the same as used by Tavakoli. The material properties are given in table 5-4.

Young's module	E	210	[GPa]
Yield strength	σ_y	275	[MPa]
Density	ρ	7850	[kg/m^3]
Poisson's ratio	μ	0.30	[-]
Strength coefficient	k	740	[MPa]
Hardening parameter	n	0.24	[-]

Table 5-4 – Material Properties for the Stern Model

5.2.5 Location of Impact

A close examining of the stern model showed that the strength of the model was a little higher towards the side than at the middle. As a consequence, the ship is considered to hit the column a little to the right of the middle. The impact location is shown in figure 5-7.

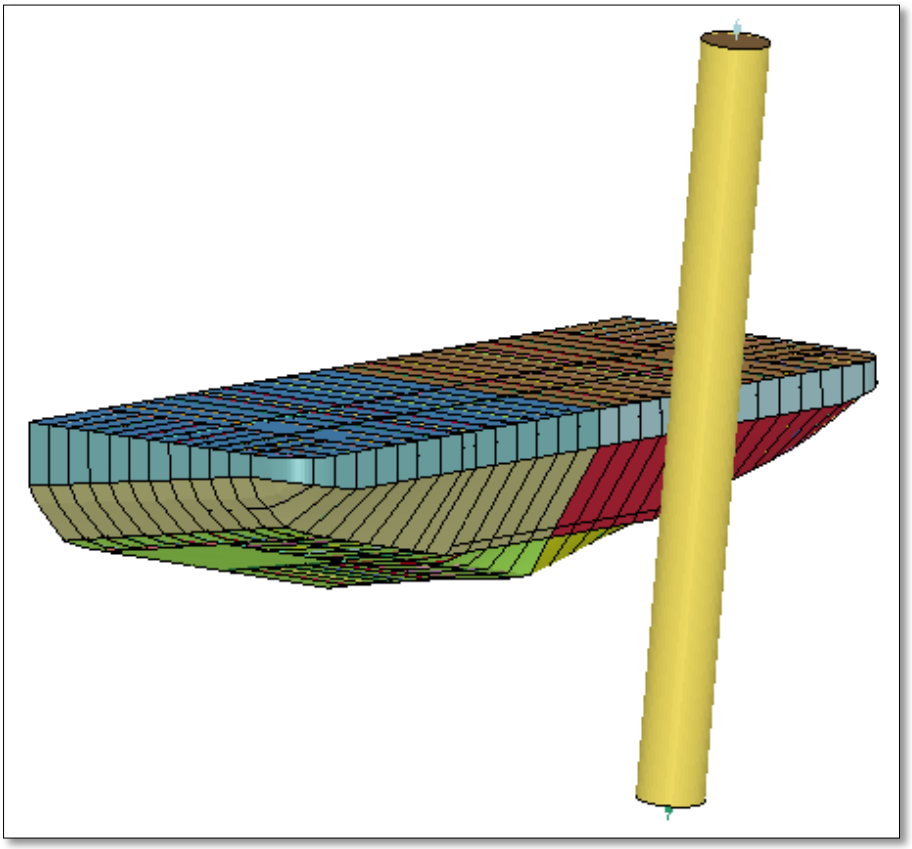

Figure 5-7 – Impact Location – Stern Model

5.3 Jacket Leg Segment

As this master thesis is a continuation of the work performed by Reny Watan during her master thesis in 2011, the finite element model of the jacket leg segment is based on what was used by Watan. However, in discussion with Prof. Jørgen Amdahl [16] it was decided that the batter-ratio should be 1/8 instead of 1/7 which was used by Watan. The diameter and thickness of the column have been varied according to table 7.1. The length of the segment is 17 m for all analyses. Figure 5-8 shows the column and its dimensions.

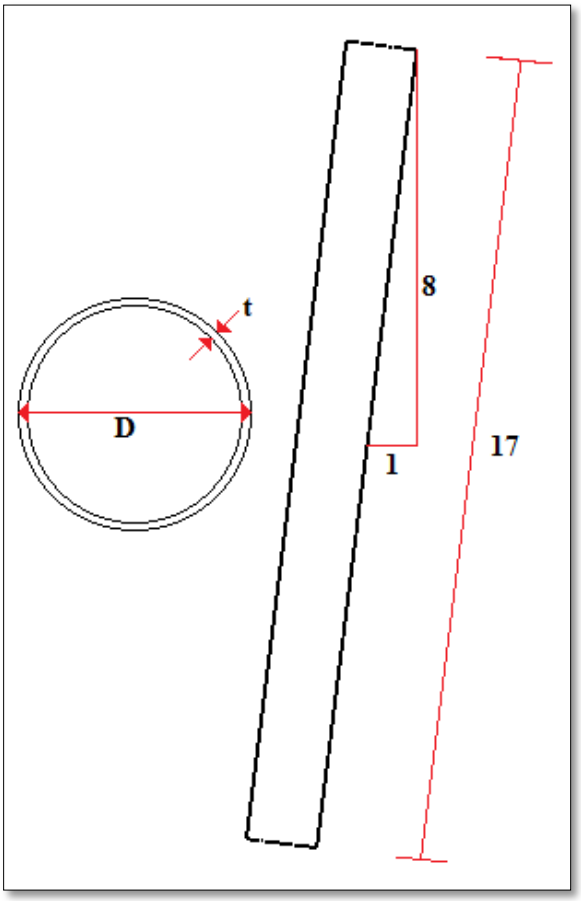

Figure 5-8 – Column Sketch – Not To Scale

5.3.1 Mesh and Elements

Convergence studies [12] of ship grounding analyses have shown that $5 < L_e/t < 10$ (where L_e is the element length and t is the shell thickness) will give a good physical representation of the structural effects during large deformations. However, since the whole column is expected to be subjected to large deformations and high stresses and strains, and since the column geometry is quite simple, the column has been meshed with 4-noded quadrilateral elements with element length = 100 mm. This gives $1.43 < L_e/t < 3.33$ which is quite small compared to the convergence studies. This has been done in order to ensure convergence of the results and in order to achieve a good representation of the circular geometry using 4-noded quadrilateral elements.

Belytschko-Lin-Tsay shell element is used for all elements. This element type has been described in section 4.3.

5.3.2 Boundary Conditions

A Jacket leg is typical divided into several segments by a network of supporting braces (see figure 5-10). The strength of the supporting structure will determine which set of boundary conditions that are appropriate. In order to find the appropriate boundary condition for this case, the jacket leg segment has been analysed using two different sets of boundary conditions:

Case 1:
The column ends are considered completely fixed in all translational and rotational degrees of freedoms. In this case the surrounding structure is assumed strong enough to resist the loads that arise when the column deforms.

Case 2:
Depending on the strength of the surrounding structure, the column ends might displace inwards in the axial direction when the column deforms. In order to model this boundary condition, the column ends are considered fixed in all rotational degrees of freedom and all translational degrees of freedoms except in the local axial direction of the column. The column ends are modelled with a spring in the axial direction to simulate the stiffness of the surrounding structure. In discussion with Prof. Jørgen Amdahl [16], it was decided that the surrounding structure would act in an elastic manner. Hence, a linear elastic spring is used.

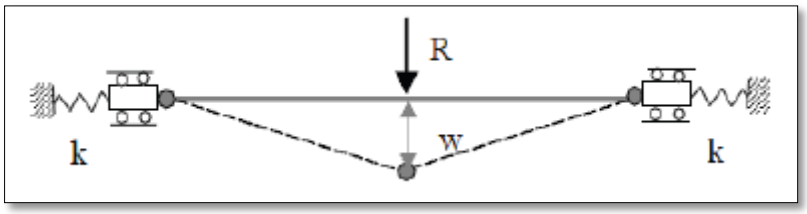

Figure 5-9 – Spring Model [7]

The spring stiffness is determined using the computer program USFOS and a previously developed jacket platform model with appropriate dimensions (figure 5-10).

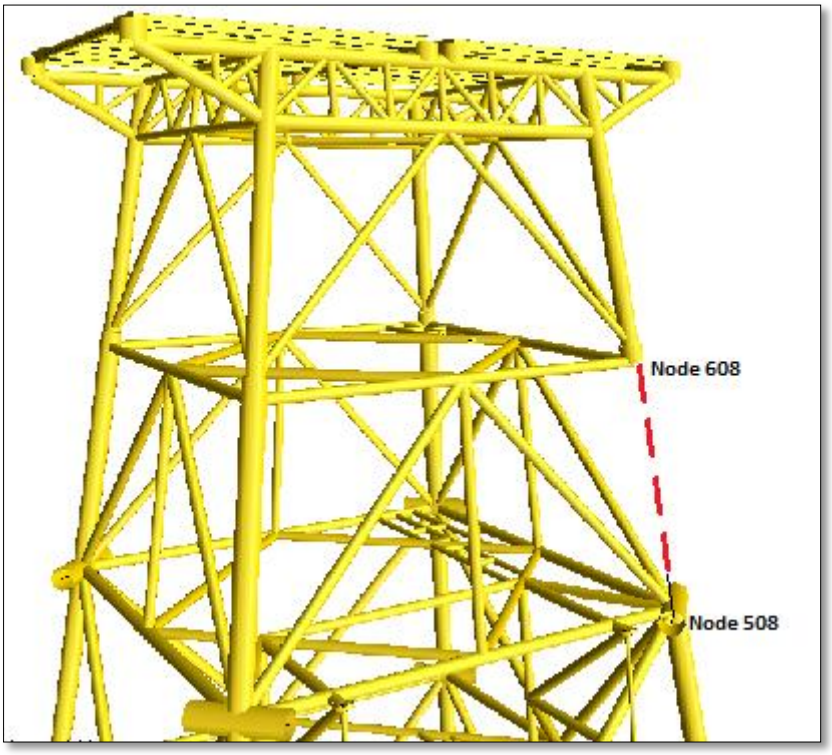

Figure 5-10 – USFOS Model

To find the stiffness, the leg segment between node 608 and 508 was removed and a known force was applied in the direction of the leg segment at both nodes. The force was applied in a stepwise manner, and the stiffness was calculated by considering the force versus displacement of the two nodes as shown in figure 5-11.

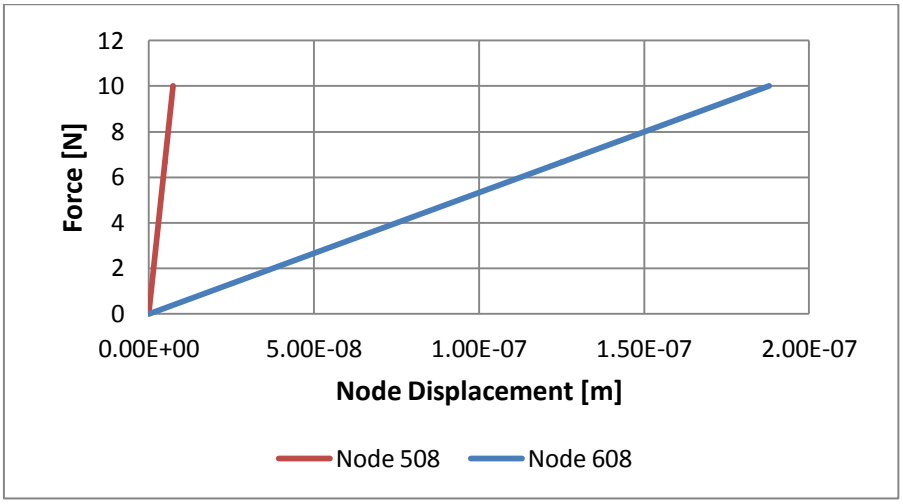

Figure 5-11 – Force–Displacement for Node 506 and 608

This resulted in the following stiffness:

Top – Node 608	K_{Top}	5,3245E+07	[N/m]
Bottom – Node 508	K_{Bottom}	1,3776E+09	[N/m]

Table 5-5 – Spring Stiffness from USFOS

When modelling the leg segment in Ls-PrePost, there are two methods of which the springs may be attached. In method A, the column is modelled with a rigid cover at the ends, and one spring with stiffness K_{Top} (or K_{Bottom}) is attached to the centre of the rigid cover as shown in figure 5-12. The rigid cover is only allowed to translate in the axial direction of the column and it is restricted from rotation. In method B, each of the top (and bottom) nodes of the column is attached to a spring so that the total stiffness is equal to K_{Top} (or K_{Bottom}). Reny Watan performed analyses using both these methods and concluded that method A is the correct method. The reason is that in method B, the nodes at the column end can displace independently of the other nodes at the same end. Hence, method A is used in this thesis.

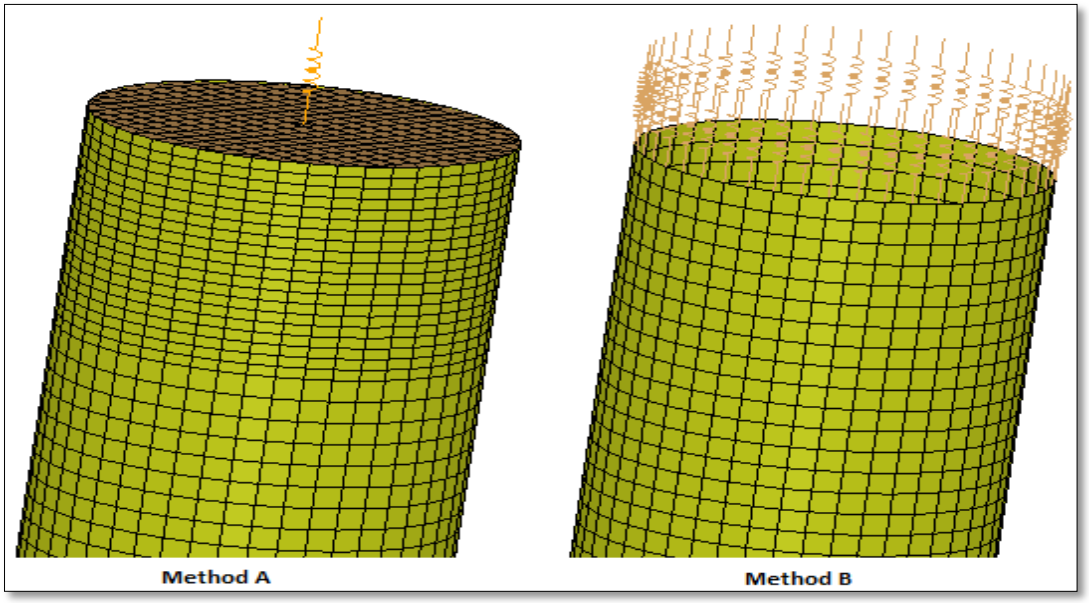

Figure 5-12 – Spring Attachment Method A and B

Figure 5-12 also shows that in method A, the meshing of the column is denser near the end. The reason for this is that the transition from a rigid material to a deformable material might be problematic if the mesh is too coarse.

5.3.3 Material Properties

The Jacket leg segment is modelled using two different material models. A power law material with isotropic hardening, as described in section 4.4.1, is used in analyses where the column is allowed to deform and dissipate compact energy. The material properties used for this model are based on the properties used by Reny Watan during her master thesis. The properties are presented in table 5-6.

Young's module	E	210	[GPa]
Yield strength	σ_y	355	[MPa]
Density	ρ	7850	[kg/m^3]
Poisson's ratio	μ	0.30	[-]
Strength coefficient	k	790	[MPa]
Hardening parameter	n	0.19	[-]

Table 5-6 – Material Properties for the Column Model [2]

A Rigid material model, as described in section 4.4.2, is used in analyses where the column is not allowed to deform or dissipate impact energy. The material properties are the same as for the power law material except that the strength coefficient and hardening parameter is not defined in this case.

5.3.4 Impact Location

The location of initial impact may have an effect on the capacity of the column. However, this has been discussed in detail by Reny Watan [2] and is not a focus in this thesis. Therefore, the initial impact location is set to middle span (in the middle of the column) for all analyses in this thesis. Figure 5-13 illustrates the impact point for beam and stern impacts.

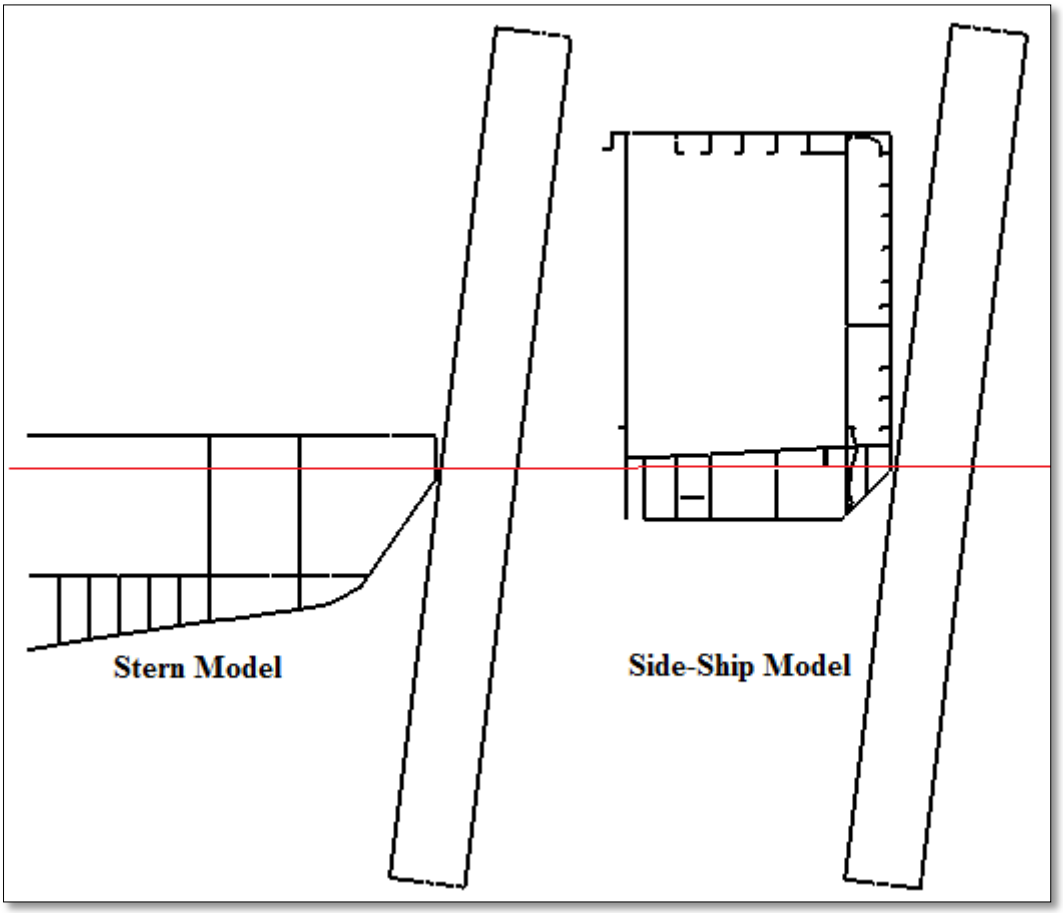

Figure 5-13 – Middle Span Impact Location

6. FEA Results – Boundary Conditions

6.1 General

The jacket leg segment might either be considered fixed or with an axial flexibility that takes into account the flexibility of the surrounding structure as described in section 5.3.2. This topic was also addressed by Reny Watan during her master thesis in 2011. Watan concluded that the difference on the response was neglectable. However, because the outcome was expected to be different and because a modelling error regarding the spring-models was found in Watan's work, the topic is being readdressed in this thesis. The results obtained from this part of the thesis will determine which boundary conditions that are used in the other parts.

To investigate the effect of boundary conditions, the jacket leg segment with a diameter of 1.5 m is considered. Only the cases with 30 mm and 60 mm column shell thickness will be discussed in detail. The comparison of the force-deformation relationships for the rest of the column thicknesses are presented in Appendix A.1.

6.2 30 mm Column

The force-deformation relationships in figure 6-1 show that the response of the column is dependent on the boundary conditions. For small energy impacts, the difference is small and fixed boundary conditions could be justified in such cases. However, the difference becomes fairly large as the column deformation increases. For example: the force required to produce a column displacement of 1.6 m using fixed boundary conditions is about 24 MN, but when the axial flexibility is taken into account the required force is about 20 MN, giving a strength reduction of about 17%.

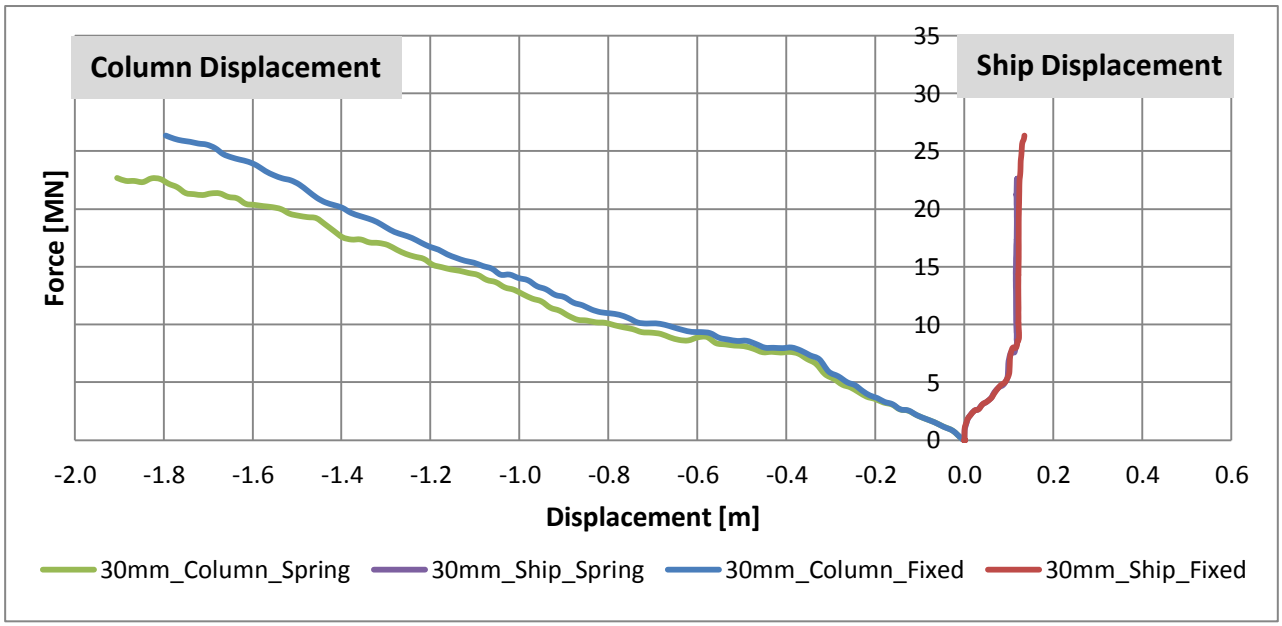

Figure 6-1 – Force-Deformation – Spring vs. Fixed Boundary - 30mm Column

The reason for the difference between the two graphs is due to the development of membrane forces in the column. This may be illustrated by an example:

Three beams are subjected to a lateral loads. Beam A has axially fixed ends, beam B has one axially fixed end while the other end is equipped with an axial spring with stiffness K_S, and beam C has one axially fixed end and one axially free end.

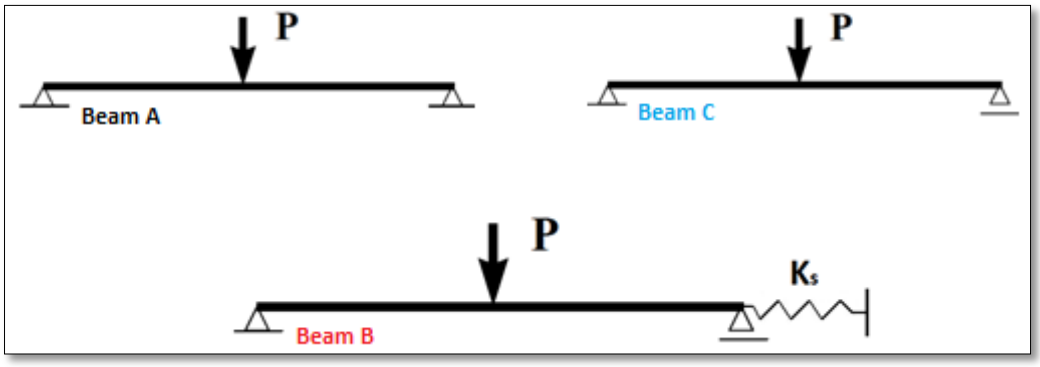

Figure 6-2 – Example beams A, B and C

The force-deformation relationships of these beams are shown in figure 6-3. Beam A will have a significant increase in strength in the post collapse range. The reason for this behaviour is that the ends are not free to displace inwards leading to the development of membrane forces in the beam that resist further deformation. Beam B will also have an increased strength in the post collapse range, but the increase in strength will be limited by the spring stiffness, K_S. However, since the ends of beam C are free to displace inwards, beam C will not develop membrane forces and the strength will therefore drop as the figure shows.

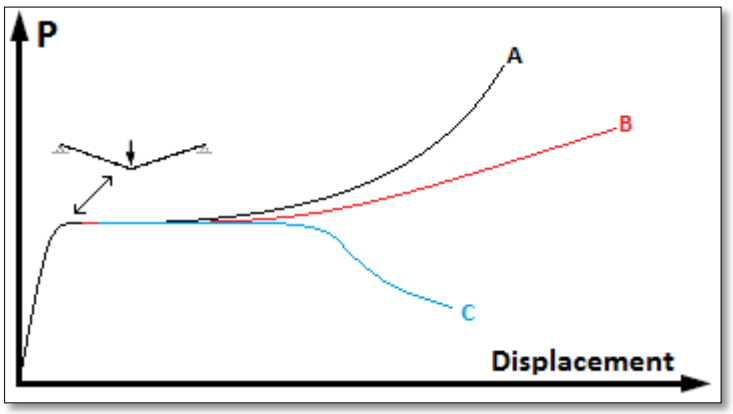

Figure 6-3 – Force-deformation for example beams A-C

Compared to the jacket leg segment, beam A corresponds to the case with fixed boundary conditions, and beam B corresponds to the case with axial flexibility. This behaviour can be verified by considering the membrane forces that are being developed in the column. A cross-section tool in LS-PrePost ("SPlane") is used to plot the membrane forces at a cross-section 4.8 m below the top of the column in the axial direction. The cross-section is locked to three

nodes so that the same section is considered as the column deforms. This is shown in figure 6-4:

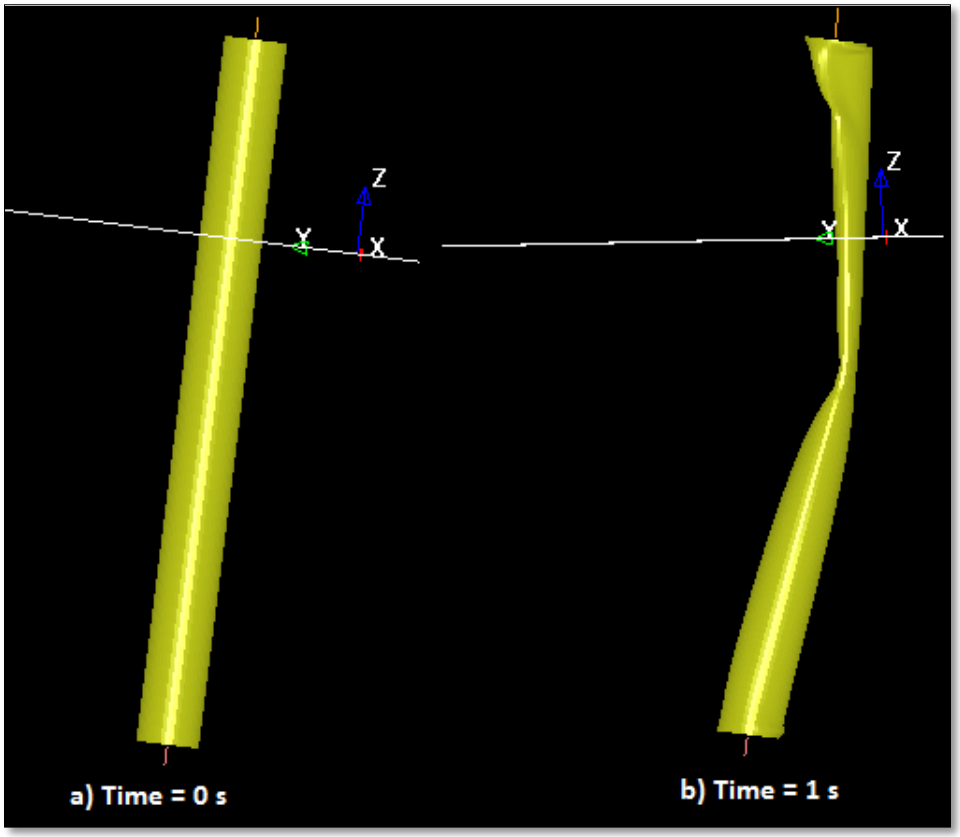

Figure 6-4 – Column Cross-Section using "SPlane" in LS-PrePost

The cross-sectional force in the local z-direction of the cross-section is plotted in figure 6-5 for both the fixed column and the column with axial flexibility. The figure shows that the membrane forces that develop in the fixed column are significantly larger than those developing in the column with axial flexibility, verifying the behaviour explained in the example above.

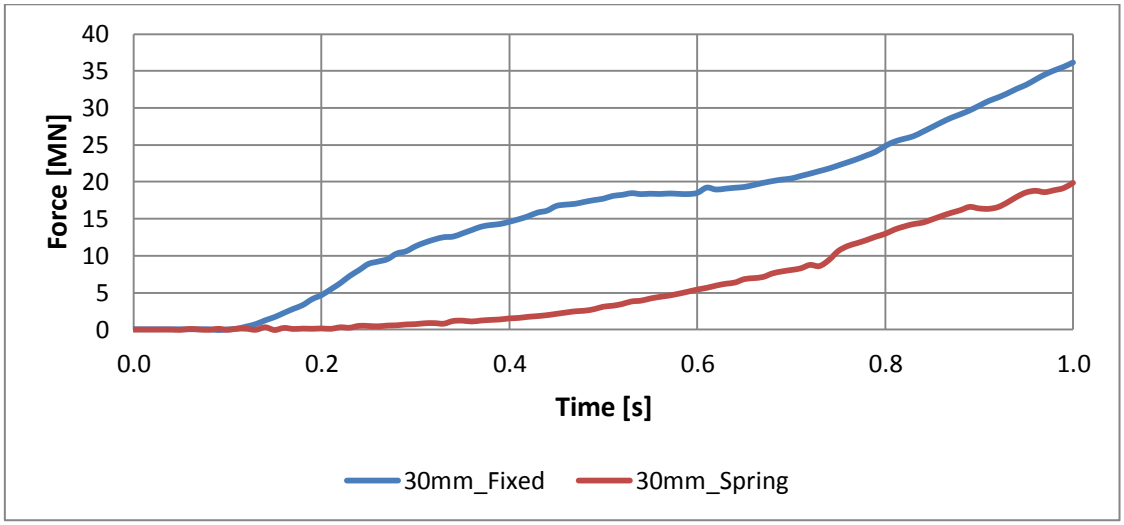

Figure 6-5 – Membrane Forces – D=1.5m – t= 30 mm

The results in this section show that the axial flexibility due to the surrounding structure will have an effect on the response of the column, especially for high energy impacts. Therefore, in order to obtain results that are as physical correct as possible, axial flexibility should be taken into account. The effect on the ship side is neglectable in this case.

6.3 60 mm Column

The force-deformation relationships for the case with 60 mm column shell thickness are shown in figure 6-6. This case is analogue to the case with 30 mm column shell thickness in the sense that fixed boundary conditions may be justified for low energy impact scenarios and in the sense that, for higher energy impacts, the force required to produce the same column deformation is larger when the column ends are considered fixed than when the axial flexibility is taken into account. For example: the required force to produce a 0.9 m deformation of the column is 46 MN for the case with fixed boundaries while the required force for the case with axial flexibility is 41 MN, giving an 11% reduction in strength.

The effect on the ship is larger than what was seen for the 30 mm case, but the effect is still quite small.

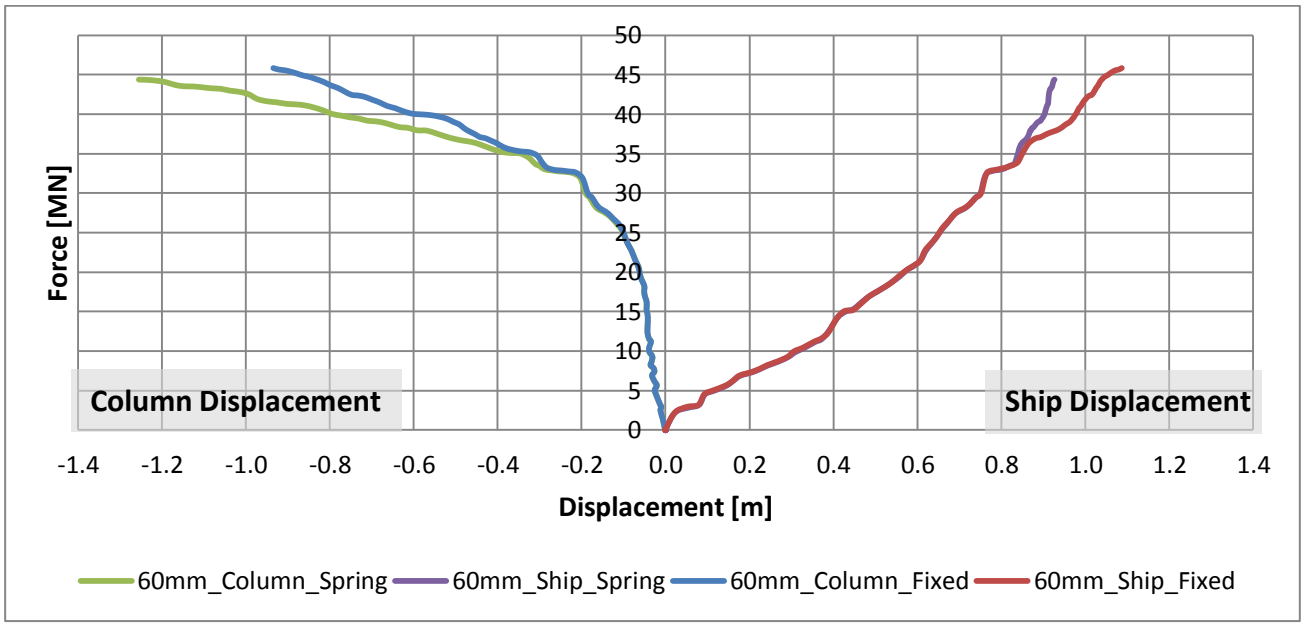

Figure 6-6 – Force-Deformation – Spring vs. Fixed Boundary - 60mm Column

The cross-sectional membrane forces that develop during the impact are plotted for both column boundary types in figure 6-7. The 60 mm columns undergo smaller deformations than for the 30 mm columns. This explains why the forces are lower in this case. The figure shows that the membrane forces are significantly larger for the fixed column than for the column with axial flexibility.

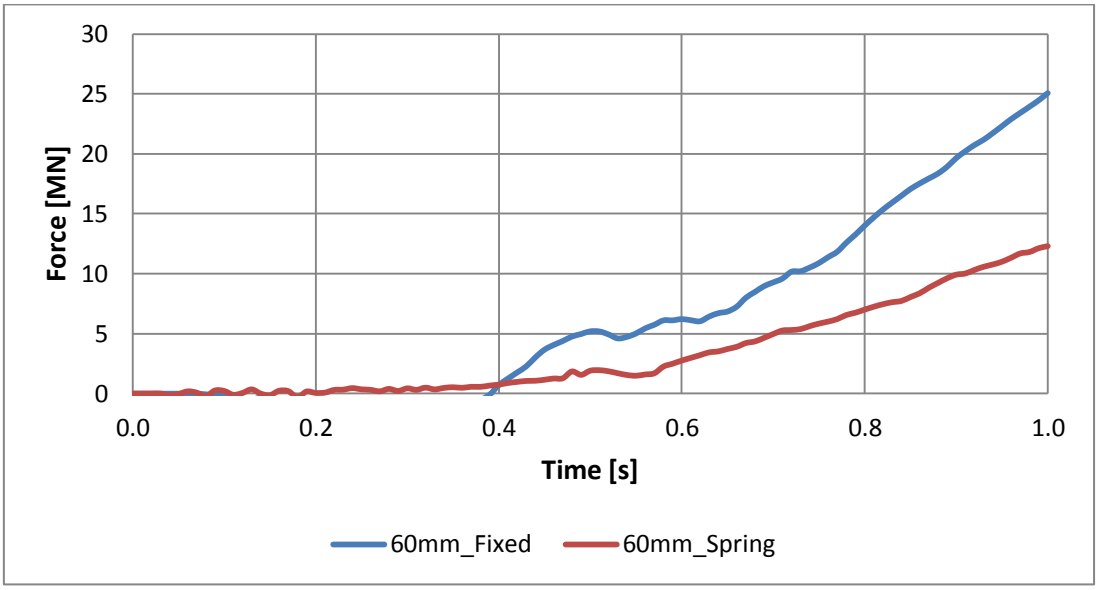

Figure 6-7 – Membrane Forces – D=1.5m – t= 60 mm

The results show that it would not be correct to assume fixed boundary conditions for the 60 mm column case either. However, the results also show that the influence of the boundary conditions becomes smaller as the column thickness is increased. In fact, the 70 mm column is almost unaffected by the choice of boundary condition (see figure A-3 in appendix A.1). But if the ship were stronger, the 70 mm column would be affected as well.

6.4 Spring Force

Table 6-1 presents the maximum spring force compared to the axial force at yield for the different column-configurations which have been subjected to beam impacts. The axial force at yield is calculated according to equation 6-1..

$$F_{yielding} = \sigma_{yield} * A_{cross-section} \quad \text{Eq. 6-1}$$

Column Diameter [m]	Column Thickness [mm]	F_{yield} [MN]	Top F_{spring}/ F_{yield} [%]	Bottom F_{spring}/ F_{yield} [%]
1.5	30	49.18	25.16	45.87
	40	65.13	15.86	34.92
	50	80.86	9.58	28.38
	60	96.36	4.68	21.46
	70	111.64	0.39	13.09
1.0	40	42.83	25.71	53.41
	50	52.98	19.87	44.57
	60	62.90	13.80	36.42
2.0	40	87.44	8.03	24.75
	50	108.74	3.26	16.49
	60	129.82	0.30	9.85
	70	150.67	0.28	7.58

Table 6-1 – Maximum Spring Force

7. FEA Results - Parameter Study

7.1 General

In this chapter, a parameter study of the jacket leg segment subjected to beam collisions is performed. The main case is the column with diameter 1.5 m. Thus, the discussion will mainly be focused on this column diameter. The column diameter and shell thickness are varied according to table 7-1:

Diameter [m]	Thickness [m]	Cross-Sectional Area [m^2]	$I = \frac{\pi}{64}(D_{outer}^4 - D_{inner}^4)$ $[m^4]$	$i = \sqrt{\frac{I}{A}}$ $[m]$
1.5m	0.03	0.139	0.037	0.520
	0.04	0.183	0.049	0.516
	0.05	0.228	0.060	0.513
	0.06	0.271	0.070	0.510
	0.07	0.314	0.081	0.506
1.0 m	0.04	0.121	0.014	0.340
	0.05	0.149	0.017	0.336
	0.06	0.177	0.020	0.333
2.0 m	0.04	0.246	0.118	0.693
	0.05	0.306	0.146	0.690
	0.06	0.366	0.172	0.686
	0.07	0.424	0.198	0.683

Table 7-1 – Parameter Study

As a consequence of the results in chapter 6, all the columns analysed in this chapter are equipped with axial flexible boundary conditions.

7.1.1 Available Strain Energy

The total available strain energy for the beam impact may, based on the main specifications of the reference ship and the impact speed, be calculated according to equation 2-4:!!

$$E_s = \frac{1}{2}(m_s + a_s)v_s^2 = \frac{1}{2}(6.878 * 10^6(1 + 0.4)) * 2^2\ [J] = 19.26\ [MJ]$$

7.1.2 Contact Area

The contact area of an impact is important for the distribution of the impact force which in turn affects the strength of the colliding structures.

For each time step, LS-DYNA prints the nodal contact pressure and force into a ncforc-file. The contact area for each time step was calculated according to equation 7-1 using MATLAB.

$$Area\ per\ time\ step = \sum_{i=1}^{Nu.of\ Nodes} \frac{(Nodal\ Force)_i}{(Nodal\ Pressure)_i} \qquad \text{Eq. 7-1}$$

The contact area calculated using MATLAB for the column with diameter 1.5 m and thicknesses 30 and 70 mm are presented in figure 7-1. The figure shows that the maximum contact area is about 2.32 m^2 for the 30 mm column and about 5.47 m^2 for the 70 mm column.

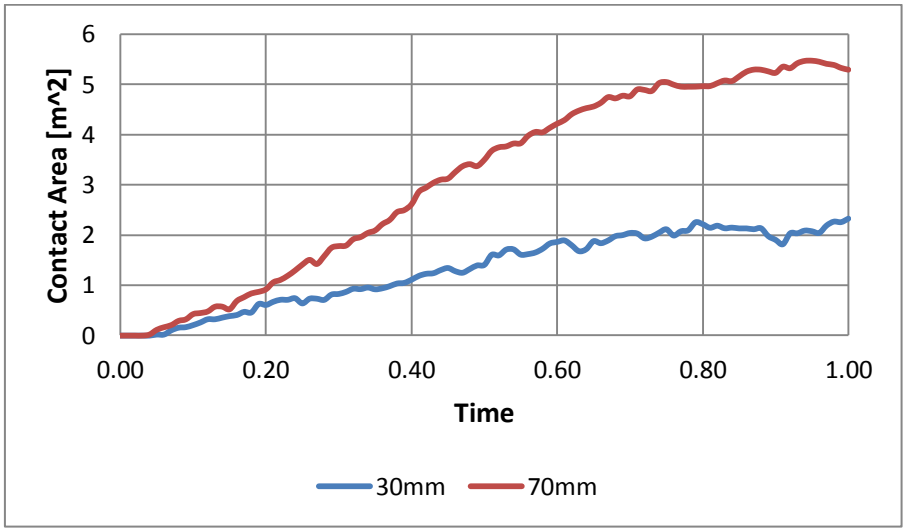

Figure 7-1 – Contact Area – 30 mm and 70 mm Column

Figure 7-2 shows the column and ship at the point of maximum contact area for the column with diameter 1.5 m and 30 mm wall-thickness. The figure shows that the column seems to have contact over the entire column width and over most of the ship height. Thus, the contact area calculated using MATLAB is quite small compared to what one could expect from visual considerations.

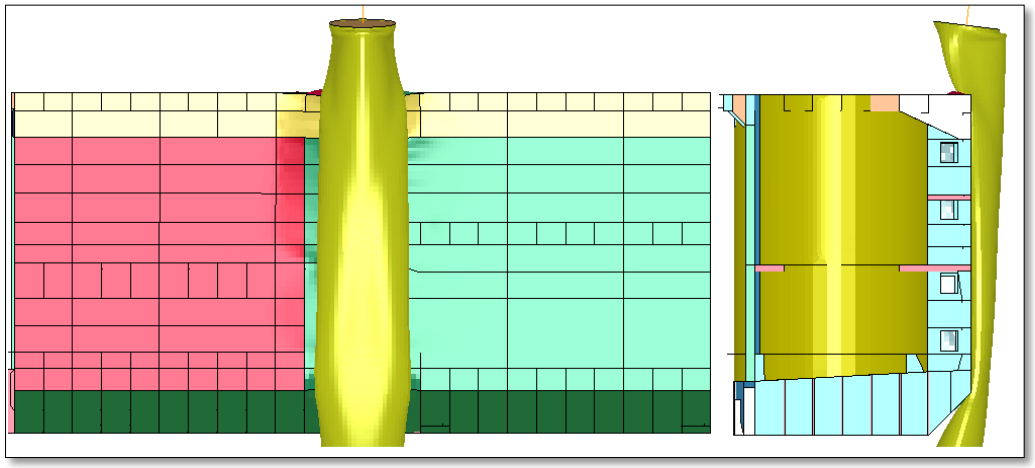

Figure 7-2 – 30 mm Column in LS-PrePost

A closer investigation of the columns verified that the results calculated using Matlab were correct. The reason is due to the deformation of the columns which is quite extensive when the column shell thickness is 30 mm. This is best illustrated by considering some cross sections of the ship and column:

z = 0.95 m (Location of first impact):

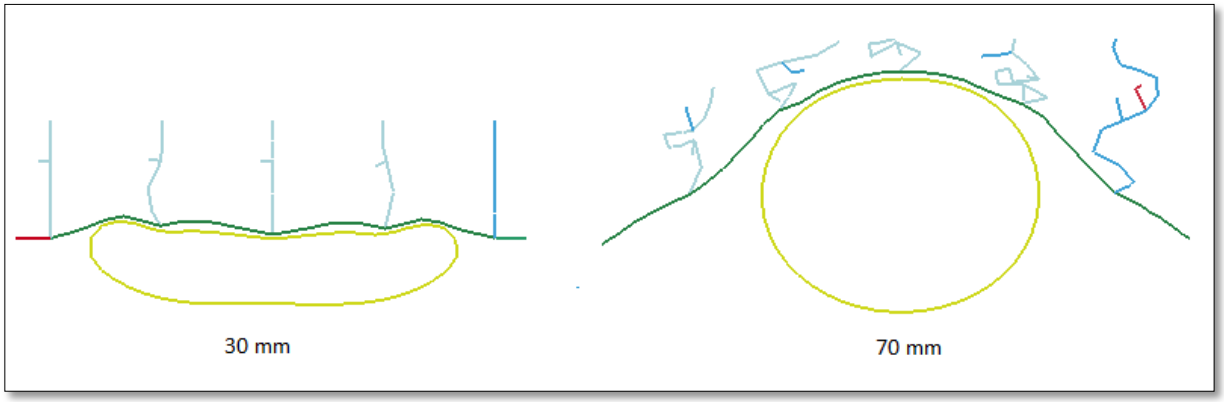

Figure 7-3 – Cross section at z = 0.95 m

z = 4 m

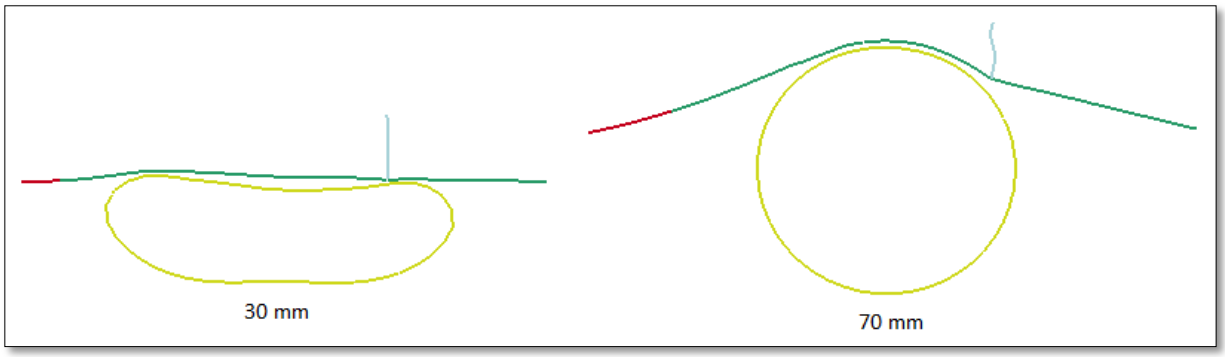

Figure 7-4 - Cross section at z = 4 m

From figure 7-3 and 7-4 it is clear that when the weaker column deforms, the contact area will be limited to the sides of the column. When the column thickness is 70 mm, the column deformation is small. In this case, the ship deforms around the column leading to a larger contact area than for the weak columns.

7.1.3 Plotting of Ship Strength

The contact area for the beam impacts is changing quite much during the impact scenario. One of the consequences of this has been that the point where the ship experiences the maximum deformation is not constant over time. Figure 7-5 shows the ship's y-displacement for two different impact moments. The column in this case is the 30 mm column with diameter = 1.5 m. The figure shows that when the impact time is 0.5 s, the point of maximum deformation is located at the bottom of the ship. However, when the time is 1.0 s, the maximum deformation will be at the top of the ship. The reason for this behaviour is that the column deforms and makes contact with the top of the ship which is considerable weaker in strength compared to the bottom of the ship.

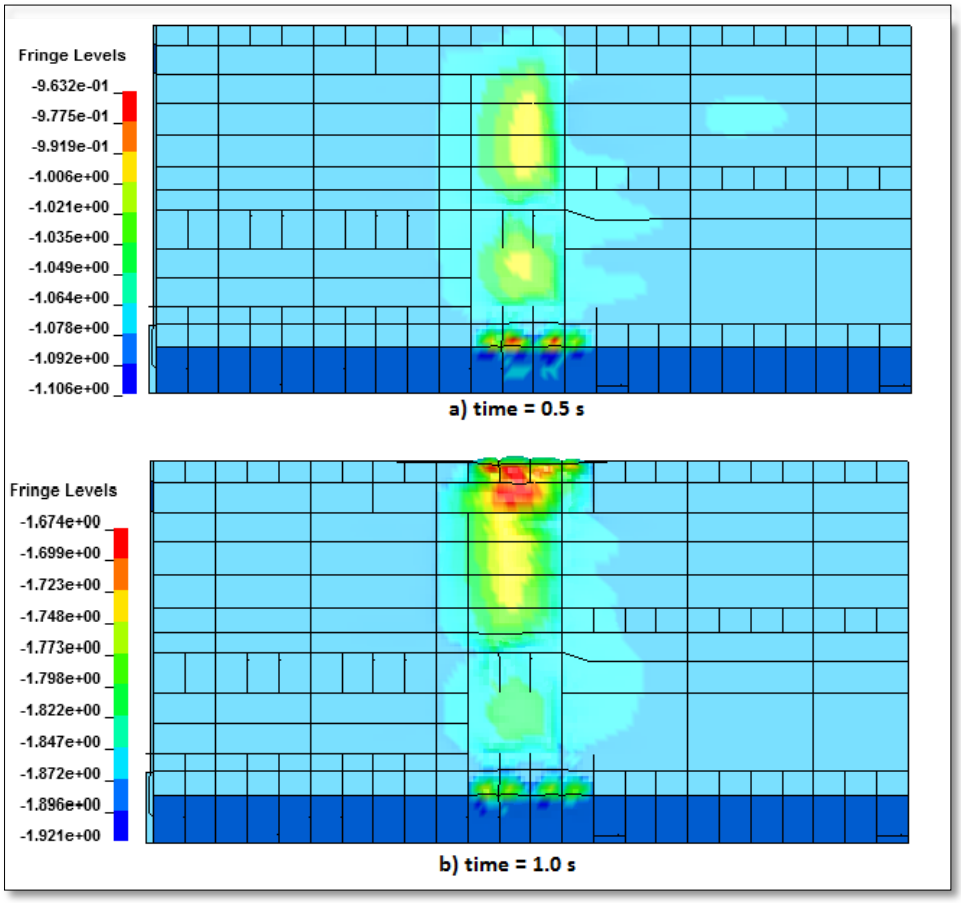

Figure 7-5 – Ship Deformation – 30mm Column Thickness

In order to present the worst structural behaviour of the ship, the maximum ship-deformation at any given time has been plotted in the force-deformation relationships. A consequence of this is that the amount of energy dissipated by the ship cannot be found simply by calculating the area under the force-deformation curve. Still, this has been presented in this way in order to show the true impact behaviour.

7.2 Force-Deformation Relationship

7.2.1 Column Diameter = 1.5 m

Figure 7-6 presents the force-deformation relationships for the different column configurations with constant diameter = 1.5 m. The column deformation is the total deformation, i.e. the local and global column deformation.

The figure shows that the strength of the column increases with increasing column shell thickness. Consequently, the strength of the ship section decreases as the column shell thickness increases. This is in accordance to what was expected prior to performing the analyses.

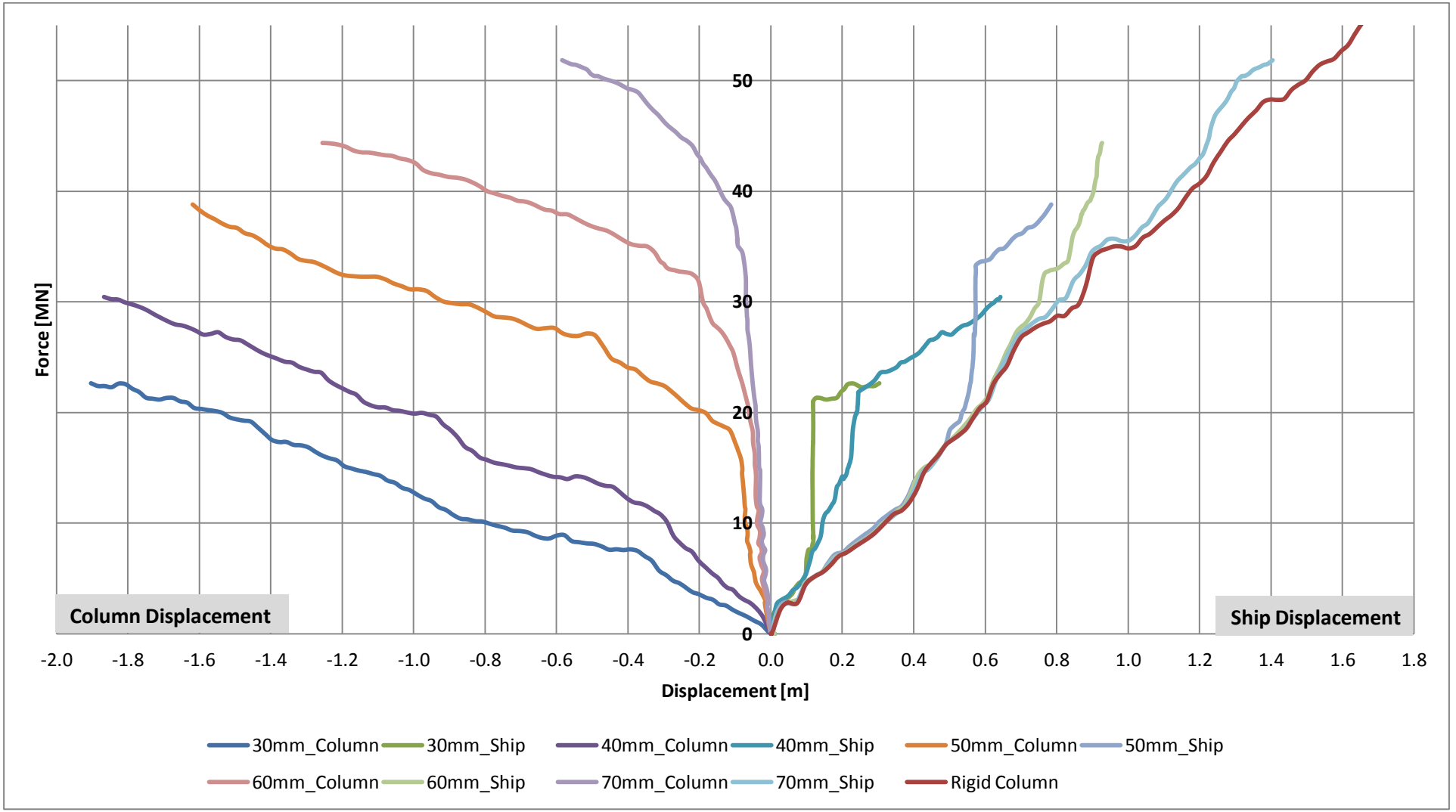

Figure 7-6 – Force-Deformation Relationships – Diameter = 1.5 m

It is interesting to see that the increase of the column strength is not consistent with respect to the increase of the column thickness. The increase in thickness and strength for the different columns at 0.20 m and 0.40 m column deformation are presented in tables 7-2 and 7-3. The tables show that there is a significant increase of the column strength when the thickness is increased from 40 mm to 50 mm. However, the increase in strength is largest when the column deformations are small. This can also be seen from figure 7-6 where the curve representing the column with shell thickness 50 mm is significantly steeper in the initial part of the impact than the curves representing the 30 and 40 mm columns. This shows that a small increase in the structural configuration may have a significant effect on the strength of the structure.

Column Thickness [mm]	Thickness Increase [%]	Force [MN]	Strength Increase [%]
30	-	3.58	-
40	133.33	6.62	84.92
50	125.00	20.21	205.29
60	120.00	31.88	57.74
70	116.67	43.37	36.04

Table 7-2 – Column Strength increase – 0.2 m Deformation

Column Thickness [mm]	Thickness Increase [%]	Force [MN]	Strength Increase [%]
30	-	3.58	-
40	133.33	6.62	60.81
50	125.00	20.21	96.09
60	120.00	31.88	46.52
70	116.67	43.37	39.86

Table 7-3 – Column Strength increase – 0.4 m Deformation

The large increase in strength as the thickness is increased from 40 mm to 50 mm is mostly a consequence of the increasing resistance against local indentation of the column. This is illustrated in figure 7-7 which shows the 40 mm and 50 mm columns at the moment where the impact force is 10 MN. At this moment, nearly all the column deformation is due to local indentation. The local indentation of the 40 mm column is quite large compared to the 50 mm column. The resistance against local indentation for the columns is discussed in detail in section 7.4.1.

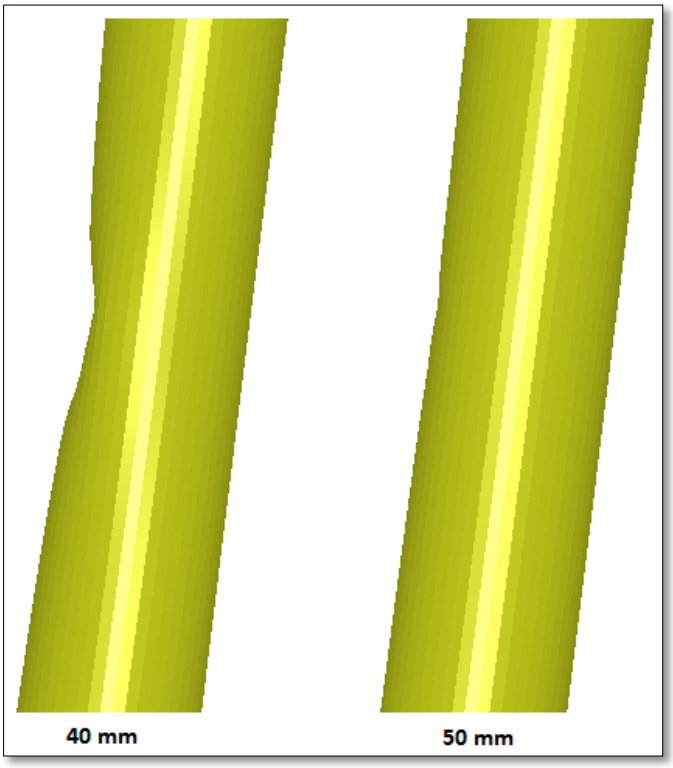

Figure 7-7 – Local Indentation at 10 MN Impact Force

From figure 7-6 it can be seen that the force-deformation curves for the different columns flattens out when the impact force reaches a certain level. This may be explained if one considers how the column deforms with respect to local deformation and global deformation. In figure 7-8 and 7-9, the global and local column deformation for the 40 mm and 50 mm columns are plotted against the impact force.

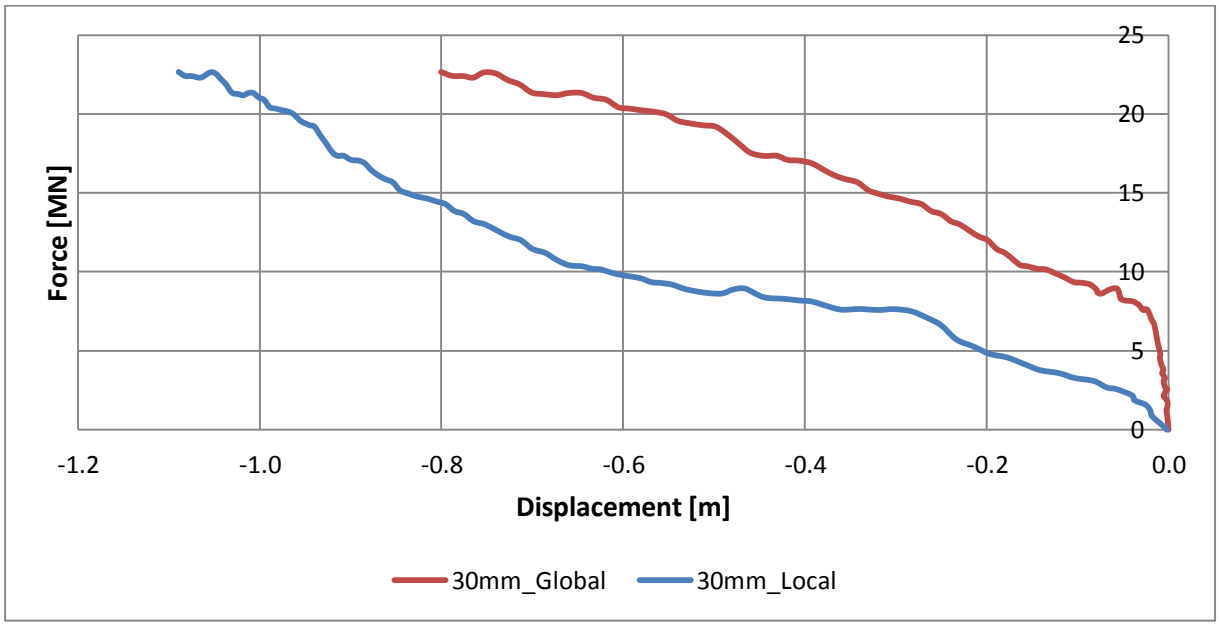

Figure 7-8 – Global and Local Deformation, 30mm Column

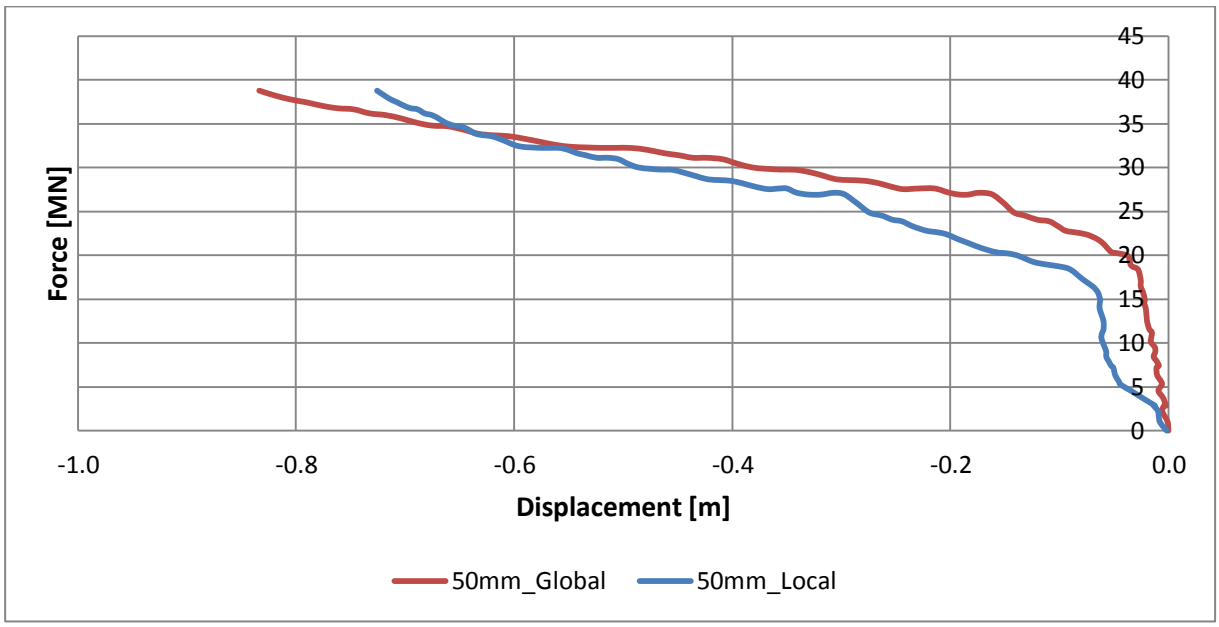

Figure 7-9 – Global and Local Deformation, 50mm Column

The figures show that the column behaviour may be separated into two phases:

1. In the initial phase of the impact scenario, the contact area is small and the total deformation of the column is governed by the local indentation of the column. If the resistance against local indentation is large, the force-deformation curve will be steep in the initial phase.

2. As the impact develops, the column reaches its plastic buckling capacity and starts to deform globally. The local indentation in phase 1 weakens the capacity of the column since the local indentation point will acts as a hinge. Thus, the total deformation increases and the force-deformation curve flatten out.

The maximum deformation of the ship and column at 30 mm and 70 mm column wall-thickness are presented in figure 7-10 and 7-11. The figure illustrates that the strength of the column is greatly dependent on the shell thickness, and that the column goes from being very weak compared to the ship to very strong as the thickness is increased from 30 mm to 70 mm. The ship is given a prescribed displacement of 2 m so the structural deformation is elements which displace less than 2 m.

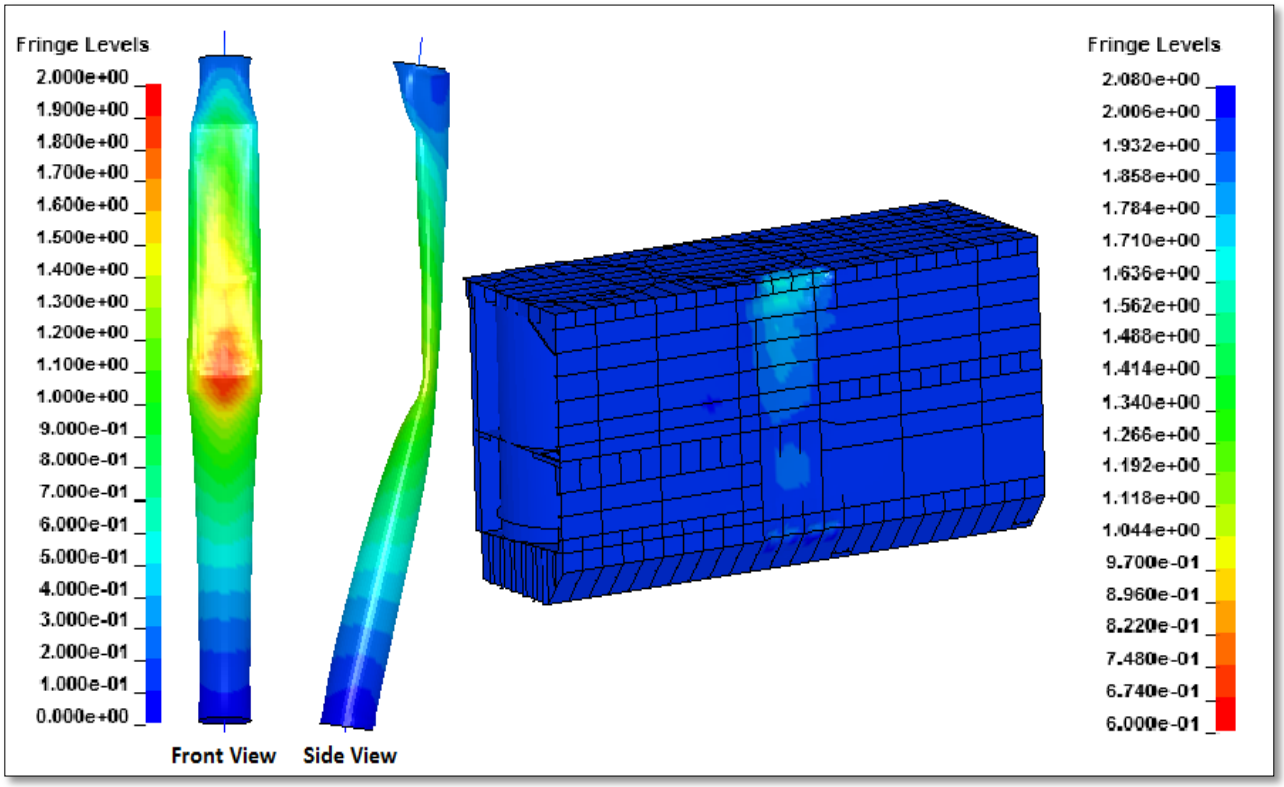

Figure 7-10 – Maximum Deformations - 30 mm Column

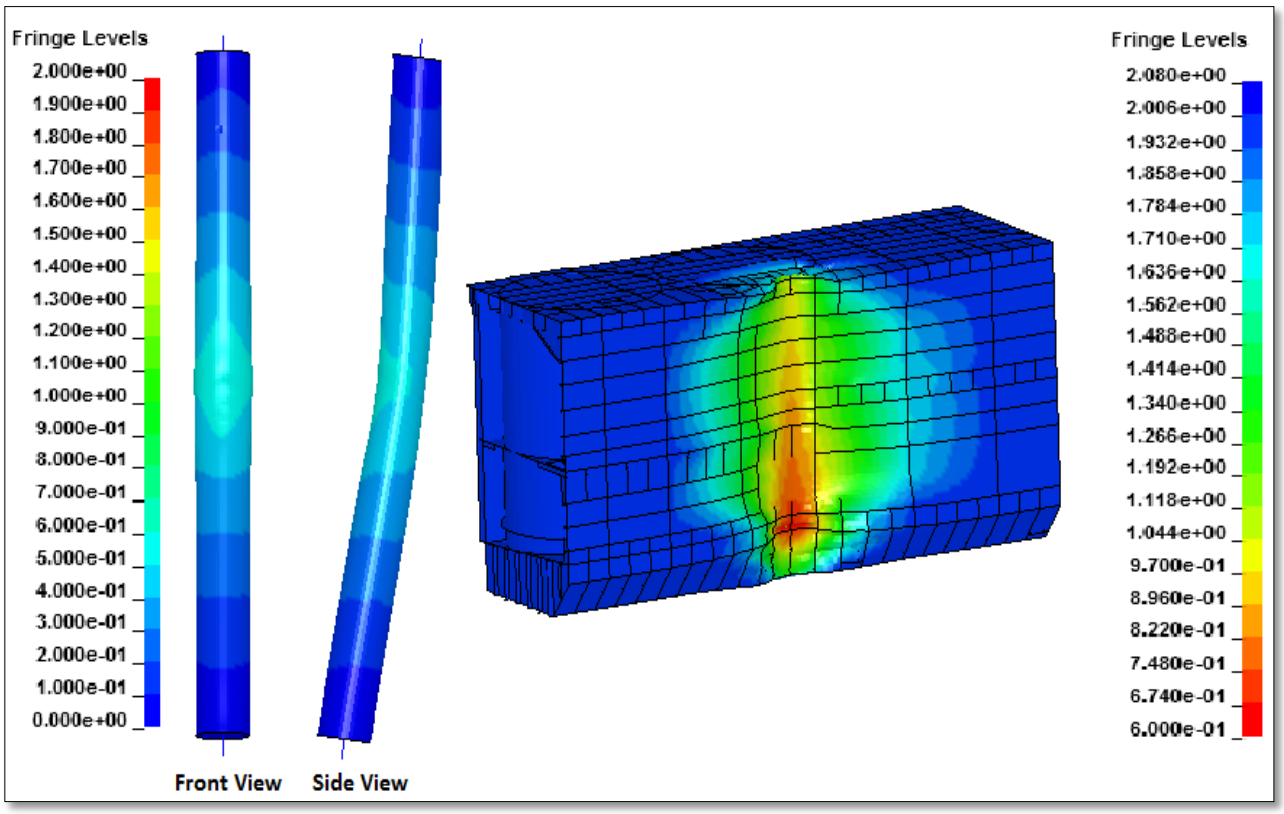

Figure 7-11 – Maximum Deformations - 70 mm Column

7.2.2 Column Diameter Variation

In this section, the effects of varying column diameter are considered. The comparison of the column diameters are presented in figures 7-12 – 7-15 where the column thickness is held constant in each figure. Force-deformation relationships with constant column diameter = 1.0 m and 2.0 m are presented in appendix A.2 and A.3, respectively.

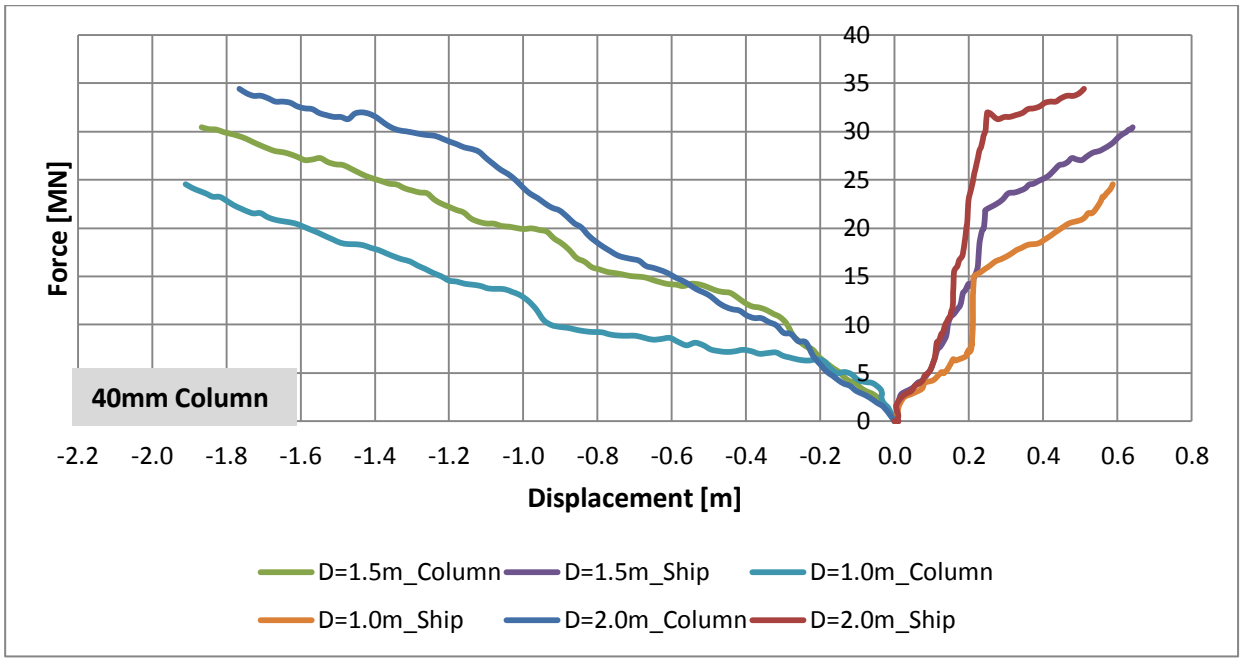

Figure 7-12 – Force-Deformation Relationships – Constant Column Thickness = 40 mm

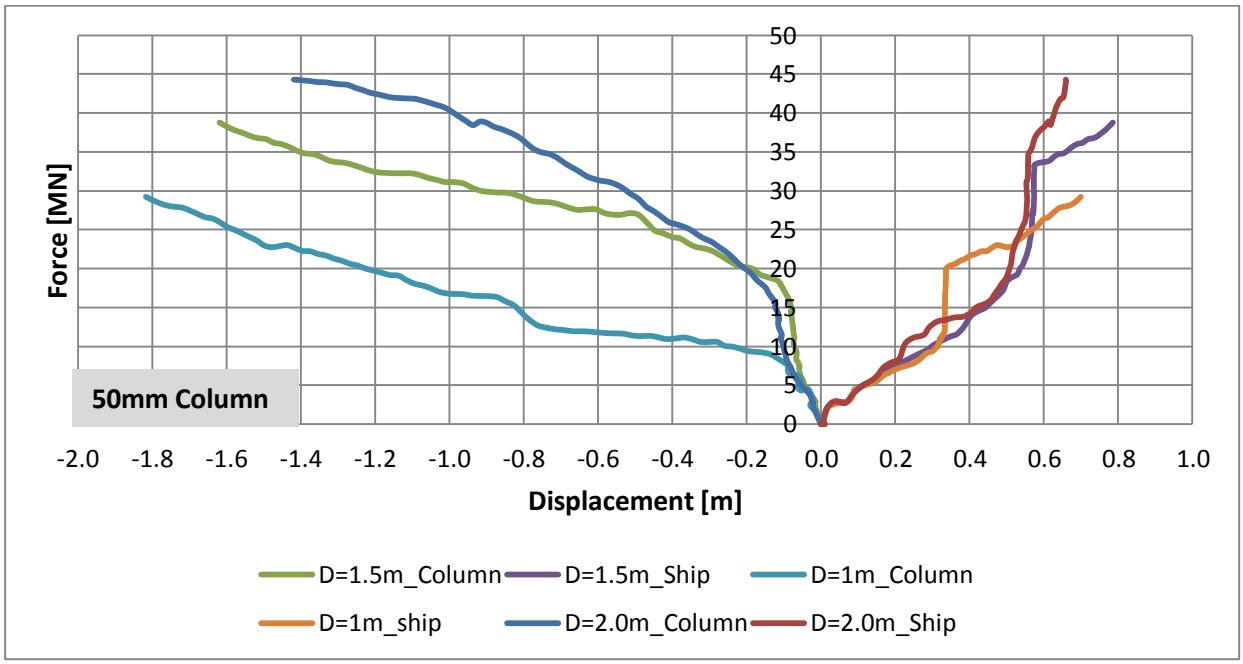

Figure 7-13 – Force-Deformation Relationships – Constant Column Thickness = 50 mm

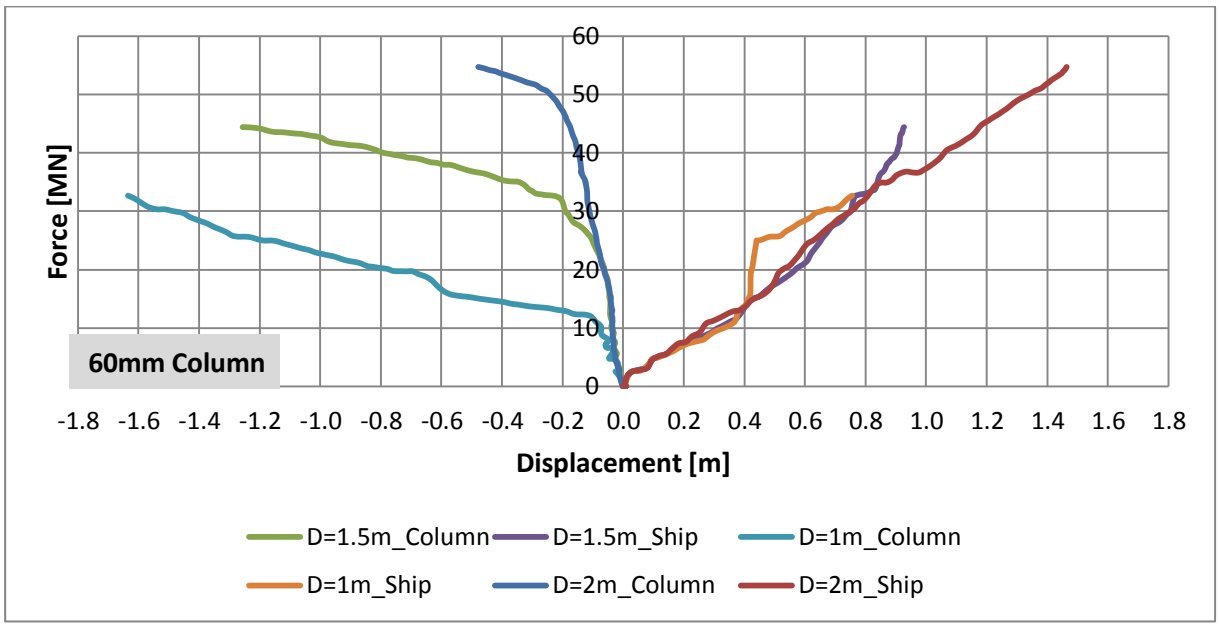

Figure 7-14– Force-Deformation Relationships – Constant Column Thickness = 60 mm

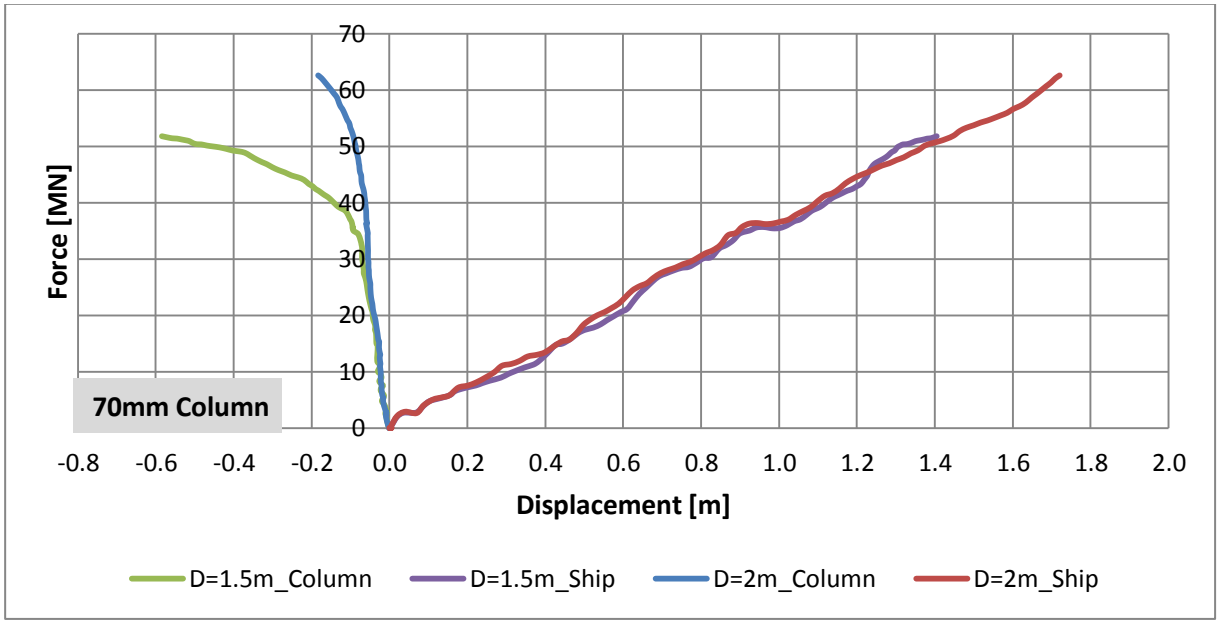

Figure 7-15– Force-Deformation Relationships – Constant Column Thickness = 70 mm

The figures show that the strength of the column increases when the column diameter increases. The increase in strength is due to several factors:

- Increasing elastic section modulus, W.
  This will in turn reduce the bending stresses in the column according to equation 7-2:

$$\sigma_b = \frac{M}{W} \qquad \text{Eq. 7-2}$$

- Increasing plastic section modulus, W_p.
  This will increase the plastic moment capacity (see equation 3-6).

- Increasing contact area.
  The increasing column diameter will increase the contact area. Hence, a larger impact force is required to produce the same contact pressure.

The results show that from a pure impact-performance point of view, a larger diameter column is best. However, the figures do not give a complete understanding of the impacts. The column deformation in the figures is the total deformation. It is also of interest to see how the total deformation is divided between global and local column deformation. Figure 7-16 and 7-17 present respectively the global and local deformation of the 40 mm column case. The deformation is normalised against the column diameter. This gives a better understanding of how large the global/local deformation is compared to the cross-sections of the columns. Plots for the rest of the column configurations are included in appendix B.

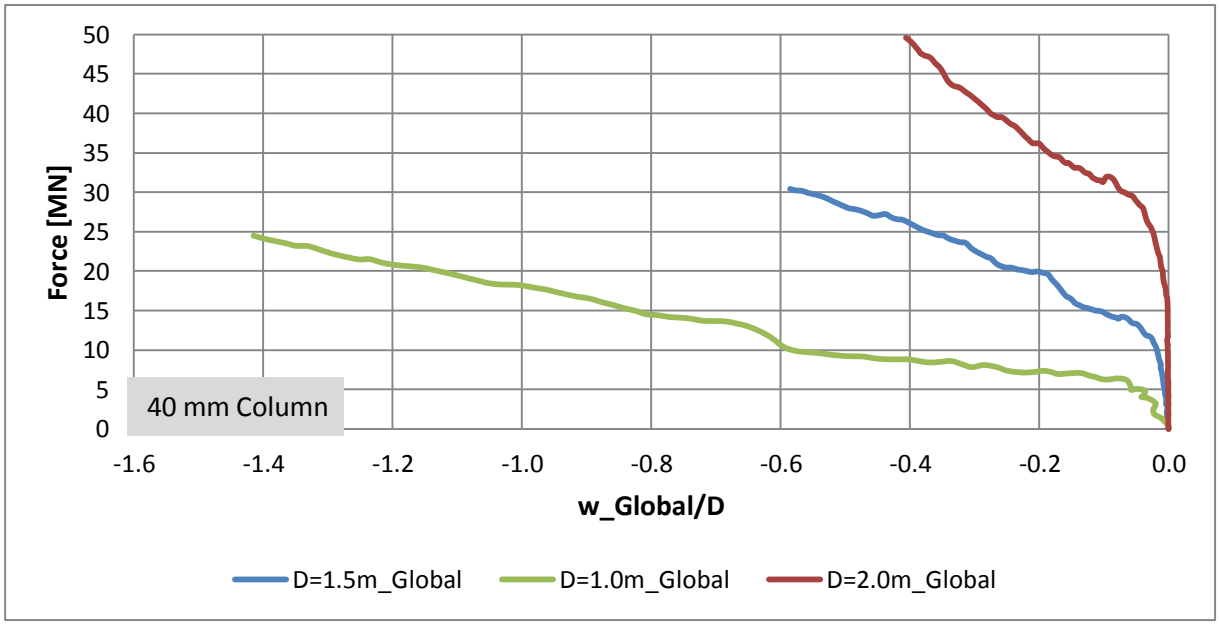

Figure 7-16 – Global Column Deformation – 40 mm Column

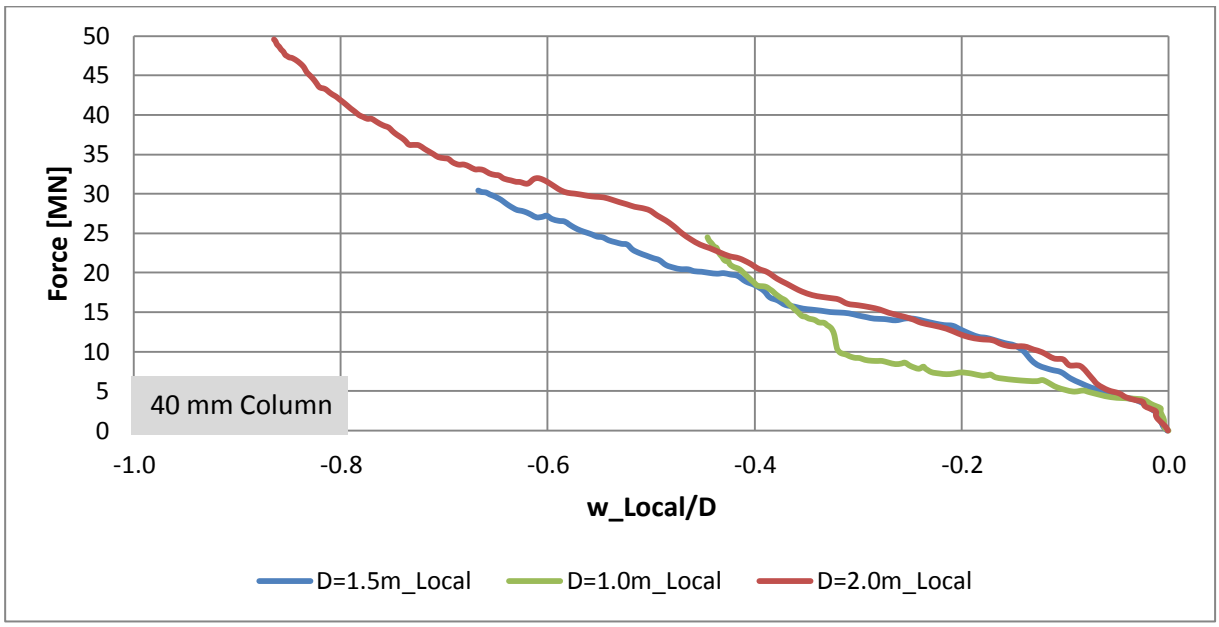

Figure 7-17 – Local Column Deformation – 40 mm Column

The figures show that the column with diameter 1.0 m is governed more by global than local deformation and that this is reversed as the column diameter is increased from 1.0 m to 2.0 m. This shows that the force-deformation relationship alone is not enough to understand the true behaviour of the impact. Local indentation of the platform-leg will significantly reduce the capacity of the dented leg. Thus, this may be of importance with respect to global analysis of the damaged platform. Also, the columns that are governed by local indentation may be more vulnerable for rupture of the column shell which will weaken the capacity even further. Considerations such as production costs may also be decisive in a design process, but this is not considered in this thesis.

7.3 Energy Dissipation & Design Categories

7.3.1 Diameter = 1.5 m

The Energy dissipation for the 30 mm and 70 mm columns is presented in figure 7-18 and 7-19, respectively.

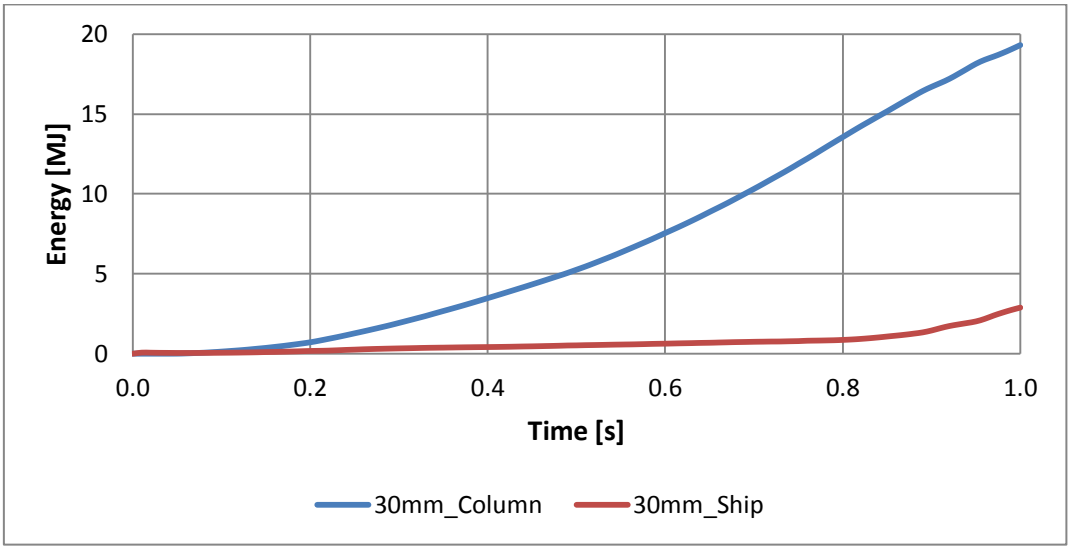

Figure 7-18 – Energy Dissipation – D=1.5 m – 30 mm Column

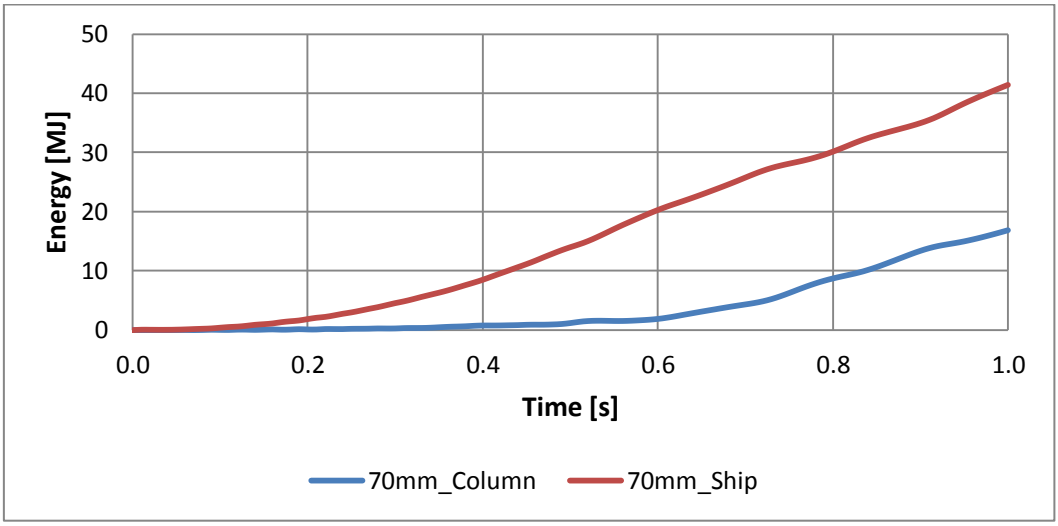

Figure 7-19 – Energy Dissipation – D=1.5 m – 70 mm Column

The total available strain energy for beam impacts was estimated to 19.26 MJ. For the 30 mm case, the impact energy is dissipated when the time is about 0.93 s. At this moment, the column has dissipated more than 90% of the impact energy while the ship dissipates about 9% of the impact energy. Thus, the column design is close to ductile design in this case. The impact force at this moment is 21.86 MN. The resulting maximum deformation of the ship and column can then be found by considering the force-deformation relationship at this force. The maximum deformation of the ship side is found to be 0.20 m, while the column deformation is 1.77 m.

For the 70 mm column case, the total available impact energy is dissipated when the time is about 0.56 s. At this moment, the column and ship dissipates about 8% and 92 % of the impact energy, respectively. The column design in this case is therefore close to the strength design category. The impact force at this moment is 35.54 MN. The maximum deformation of the column is found to be 0.09 m, and the maximum deformation of the ship is 1 m.

The impact force, energy dissipation and maximum deformation of the column and ship at the moment where the total strain energy is dissipated are presented in table 7-4 for the different column configurations. The table shows that the remaining columns may be categorised as within the shared-energy region.

Column Thickness	Impact Force [MN]	Energy Dissipation - Column [%]	Energy Dissipation - Ship [%]	Column Deformation [m]	Ship Deformation [m]
30 mm	21.86	91	9	1.77	0.20
40 mm	24.88	72	28	1.38	0.39
50 mm	29.06	49	51	0.80	0.57
60 mm	35.02	29	71	0.35	0.84
70 mm	35.54	8	92	0.09	1.00

Table 7-4 – Energy Dissipation – Column Diameter = 1.5 m

7.3.2 Diameter = 1.0 m

Table 7-5 shows that the 40 mm column configuration is close to ductile design, while the other column configurations are classified as within the shared-energy region. It is interesting to see that the column dissipates the same percentage of the total strain energy for both the 50 mm and 60 mm case.

Compared to the case with column diameter = 1.5 m, the columns with diameter 1.0 m dissipates a larger percentage of the total available strain energy. The difference is especially large for the 60 mm column which dissipated only 29 % of the impact energy when the column diameter was 1.5 m.

Column Thickness	Impact Force [MN]	Energy Dissipation - Column [%]	Energy Dissipation - Ship [%]	Column Deformation [m]	Ship Deformation [m]
40 mm	22.34	91	9	1.78	0.55
50 mm	22.76	67	33	1.48	0.50
60 mm	24.49	67	33	1.12	0.44

Table 7-5 – Energy Dissipation – Column Diameter = 1.0 m

7.3.3 Diameter = 2.0 m

Table 7-6 shows that the column is closed to strength designed for both 60 mm and 70 mm columns, while the 40 mm and 50 mm columns are within the shared-energy region.

All the column configurations, except the 40 mm case, show a reduction in energy dissipation compared to the case with column diameter 1.5 m. The 40 mm case dissipates 11% more of the impact energy in this case. The 60 mm thickness case shows a significant reduction in the energy dissipation (from 29% for the column with diameter =1.5 m to 10% in this case) and is now close to strength designed while it was classified as within the shared energy region when the column diameter was 1.5 m.

Column Thickness	Impact Force [MN]	Energy Dissipation - Column [%]	Energy Dissipation - Ship [%]	Column Deformation [m]	Ship Deformation [m]
40 mm	29.62	83	17	1.26	0.24
50 mm	33.58	43	57	0.69	0.56
60 mm	36.65	10	90	0.14	0.96
70 mm	36.93	4	96	0.06	1.02

Table 7-6 – Energy Dissipation – Column Diameter = 2.0 m

7.4 Resistance against Local Indentation

7.4.1 General

The resistance to local indentation of the column is very important since local indentation reduces the capacity of the platform leg and therefore the platform. The local indentation is estimated using LS-PrePost and compared with the NORSOK recommended curves as described in section 3.4.

One of the factors which is included in the NORSOK curves is the width of the collision, b. When the impact is first initiated, the contact width is close to zero. However, more of the ship will come into contact with the column as the impact develops. The maximum contact width for the beam impacts was estimated to 6.82 m which is almost the height of the ship-model. Therefore, the results are compared to NORSOK curves with b = 0 m and b = 6.82 m. The maximum b/D ratios for the different columns are presented in table.7-7

Column Diameter [m]	b/D
1.5	4.55
1.0	6.82
2.0	3.41

Table 7-7 – Maximum b/D ratios

Only the results from the cases with column diameter = 1.5 m and 1.0 m will be discussed in this section. The discussion in section 7.4.2 is, due to similarity of the results, also valid for the columns with diameter = 2.0 m. The comparison between the FEA results for the 2.0 m case and the NORSOK curves is included in appendix C.1.

7.4.2 Diameter = 1.5 m

The FEA results and the NORSOK curves are presented in figure 7-20 for the columns with diameter = 1.5 m. A circle indicates approximately where the NORSOK b=6.82 curve is valid, i.e. where the column has maximum contact over the ship height. These points are based on observations of contact at the top of the ship using Ls-PrePost.

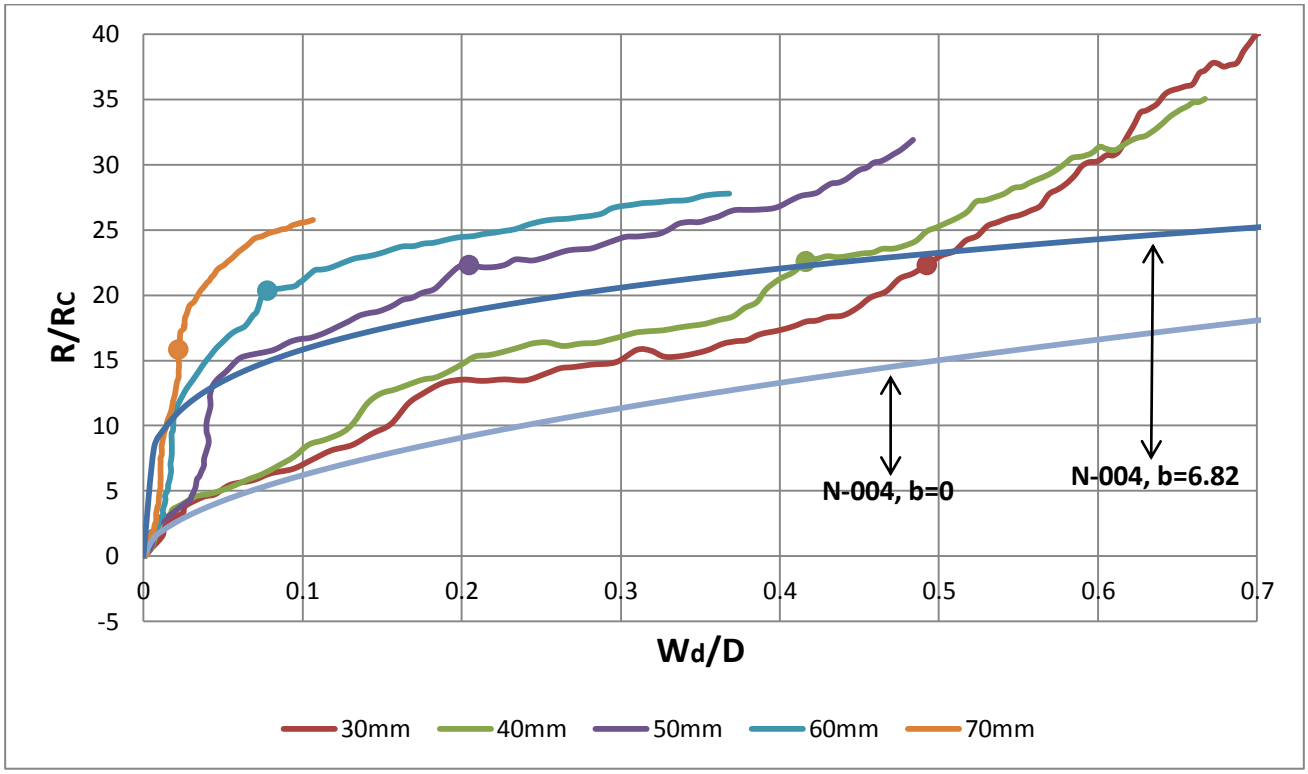

Figure 7-20 – Resistance to Local Indentation – Column Diameter = 1.5 m

The force-deformation relationships for the columns in figure 7-6 showed that the strength of the column increased significantly when the thickness was increased from 40 mm to 50 mm. The curves in figure 7-20 show the same tendency for the local indentation. Thus, the increase in strength of the column may be explained by the increasing resistance against local indentation.

The weakest columns in figure 7-20 follows the NORSOK b=0 curve quite good for small deformations. Then, the strength increases as a result of the increasing contact area. The point where the columns reach the maximum contact width also corresponds well with the NORSOK curves for these columns. However, it would be fairly conservative to use the NORSOK curves for strength prediction of the three strongest columns which show a significant increase in strength compared to both NORSOK curves. Also, the figure shows that the strength of the two weakest columns increases well beyond the "N-004, b=6.82" curve for large deformations. It is therefore seen that the NORSOK curves are quite inconsistent with respect to the strength prediction even though the FEA results are normalised.

To understand why the NORSOK curves are so inconsistent, one must consider how the NORSOK curves are developed. The NORSOK curves are based on the assumption of a perfectly rigid ship [10]. A cross-section of the 30 mm and 70 mm column cases, shown in figure 7-21, shows that the 30 mm case is quite close to the assumption of a rigid ship while the 70 mm column acts more like a rigid column. When the ship deforms, the impact force is

distributed around the column as shown in figure 7-22. Hence, as the column thickness is increased from 30 mm, the calculation model becomes less and less valid.

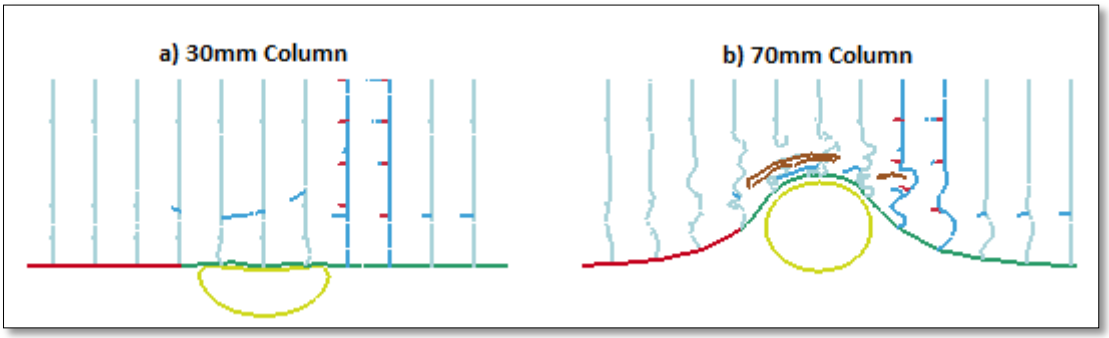

Figure 7-21 – Cross-Section of Local Indentation

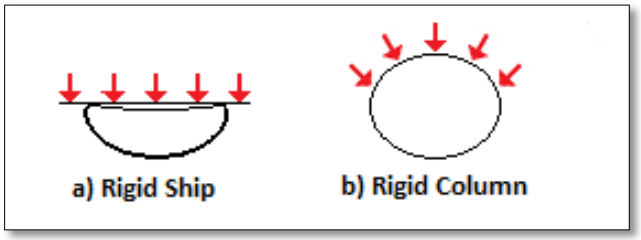

Figure 7-22 – Impact Force Distribution

In order to check that the discussion above is valid, the resistance to local indentation for the different column-configurations using a rigid ship is considered. Since the result are normalised, the curves are now expected to be similar for all column thicknesses. The results are presented in figure 7-23 and show that, for $w_d/D < 0.35$, the results are very similar. The circle that indicates when the maximum contact width is reached corresponds well with the NORSOK b=6.82 curve for all column configurations. However, the curves show some deviation from each other for $w_d/D > 0.35$ and the strength of all column configurations increases well beyond the NORSOK b=6.82 curve for all curves.

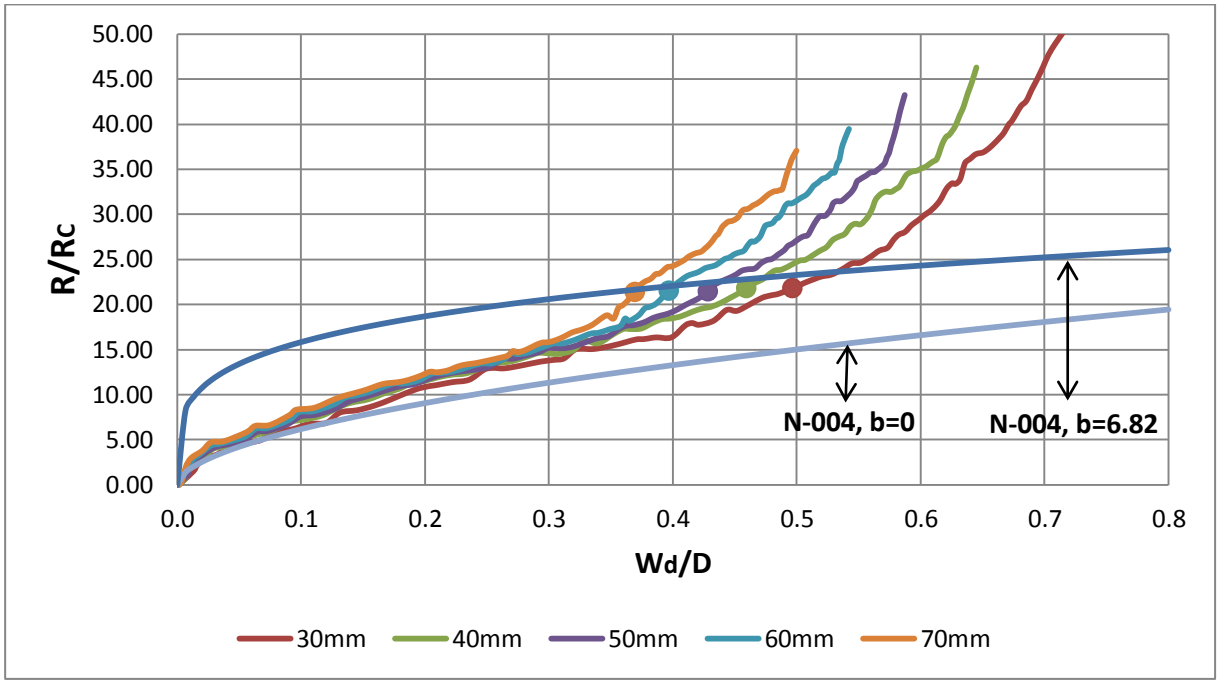

Figure 7-23 – Resistance to Local Indentation – Rigid Ship – Column Diameter = 1.5 m

The increase in strength above the NORSOK b=6.82-curve is a consequence of several factors:

- *Increasing contact area.*
  Most of the contact area develops until the column reaches its maximum contact width. However, the contact area still increases a little after this point leading to a further increase in the resistance. The contact area for the 30 mm case is presented in figure 7-24. The time when the column reaches its maximum contact width is about 0.54 s. The figure shows that the contact area continues to increase after this point.

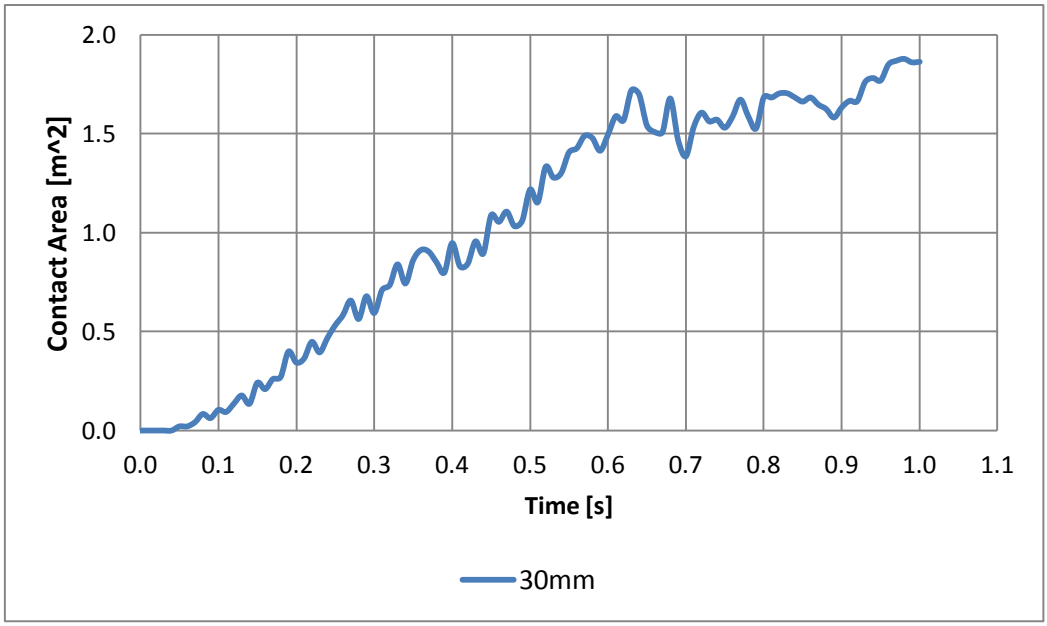

Figure 7-24 – Contact Area – 30 mm Column – Rigid Ship

- *Increasing tension forces in the column.*
  When the column deforms, membrane forces will develop that will increase the resistance against local indentation. A plot of the membrane forces in the column can be seen in figure 6-5 for the 30 mm column. The membrane forces are small until the impact time is about 0.5 s. After this, the forces increase leading to an increase of the resistance against local indentation towards to end of the impact scenario.

- *Strain hardening effects.*
  A plot of the stress-strain relationship measured at a node in the dented region shows that the columns experience some strain-hardening. The stress-strain relationship is presented in figure 7-25. The stress is the Von-Mises stress and the strain is an effective strain as defined in equation 7-3 [14]

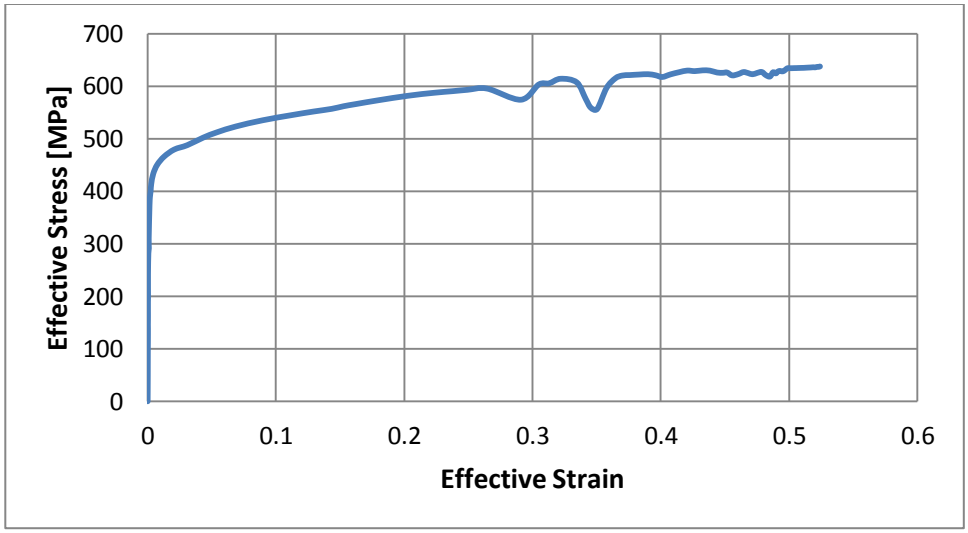

Figure 7-25 – Stress-Strain Relationship – Strain Hardening Effects

$$\varepsilon^{effective} = \sqrt{\frac{2}{3}\varepsilon_{ij}\varepsilon_{ij}} \qquad \text{Eq. 7-3}$$

where ε_{ij} is the engineering strain-tensor components.

7.4.3 Diameter = 1.0 m

The FEA results from the analyses where the column diameter = 1.0 m are compared with the NORSOK curves in figure 7-26. The circles in the graphs indicate approximately where the NORSOK b=6.82 m curve is valid, i.e. where the column has maximum contact over the ship height.

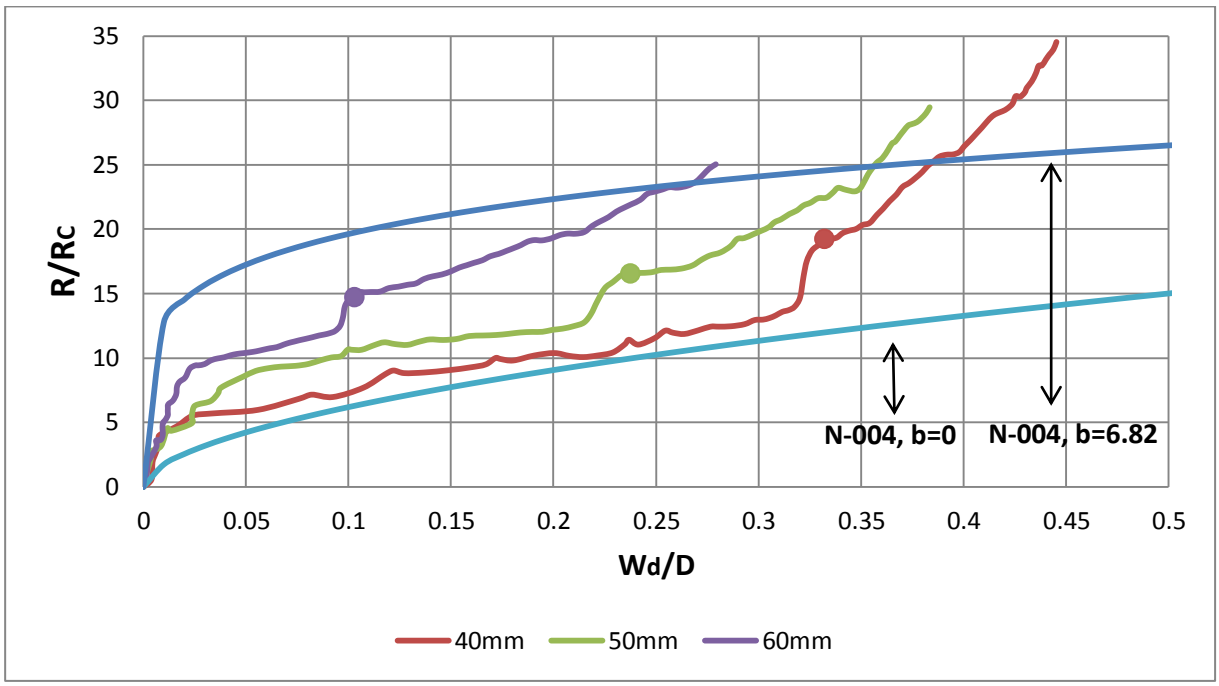

Figure 7-26 – Resistance to Local Indentation – Diameter = 1.0 m

The results show that the strength increases more steadily with increasing column--thickness than what was the case for the columns with diameter =1.5 m.

The NORSOK curve with b = 0 m gives a good representation of the initial phase for the weakest column. However, at the point where the curves indicate that the NORSOK b=6.82 m curve should be valid, the actual strength is quite low compared to NORSOK. Hence, NORSOK is quite un-conservative in this case.

7.4.4 Design Curve for Ductile Design

The curves provided by NORSOK assume that the contact-width/column-diameter ratio (b/D-ratio) is constant. However, the b/D ratio will not be constant throughout the impact scenario. This behaviour leads to a problem when applying the NORSOK curves: Which b/D ratio should be used? If the b/D ratio is assumed to be small throughout the impact scenario, the resistance estimated by NORSOK may be very conservative. However, if the b/D ratio is assumed to be large, the resistance estimated by NORSOK may be un-conservative.

In this section, an empirical design curve that takes into account the increasing contact width is proposed. The design curve is intended for structures that may be classified as ductile designed. The results in the previous chapters show that the strength of columns that may not be classified as ductile designed is very hard to predict. Hence, nonlinear finite element analyses are recommended in such cases. However, the design curve may be used as a conservative lower estimate of the resistance against local indentation.

The design curve is assumed to follow the curve of the 30 mm case in figure 7-23, where the ship is considered perfectly rigid, until the curve intersects with the NORSOK curve which

assumes maximum contact-width (maximum b/D-ratio). The increase in strength above the NORSOK curve is therefore neglected in order to be conservative.

The design curve is given by equation 7-4 until the intersection point. Then, the design curve follows the NORSOK curve as shown in figure 7-27.

$$396.05\left(\frac{B}{D}\right)^4 - 253.99\left(\frac{B}{D}\right)^3 - 9.2047\left(\frac{B}{D}\right)^2 + 60.258\frac{B}{D} + 0.6033 \qquad \text{Eq. 7-4}$$

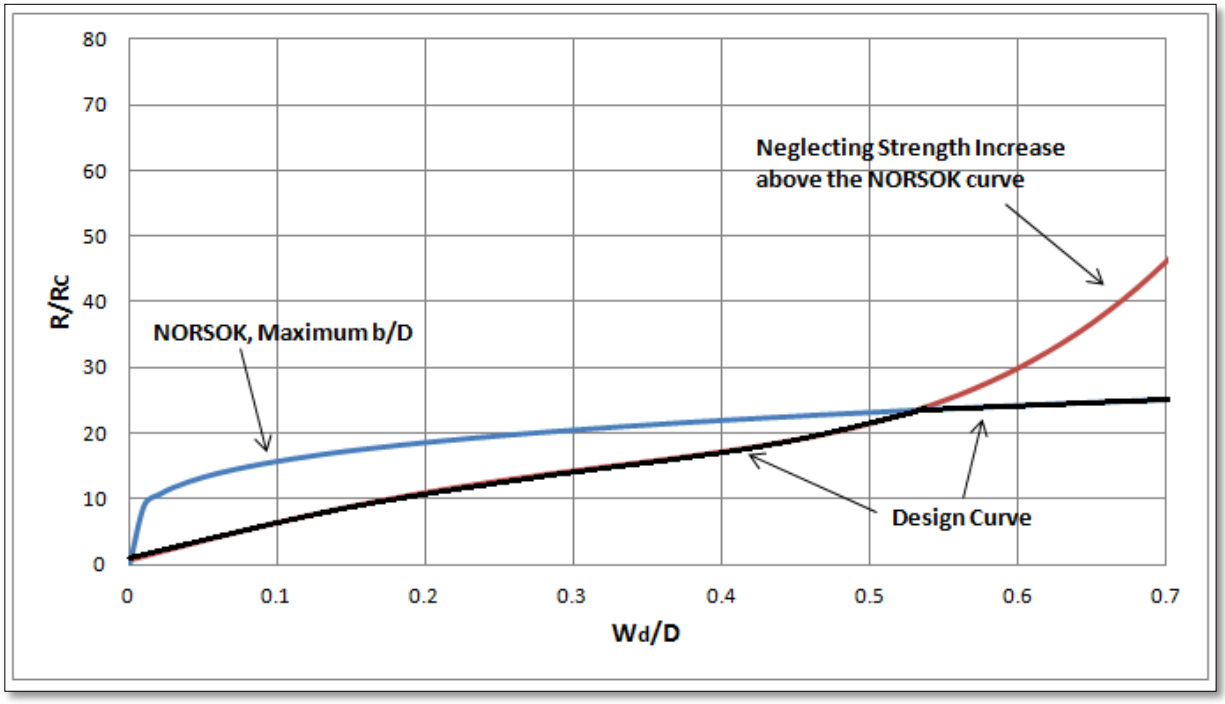

Figure 7-27 – Design curve for Ductile Design

The design curve is compared against the integrated analyses using column diameter =1.5 m in figure 7-28. Since the design curve represents ductile design, only the two weakest columns are considered. The figure shows that the design curve gives a good representation of the resistance against local indentation for these columns. The comparison between the design curve and the FEA results from the integrated analyses using column diameter = 1.0 m and 2.0 m is included in appendix C.2 The design curve gives a good representation of the strength of the weakest columns in these cases as well.

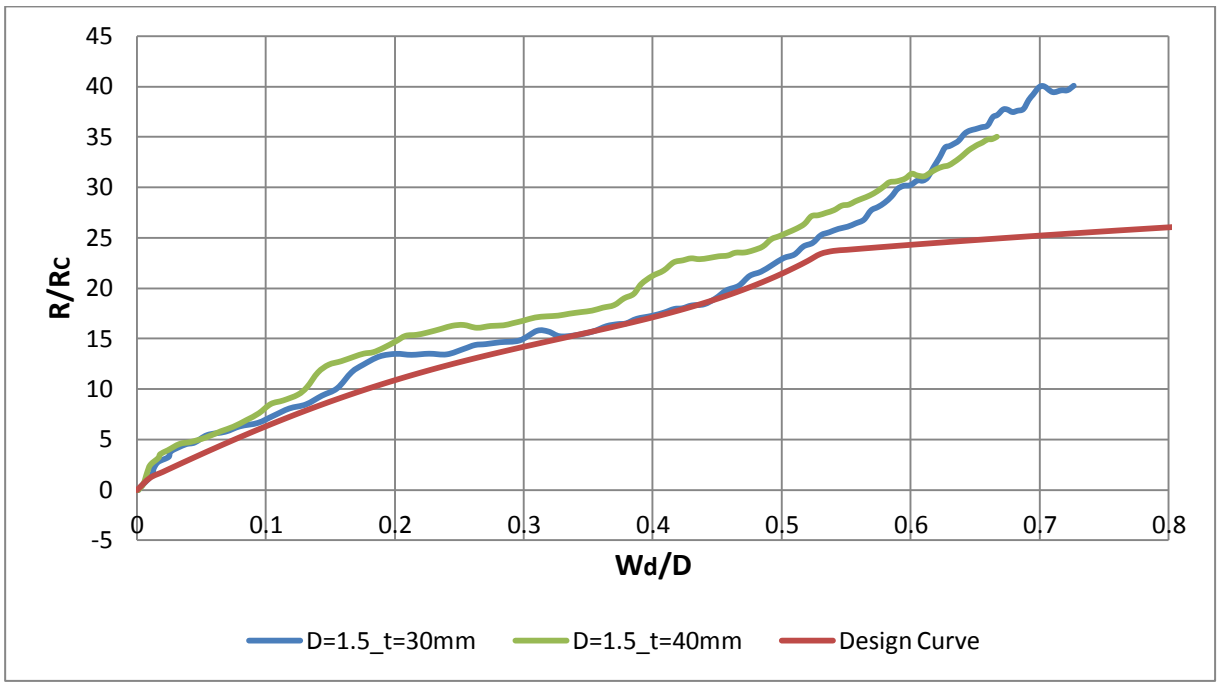

Figure 7-28 – Comparison with Design Curve – Column Diameter =1.5 m – Beam Impact

7.5 Comparison with Simple Calculations

In this section, the FEA results are compared against the ideal rigid plastic behaviour that takes into account the increase in strength due to the development of membrane forces during large column deformations. The ideal non-dimensional force-deformation equations were derived in section 3.3 for a point loaded clamped beam with a cylindrical cross-section.

The calculation procedure in section 3.3 assumes that the beam is not subjected to any local damage, i.e. all the beam deformation is global deformation. Thus, in order to compare the FEA results with the calculated force-deformation relationship, only the global deformation of the column is considered.

The comparison between the FEA results and the theoretical model is presented in figure 7-29 for the columns with diameter 1.5 m. The results for the other two column-diameters are included in appendix D.1.

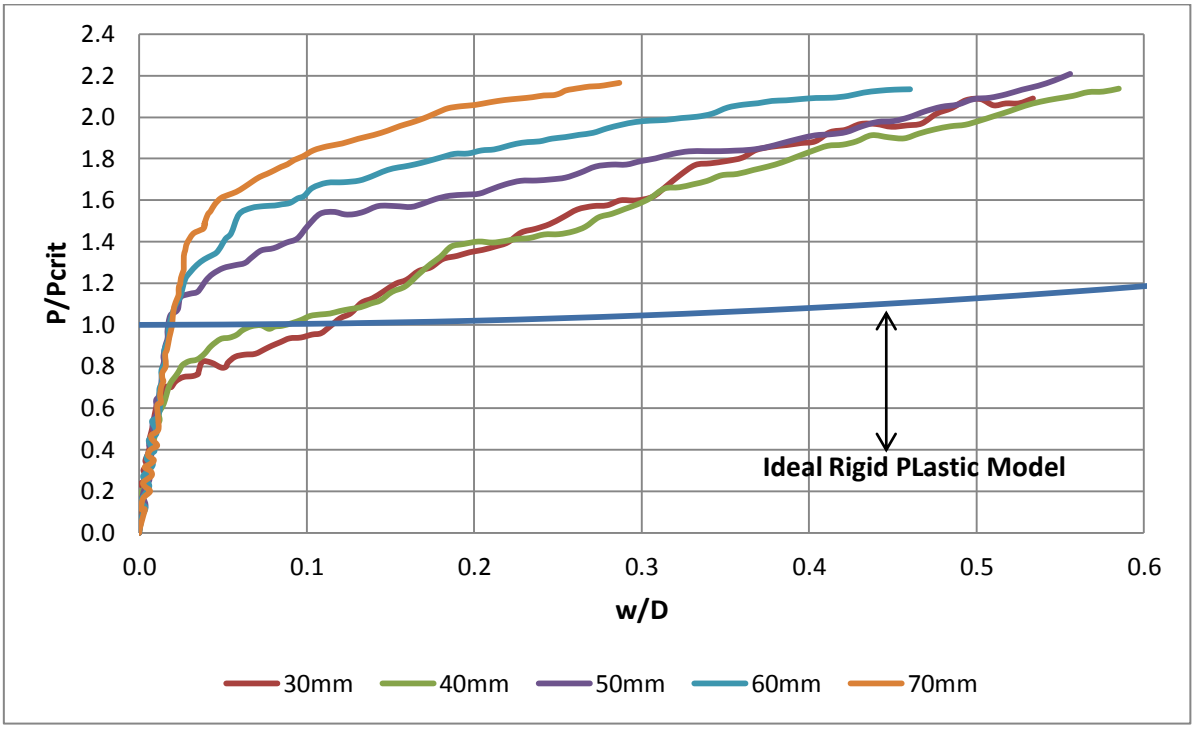

Figure 7-29 – FEA Results vs. Point Loaded Model – Column Diameter = 1.5 m

The results show that the simple calculation model presented in section 3.3 is not a good basis for comparison in this case. This statement is based on two key-observations:

1. The plastic buckling capacity of the three strongest columns is quite large compared to the ideal model (about 40% larger for the 70 mm column).

2. All the column configurations show a significant increase in post-buckling strength compared to the calculation model.

Thus, the point-load calculation model is quite conservative compared to the FEA results. The assumption of a point load at the middle of the column might be a reasonable assumption in the initial phases of the impact. However, as the impact develops, the contact area increases. Hence, the assumption of a point loaded beam becomes quite unrealistic. A remedy for this might be to consider a beam subjected to a distributed load when calculating the theoretical force-deformation relationship. The mechanism is assumed to be the same as in section 3.3, but the loading is now a distributed loading, q. The width of the distributed load is denoted "a".

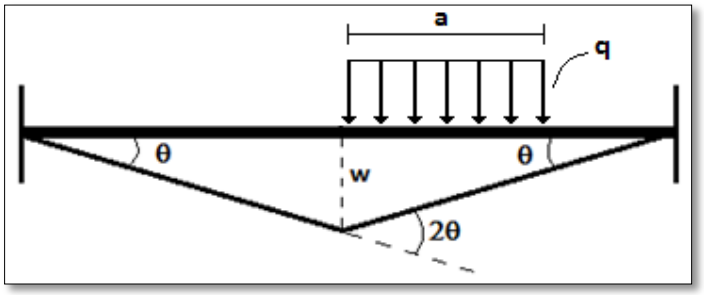

Figure 7-30 – Three Hinge Collapse Mechanism – Distributed Load

In order to find the new normalising force, the external work needs to be calculated:

$$E_{external} = \int q(x)w(x)\,dx \qquad \text{Eq. 7-5}$$

If the origin is defined to be at the middle of the beam with positive x-axis in the direction of the distributed load, the external work can be calculated as:

$$E_{external} = q\int_0^a w\left(1-\frac{2}{l}x\right)dx \qquad \text{Eq. 7-6}$$

$$E_{external} = qw\left[x-\frac{1}{l}x^2\right]_0^a \qquad \text{Eq. 7-7}$$

$$E_{external} = qwa\left(1-\frac{1}{l}a\right) = Pw\left(1-\frac{1}{l}a\right) \qquad \text{Eq. 7-8}$$

The normalised force-deformation relationship becomes the same as before, but with a new P_{crit}.

$$P_{crit} = 8\frac{M_p}{l}\left(1-\frac{1}{l}a\right)^{-1} \qquad \text{Eq. 7-9}$$

The maximum width of the impacts is approximately 6.82 m for the beam impacts. The load-width, "a", in equation 7-9 is therefore set to 6.82 m. The comparisons between the new idealised force-displacement relationship and the FEA results are shown in figures 7-31 – 7-33 for the columns with diameter 1.5 m, 1.0 m and 2.0 m, respectively.

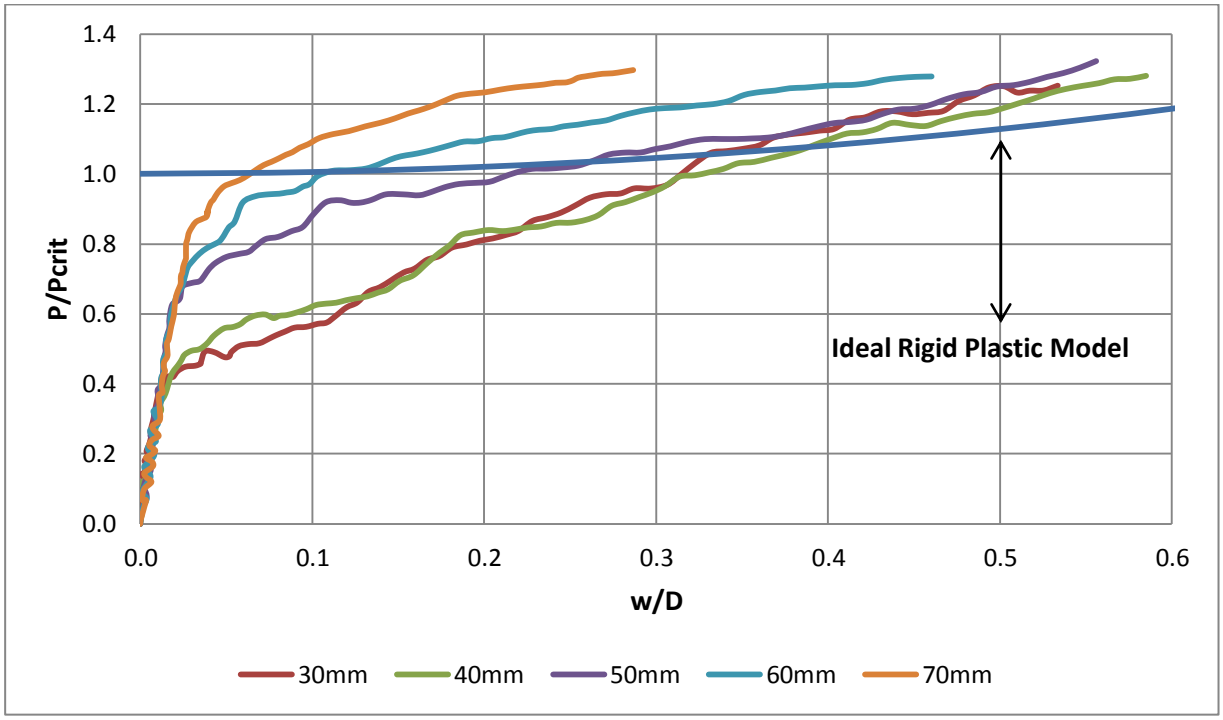

Figure 7-31 – FEA Results vs. Distributed Load Model – Column Diameter = 1.5 m

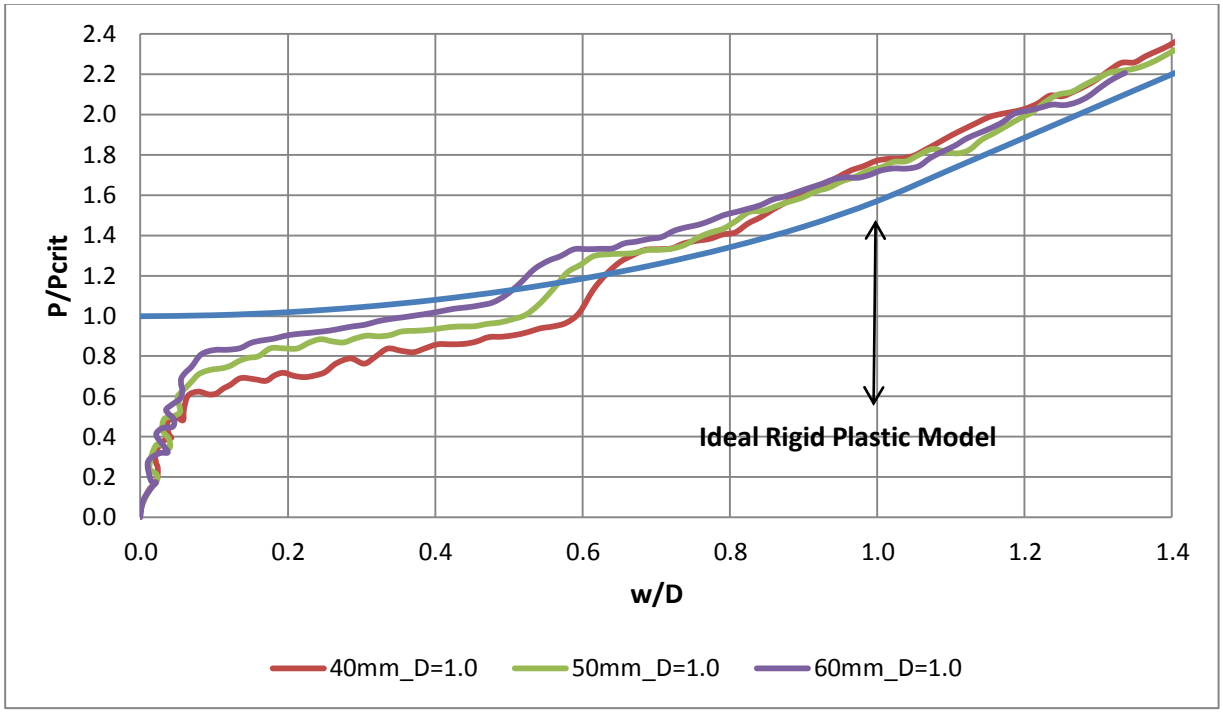

Figure 7-32 – FEA Results vs. Distributed Load Model – Column Diameter = 1.0 m

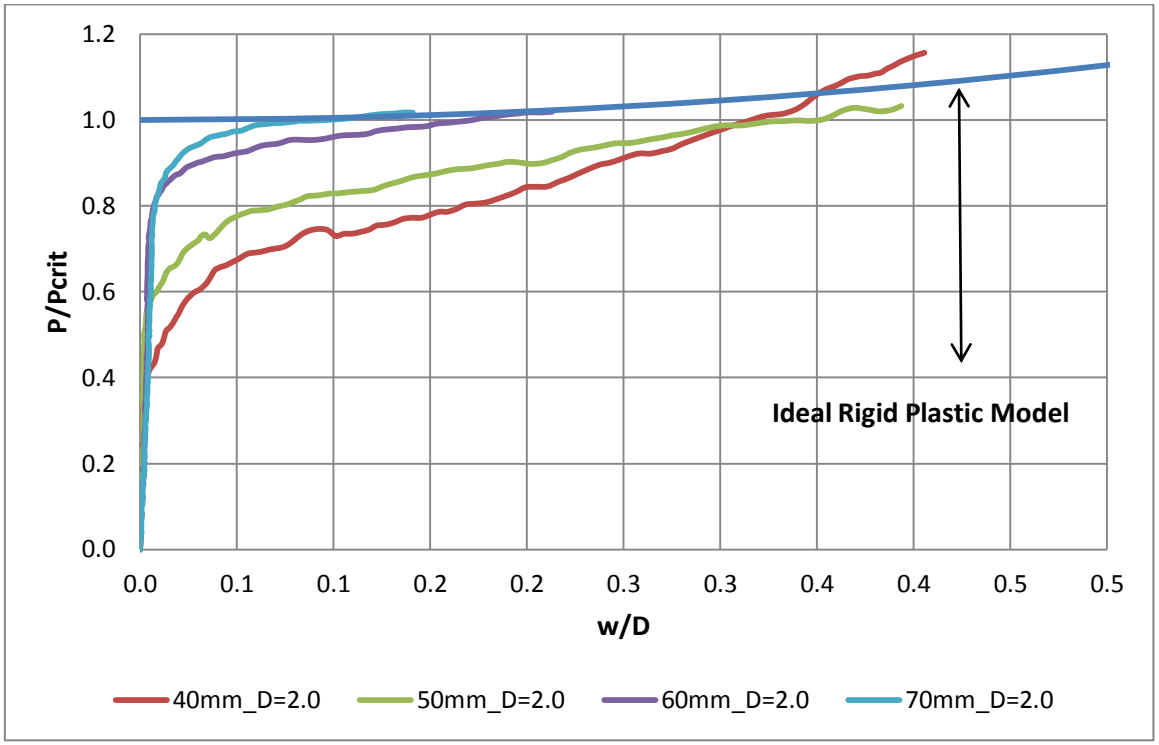

Figure 7-33 – FEA Results vs. Distributed Load Model – Column Diameter = 2.0 m

The results show that the plastic buckling capacity of the columns is very dependent on the severity of the local indentation of the columns. The weaker columns have large local indentations which reduces the buckling capacity compared to the stronger columns. For example: the 30 mm column in figure 7-31 is subjected to large local indentations and buckles at approximately 45 % of the ideal rigid plastic while the 70 mm column is subjected to small local indentations and buckles at approximately 87 % of the ideal load.

The results show that the distributed-load model is a much better model than the point-load model. However, there are still some remarks:

- The strongest columns in figure 7-31 and 7-33 are subjected to small local indentations and should therefore reach the plastic capacity as predicted by the calculation model.

- Some of the columns still show an increase in strength in the post-buckling range compared to the calculation model for large deformations.

- The calculation model assumes completely clamped boundary conditions. However, the columns have been analysed using axial flexible boundary conditions. Thus, the increase in strength for large deformations should be lower than what the calculation model predicts in its current configuration.
- The model assumes that the column is subjected to a distributed load throughout the impact scenario. A better model might be one that takes into account the gradual

increase in contact area.

- It would be quite un-conservative to use the estimations of the simplified model in an actual design process, especially for the columns which are subjected to large local indentations.

7.5.1 Model with Reduced Capacity

The ideal rigid model in the previous section does not take into account that the plastic moment capacity of the column will be reduced due to local indentations. This is why the buckling capacity of the weaker columns is low compared to the stronger columns. The reduction of the capacity may be taken into account according to figure 3-13. However, NORSOK does not provide any information of how large local dent that should be taken into account.

In order to suggest some design values that may be used, the $^{w_d}/_{D}$ value at the moment where the column starts to buckle has been estimated for each column-configuration. This is plotted against the $^{D}/_{t}$ ratio for the columns in figure 7-34. A linear relationship has been fitted to the points with equation:

$$^{w_d}/_{D} = 0.0072\,^{D}/_{t} - 0.1141 \qquad \text{Eq. 7-10}$$

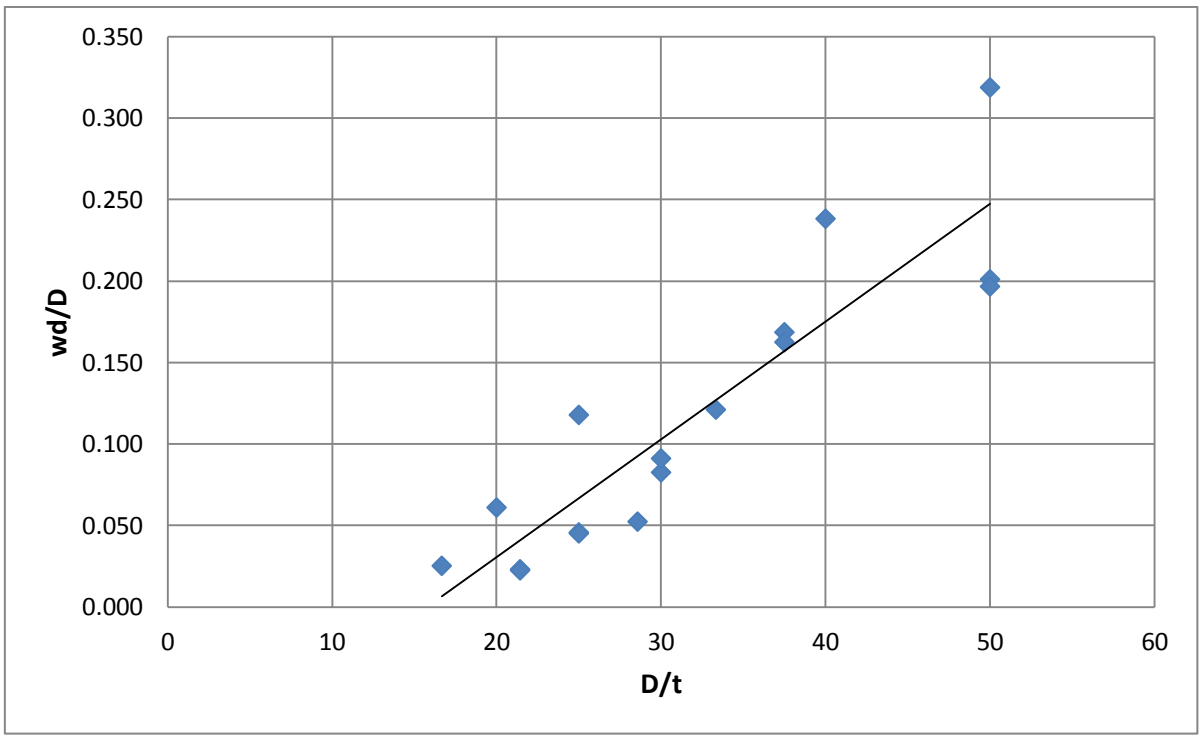

Figure 7-34 – Dent-size vs. D/t – ratio

The figure shows that the points are quite scattered for high $^{D}/_{t}$ ratios, but the linear relationship gives a good representation of the points for lower $^{D}/_{t}$ ratios. However, more analyses should be performed in order to verify the behaviour.

The reduced moment capacity for the different column-configurations has been calculated based on the points in figure 7-34 and equation 3-35 – 3-37 and are presented in table 7-8:

Diameter [m]	Thickness [m]	Mp [MNm]	Mp Reduced [MNm]
1.5m	0.03	23.02	11.35
	0.04	30.28	16.27
	0.05	37.33	25.48
	0.06	44.19	33.94
	0.07	50.86	42.63
1.0 m	0.04	13.09	8.08
	0.05	16.03	11.70
	0.06	18.85	15.65
2.0 m	0.04	54.56	19.60
	0.05	67.51	30.16
	0.06	80.19	49.02
	0.07	92.60	69.52

Table 7-8 – Reduced Moment Capacity

Since the model that assumes a distributed loading gave the best representation of the FEA results, this model is used in this section as well. Reduced ideal rigid collapse loads, Pcrit, have been calculated based on the reduced moment capacity in table 7-8.

The comparison between the FEA results and the theoretical model with reduced capacity is presented in figure 7-35 for the columns with diameter 1.5 m. The comparisons for the other two column-diameters are similar to the 1.5 m-case and are included in appendix D.2.

The comparison shows that the simplified model with reduced capacity gives a good representation of the plastic buckling capacity of the different columns. However, the model becomes too conservative in its representation of the behaviour in the post-buckling range.

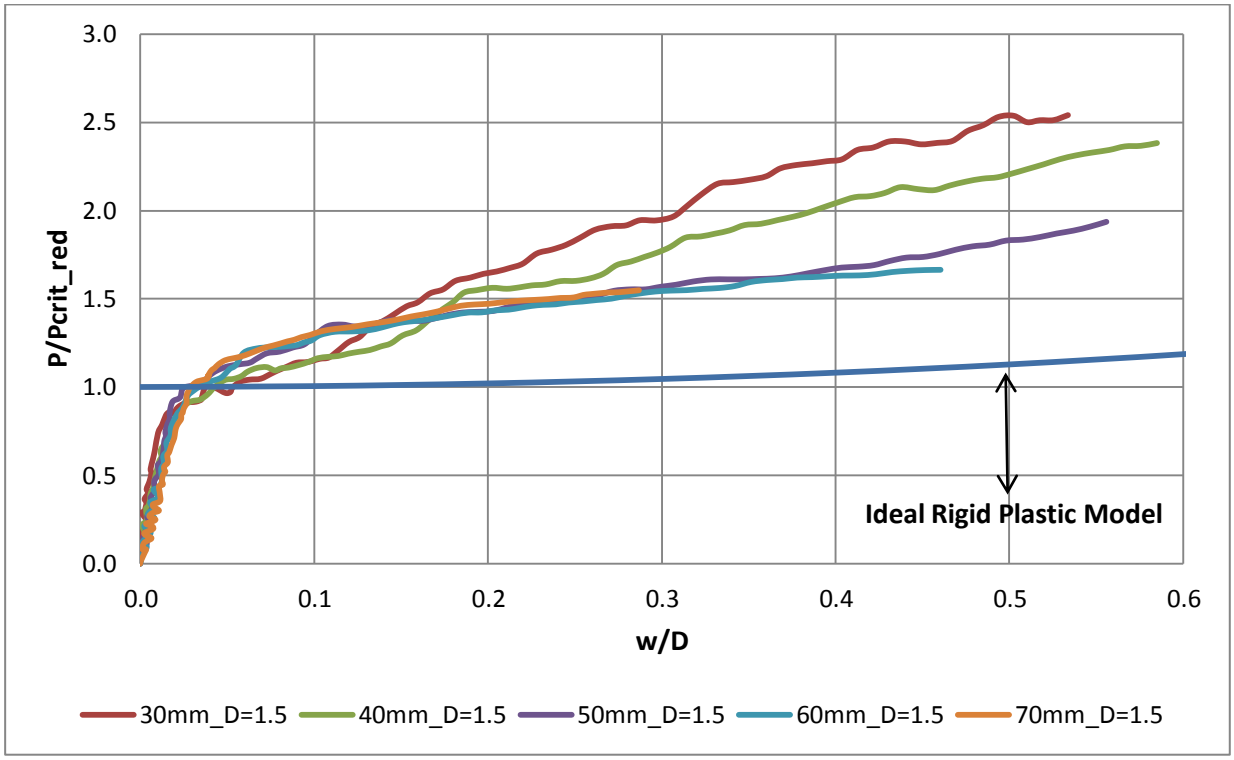

Figure 7-35 – Simplified Model with Reduced Capacity – Column Diameter = 1.5 m

8. Stern Impact – Results

8.1 General

In the previous chapters, beam impacts have been considered. However other impact scenarios may be more critical. In this chapter, stern impacts against the unstiffened column segment are considered.

The column diameter is held constant = 1.5 m for all analyses and the column thickness is varied from 30 mm to 70 mm.

8.1.1 Available Strain Energy

The total available strain energy for the stern impact may be calculated according to equation 2-4. The reference ship for the stern model is not known, so it is assumed that the ship's displacement is equal to that of the reference ship for the beam model.

$$E_s = \frac{1}{2}(m_s + a_s)v_s^2 = \frac{1}{2}(6.878 * 10^6(1 + 0.1)) * 2^2\ [J] = 15.13\ [MJ]$$

8.2 Force-Deformation Relationship

The force-deformation relationships for the different column-configurations are presented in figure 8-1. The column deformation is the total deformation as defined earlier. The discussion in section 7.2.1 regarding the behaviours of the force-deformation relationships in figure 7-6 is also valid for the force-deformation relationships in figure 8-1. The focus in this section will be on the differences between the stern and beam impact scenarios. .

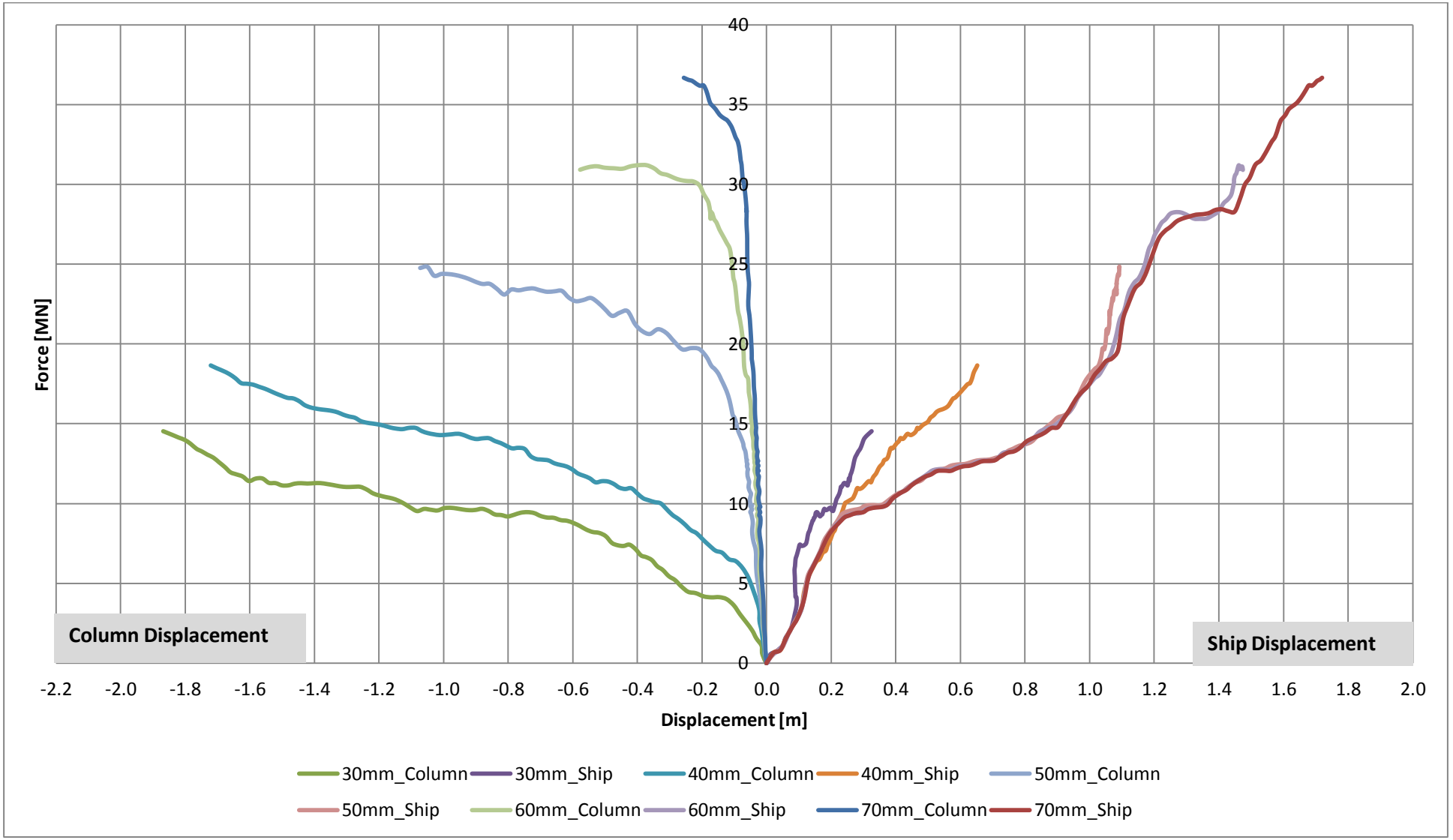

Figure 8-1 – Force Deformation Relationships – Stern Impact – Column diameter = 1.5 m

The results show that the strength of the column increases as the column thickness increases. It is interesting to see that, as was the case for the beam collisions, the column strength increases significantly when the column thickness is increased from 40 mm to 50 mm. However, other than this, the results are quite different compared to the beam collisions. Table 8-1 presents some column deformations and required impact force for beam and stern impacts. Table 8-2 presents the same for the ship-side.

Column Thickness [mm]	Column Deformation [m]	Impact Force – Beam Collision [MN]	Impact Force – Stern Collision [MN]
30	1.0	12.60	9.71
40	1.0	20,01	14.30
50	0.8	29.06	23.43
60	0.4	35.25	31.19
70	0.2	42.97	36.21

Table 8-1 – Comparison of Column Strength – Beam vs. Stern Collision

Column Thickness [mm]	Ship Deformation [m]	Impact Force – Beam Collision [MN]	Impact Force – Stern Collision [MN]
30	0.1	7.02	7.34
40	0.2	14.17	8.14
50	0.4	13.84	10.61
60	0.8	32.88	13.87
70	1.0	35.48	17.37

Table 8-2 – Comparison of Ship Strength – Beam vs. Stern Collision

Table 8-1 and 8-2 show that the required force to produce a given deformation is, for most cases, smaller for both ship and column when stern impacts are considered. The only exception is the ship deformation when the column thickness is 30 mm. The largest difference is with respect to the ship-side which shows a strength reduction of over 50 % when the column thickness is 60 mm.

The differences discussed above are mainly due to the following reasons:

1. The strength of the stern model is lower compared to the more compact beam-model. This effect becomes more and more important when the column thickness is increasing.

2. The contact area is smaller.
   Thus, a smaller force is required in order to produce the same pressure.

3. The overall deformation of the column is smaller for the stern impacts.
   This is illustrated in figure 8-2.

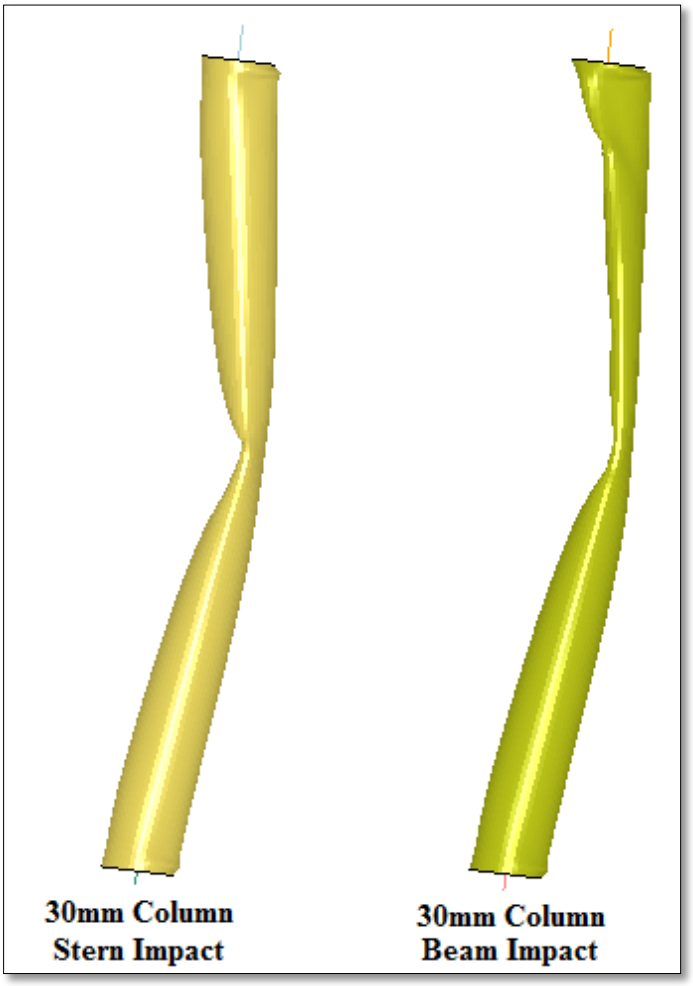

Figure 8-2 – Overall Column Deformation – Beam vs. Stern Impact

The maximum deformation of the ship and column are presented in figures 8-3 and 8-4 for respectively the 30 mm and 70 mm case. When the column thickness is 30 mm, the column deformation is large and the ship deformation small. When the column thickness is 70 mm, the ship deformation is large and column deformation small. The ship is given a prescribed displacement of 2 m so the structural deformation is elements which displace less than 2 m.

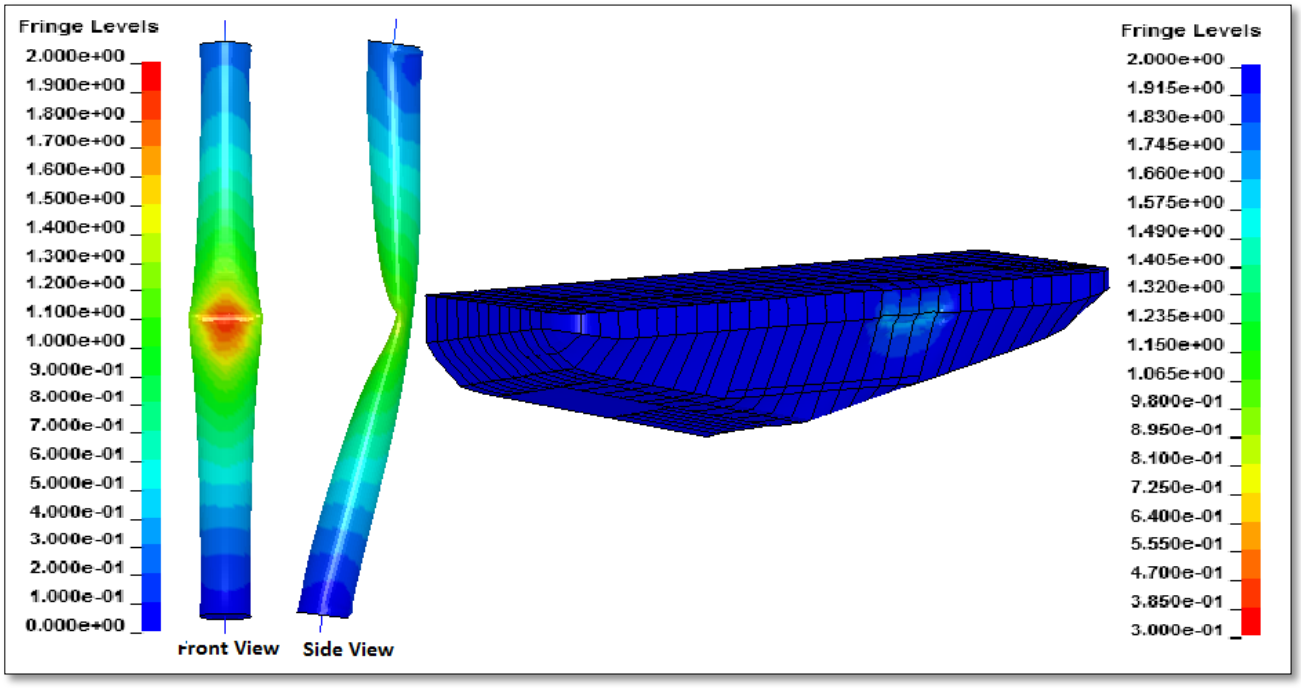

Figure 8-3 – Deformation Levels - 30 mm Column – Stern Impact

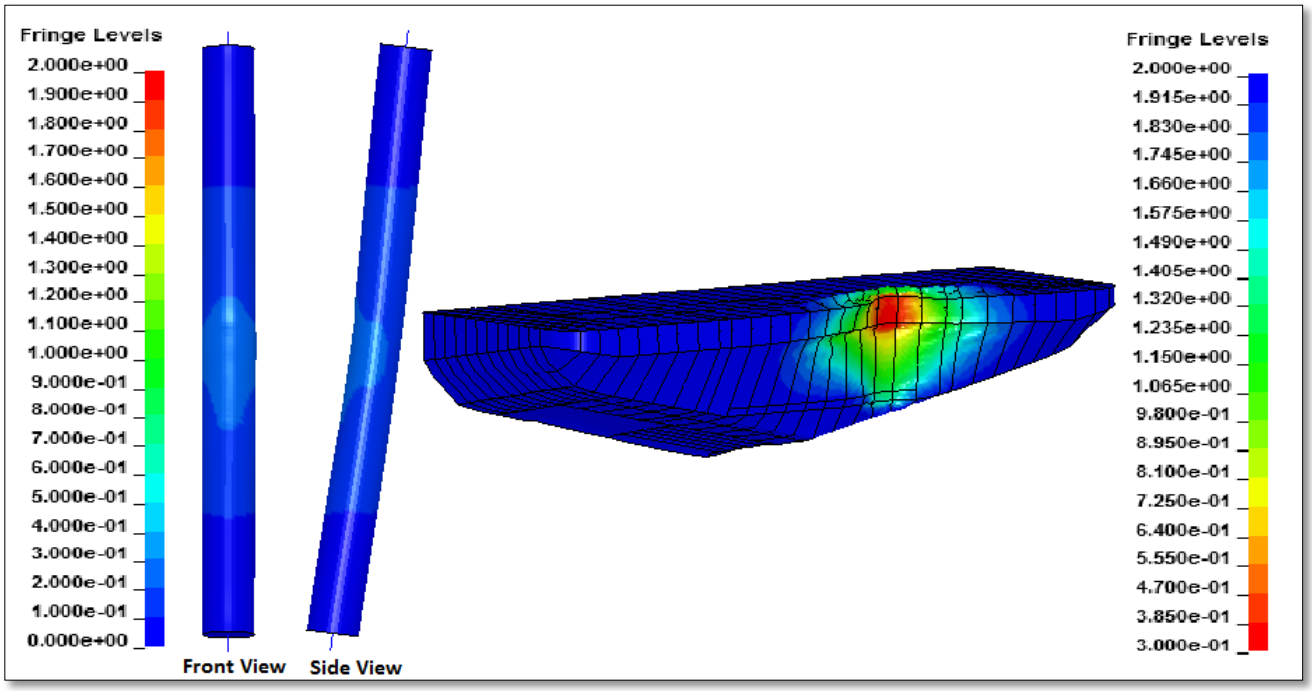

Figure 8-4 – Deformation Levels - 70 mm Column – Stern Impact

8.3 Energy Dissipation & Design Categories

The impact force, energy dissipation and maximum deformation of the ship and column at the moment where the total available strain energy is dissipated is presented in table 8-3 for the different column configurations.

Column Thickness	Impact Force [MN]	Energy Dissipation - Column [%]	Energy Dissipation - Ship [%]	Column Deformation [m]	Ship Deformation [m]
30 mm	14.12	87	13	1.82	0.30
40 mm	15.45	76	24	1.29	0.51
50 mm	20.94	22	78	0.34	1.05
60 mm	25.90	8	92	0.11	1.18
70 mm	26.57	5	95	0.06	1.21

Table 8-3 – Energy Dissipation – Column Diameter = 1.5 m

The table show that the 30 mm column dissipates most of the strain energy and may almost be categorized as ductile designed. The two strongest columns both dissipate less than 10% of the strain energy and may be considered strength designed. The other columns are classified as within the shared-energy region.

The previous section showed that the strength of the columns which are subjected to stern impacts is generally lower than the columns subjected to beam impacts. However, table 8-3 shows that the 4 strongest columns dissipate a less percentage of the total strain energy compared to the beam impacts. The difference is especially large for the 50 mm and 60 mm columns. The 60 mm column was classified as within the shared-energy region for the beam impact scenario, but is now classified as strength designed. The reason for this behaviour is, as previously mentioned, that the strength of the stern-model is lower compared to the more compact beam-model. Also, the total available strain energy is larger for the beam impact scenarios due to a larger hydrodynamic mass.

8.4 Resistance against Local Indentation

The normalised resistance against local indentation for the stern model are presented in figure 8-5. The FEA results are plotted against NORSOK curves with collision width, b, equal to 0.83 m and 3.55 m. 0.83 m is the width of the stern edge and 3.55 m is the maximum collision width.

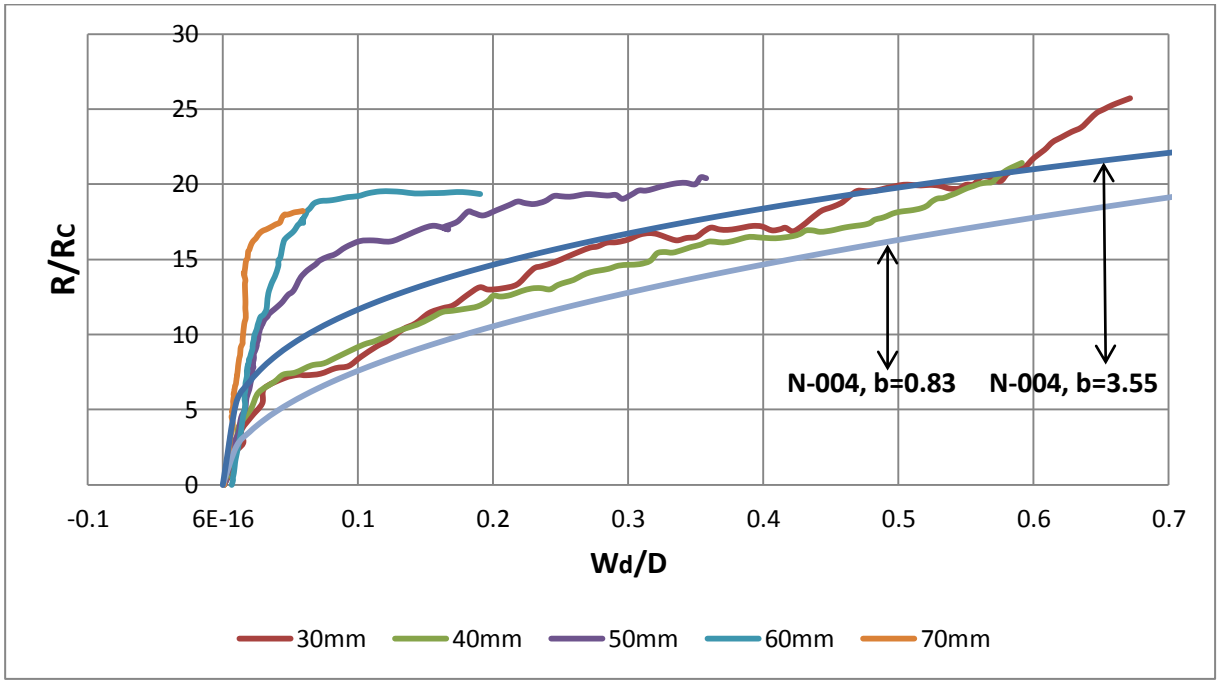

Figure 8-5 – Resistance to Local Deformation – Diameter = 1.5 m – Stern Impact

The results show that the NORSOK curves give a good representation of the two weaker columns. However, the NORSOK curves are very conservative compared to the three strongest columns. The reason for this is, as discussed in section 7.4.2, that the NORSOK curves are based on the assumption of a rigid ship, an assumption which becomes less and less valid as the column thickness increases.

Compared to the resistance against local indentation for the beam impacts, it is observed that the stern impact resistance is generally larger for small deformations and smaller for larger deformations. This is in accordance with how the contact area develops for the two impact scenarios. Initially, the contact area is largest for the stern impacts. Then, after about 0.2 s, the contact area for the beam impacts becomes larger. The contact area for the 40 mm column-configurations is plotted in figure 8-6 for both beam and stern impact scenarios. The figure shows that the contact area for the stern case increases little after about 0.3 s. This might explain why the weaker columns in figure 8-5 do not show the same increase in strength for large deformations as the weaker columns in figure 7-20. A comparison of the contact area for stern and beam impact scenarios for all column-thicknesses is included in appendix E. The columns in appendix show the same behaviour as figure 8-5.

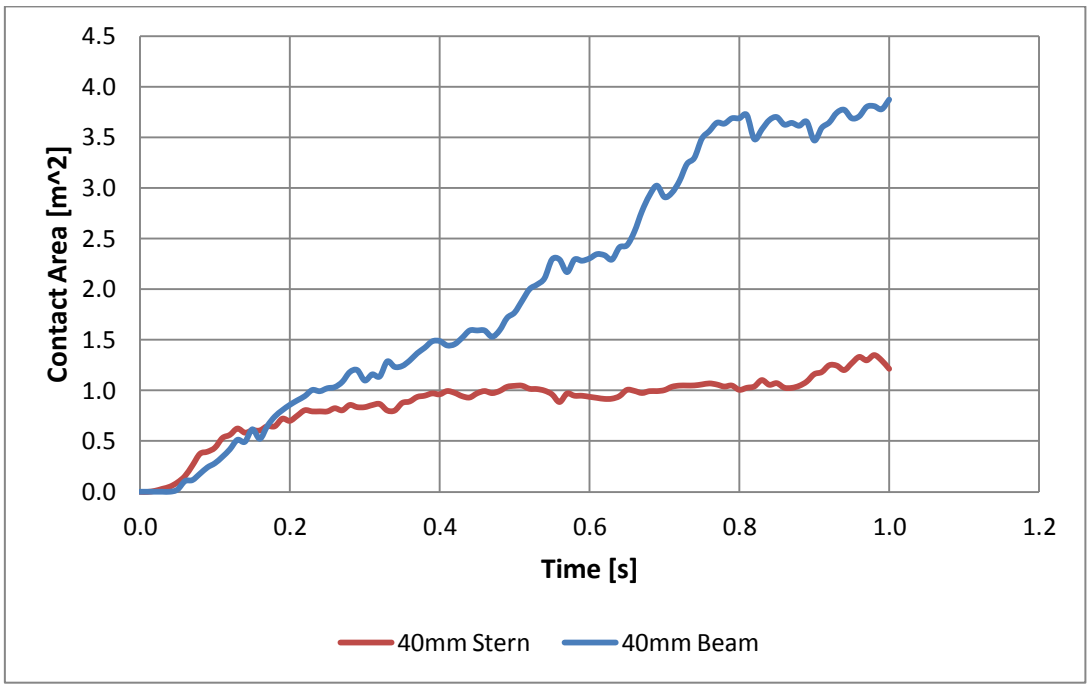

Figure 8-6 – Contact Area – Stern vs. Beam Impacts – 40mm Column

Another reason why the curves in figure 8-5 do not increase as much as the curves in figure 7-20 is because the membrane forces that develops in the column is lower during the stern impact compared to the beam impact. A comparison of the membrane forces at a cross-section just above the dented region is presented in figure 8-7. The maximum membrane force is about 13.8 MN for stern impacts and 20.57 MN for beam impacts.

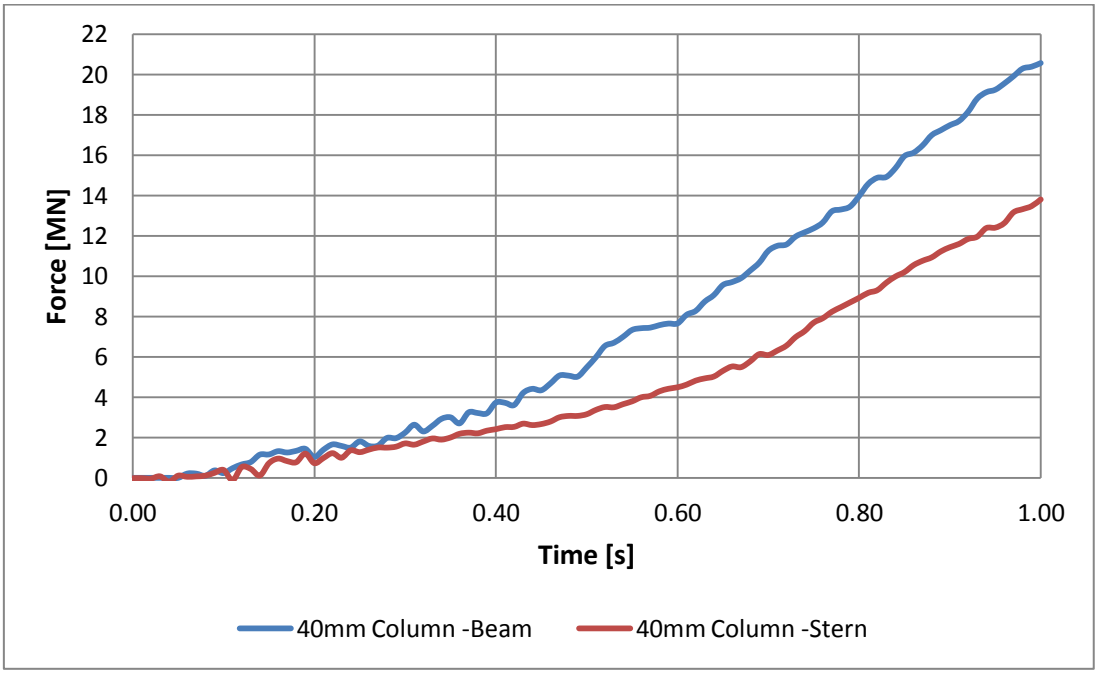

Figure 8-7 – Membrane Forces – Beam vs. Stern Impact

8.4.1 Comparison with the Design Curve

Figure 8-8 presents a comparison between the two weakest columns and the design curve for ductile design that was established in section 7.4.4. The figure shows that the design curve represents the FEA results quite well and that the design curve is mostly on the conservative side. The NORSOK curve with contact-width = 1.5 m is used as an intersection curve with equation 7-4 in this case. This is because the two weakest columns do not reach the maximum contact width of 3.55 m that was used in figure 8-5.

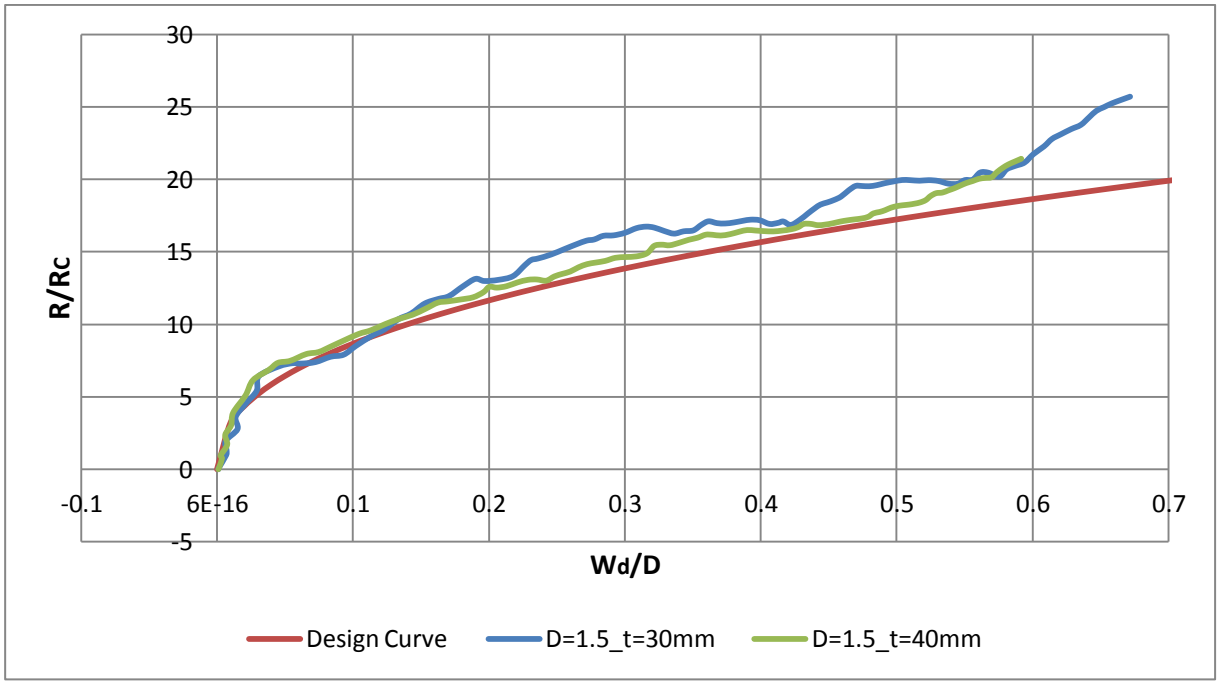

Figure 8-8 – FEA vs. Design Curve – Column Diameter =1.5 m – Stern Impact

8.5 Comparison with Simple Calculations

In this section, the FEA results from the stern impact analyses are compared with the ideal rigid plastic force-deformation relationship. The results will be compared against both the point-load model (figure 3-4) and the model which is subjected to a distributed load (figure 7-30).

Since the contact area is small compared to the beam impact scenario, the point-load model should give a better representation of the results in this case. The results compared with the point-load model are presented in figure 8-9.

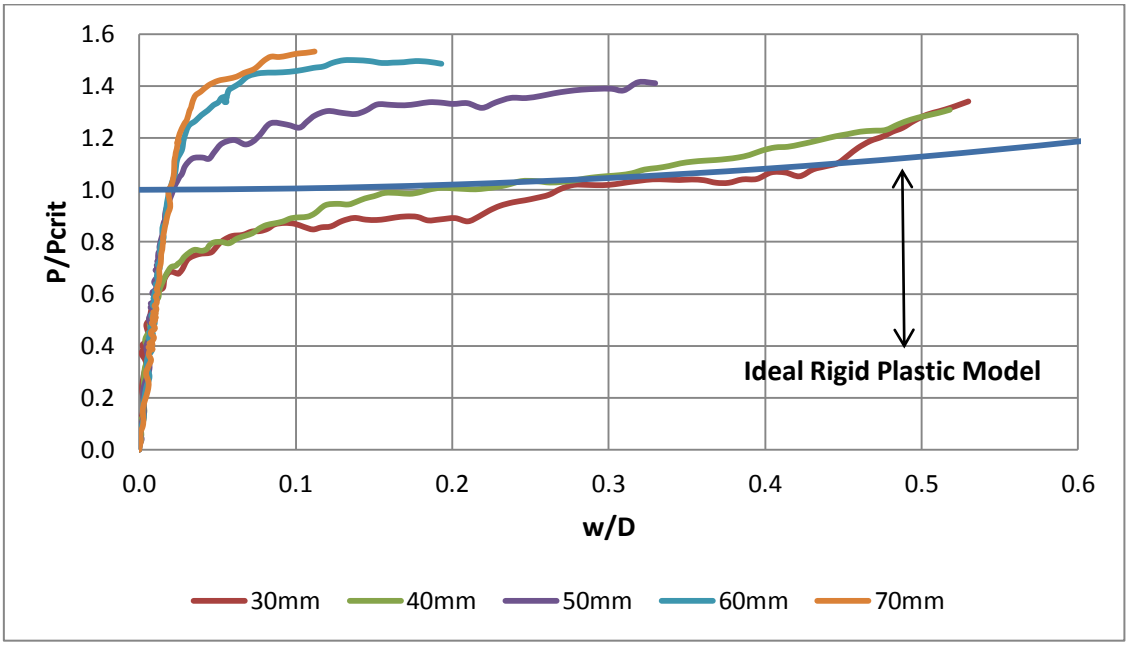

Figure 8-9 – FEA Results vs. Point Loaded Model – Stern Impact

The figure shows that the point loaded model does give a better representation of the results in this case, especially for the two weaker columns. However, since the plastic buckling capacity of the three stronger columns is higher than the capacity of the ideal model, and since the strength of the weaker columns increases beyond the ideal model for large deformations, the model does not give a good enough representation of the results. The results are therefore compared to the model which is subjected to a distributed load. The width of the maximum load distribution, "a", now increases with increasing column thickness and is given in table 8-4. The comparison between the new model and the FEA results is presented in figure 8-10.

Column Thickness	Load Width, "a" [m]
30 mm	1.04
40 mm	1.20
50 mm	3.33
60 mm	3.55
70 mm	3.55

Table 8-4 – Load Width – Stern Impact

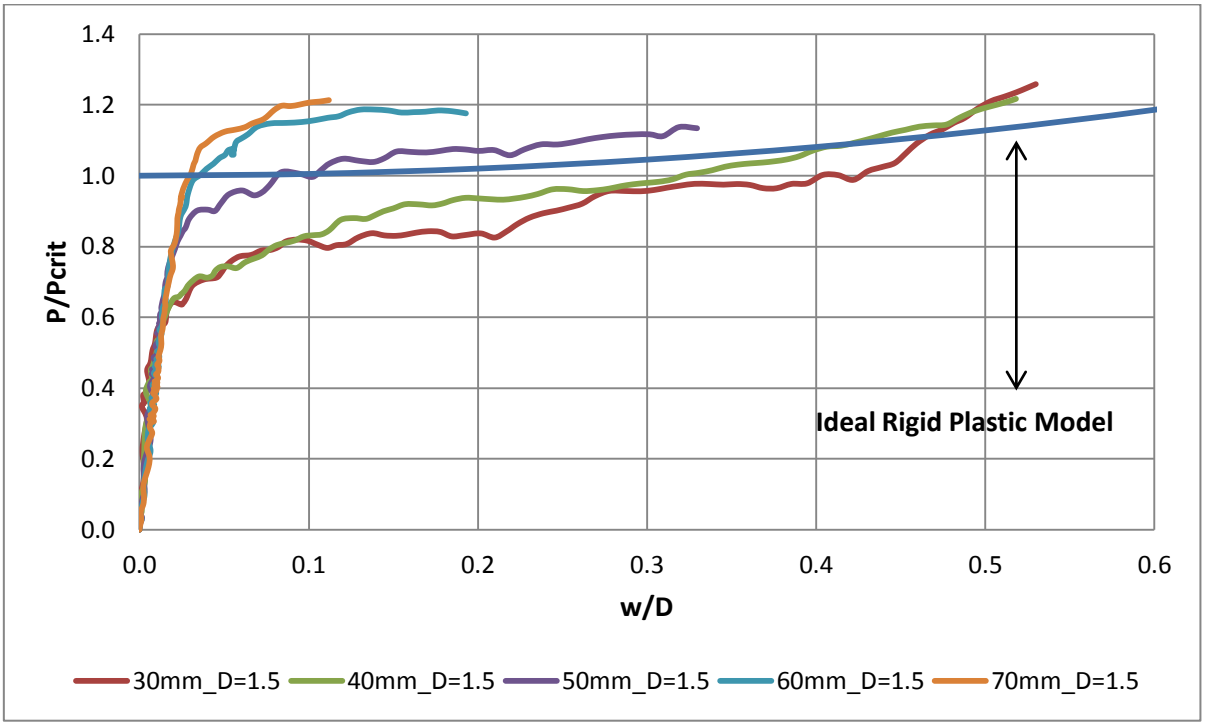

Figure 8-10 – FEA Results vs. Distributed Load Model – Stern Impact

The figure shows that the theoretical model now gives a better representation of the three strongest columns. The load-width for the weakest columns is close to 1 so the difference is small compared to the point-load model. These columns buckles at about 63 % of the ideal capacity which is probably realistic since the columns are subjected to large local deformations.

However, there are some remarks:

- The buckling capacity of the two strongest columns is still higher than the ideal capacity.

- The post buckling strength of the columns increases beyond the ideal model for large deformations.

- The ideal model assumes clamped boundaries and thus over-estimates the increase in strength in the post-buckling region.

- The ideal model assumes a constant distributed load. A more realistic method would be to take into account the gradual increasing contact area.

- The model yields quite un-conservative estimates of weak columns. The results show that it is important to consider the reduction in strength due to local indentation.

Model with Reduced Capacity

The reduced moment capacity for the different column-configurations that are subjected to stern impacts is presented in table 8-5:

Diameter [m]	Thickness [m]	Mp [MNm]	Mp Reduced [MNm]
1.5m	0.03	23.02	5.69
	0.04	30.28	8.24
	0.05	37.33	14.91
	0.06	44.19	20.19
	0.07	50.86	25.35

Table 8-5 – Reduced Moment Capacity – Stern Impacts

The reduced moment capacity are calculated according to equations 3-35 – 3-37 and are based on estimations of the indentation depth at the moment where the column starts to buckle. Reduced ideal rigid collapse loads, Pcrit, for the distributed-load model are calculated based on the reduced moment capacity.

The comparison between the FEA results and the theoretical model with reduced capacity is presented in figure 8-11 for the columns subjected to stern impacts. The figure shows that the ideal model is quite conservative in its representation of the plastic buckling capacity.

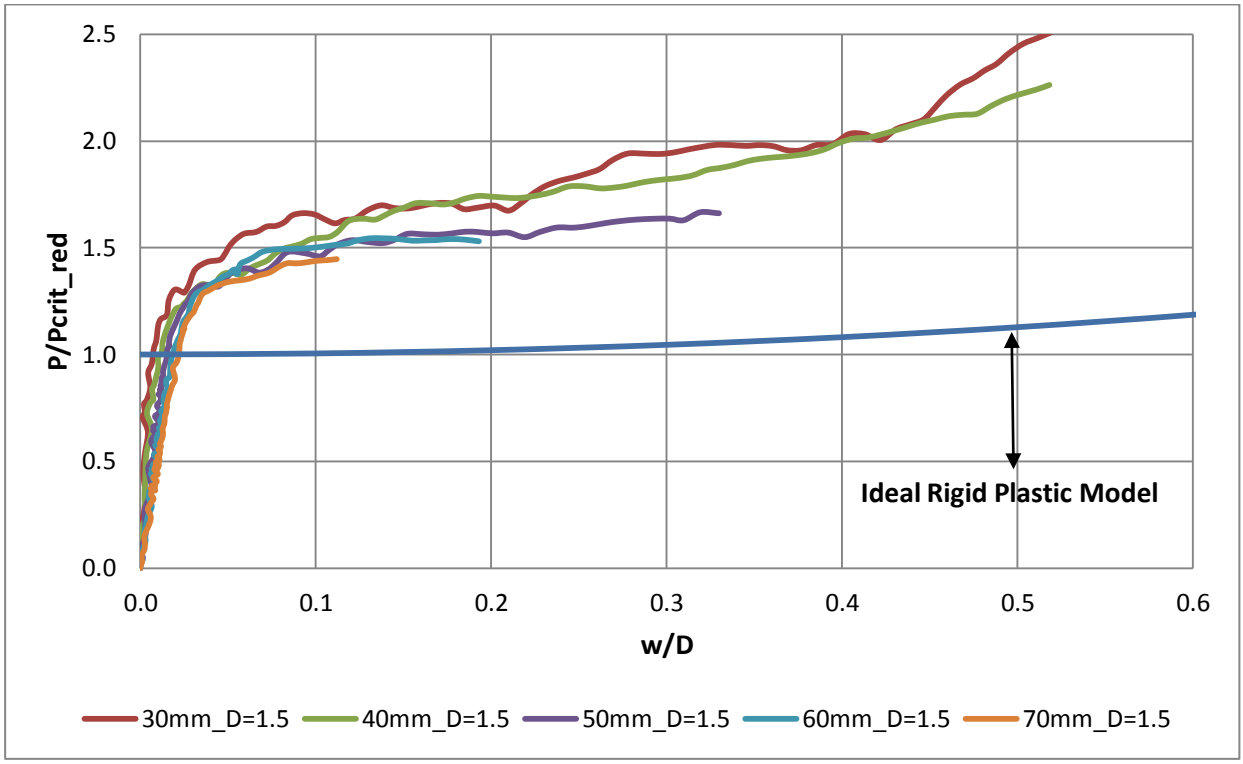

Figure 8-11 – Simplified Model with Reduced Capacity –Stern Impacts

9. Effect of Ring Stiffeners

The capacity of the platform leg-segment may be improved by applying stiffeners. In this chapter, the effect of ring-stiffeners on the column with diameter = 1.5 m and thickness 50 mm is considered.

Ring-stiffeners applied in the collision-zone of a platform leg are unusual. Therefore, literature on realistic stiffener-scantlings was not found. Based on a discussion with Professor Jørgen Amdahl [16], the following stiffener-scantlings have been considered:

Design Nr.	Stiffener Details (units in mm)	Increase in Total Volume [m^3]
1	Spacing = 750, L-Profile, W160x10/F80x15	0.234
2	Spacing = 500, L-Profile, W160x10/F80x15	0.345
3	Spacing = 500, L-Profile, W160x15/F80x20	0.494
4	Spacing = 500, L-Profile, W220x15/F110x20	0.634

Table 9-1 – Ring Stiffeners

The increase in strength will be compared against the increase in strength by increasing the column thickness to 60 mm. The column volume increases 0.753 m^3 when the column thickness is increased 10 med mer. The production costs are not considered.

The force-deformation relationships of the 50 mm unstiffened column, the 4 stiffener designs and the 60 mm unstiffened column are presented in figure 9-1.

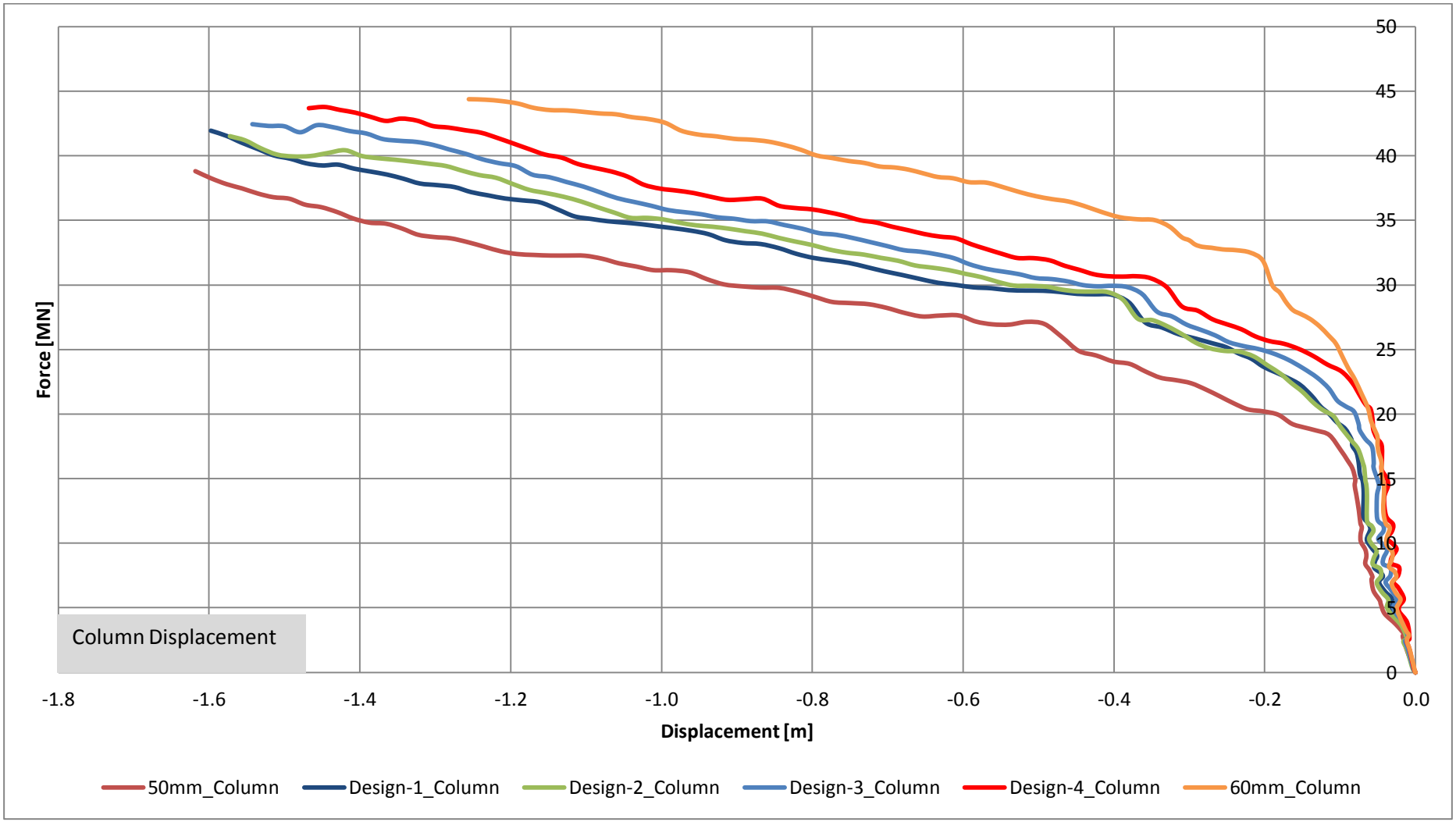

Figure 9-1 – Force-Deformation Relationship – Effect of Ring Stiffener

The energy dissipation is presented in table 9-2. The maximum difference between the energy dissipation of the 50 mm unstiffened column and the 50 mm column with stiffeners is about 5 % from. However, the reduction from the unstiffened 50 mm column to the unstiffened 60 mm column is about 20%.

Column	Impact Force [MN]	Energy Dissipation - Column [%]	Energy Dissipation - Ship [%]	Column Deformation [m]	Ship Deformation [m]
50 mm unstiff.	29.06	49	51	0.80	0.57
Design 1	30.17	46	54	0.63	0.66
Design 2	31.14	46	54	0.62	0.67
Design 3	31.24	45	55	0.57	0.68
Design 4	32.07	44	56	0.53	0.71
60 mm unstiff.	35.02	29	71	0.35	0.84

Table 9-2 – Energy Dissipation – Ring Stiffener

The results show that the effects of the ring-stiffeners are smaller than the effect of increased column thickness. Increased ring-stiffener scantlings would help, but larger scantlings than those in table 9-1 would be quite unrealistic for this diameter.

10. Discussion & Conclusions

In this Master Thesis, analyses of unstiffened and stiffened platform leg-segments subjected to beam and stern impacts have been considered. Parameter studies of column-design and impact scenarios have been performed. The results from the finite element analyses have been compared against theoretical calculations and recommended practice given in NORSOK N-004 [4].

As a general conclusion, the thesis shows that the need for accurate finite element analyses in structural design is ever present. Theoretical calculation-models are often based on unrealistic assumptions and simplifications, and may be conservative in some cases and un-conservative in other. Thus, one should not use simplified theoretical methods without concern for the effects of the simplifications.

In the following, a brief discussion and concluding remarks about the specific topics of this thesis is presented.

Boundary Conditions

The column with diameter 1.5 m has been analysed using two different sets of boundary conditions. In the first case, the surrounding structure of the impacted leg-segment is considered strong enough to withstand the collision forces during large deformations of the leg-segment. The column-ends are therefore assumed fixed in all rotational and translational degrees of freedom. In the second case, it is assumed that the surrounding structure is not strong enough to withstand the collision forces. Thus, when the leg-segment deforms, the ends may displace inwards. The column in this case is considered fixed in all degrees of freedom except for the translational degree of freedom in the local axial direction of the column where the column-ends have been fitted with an elastic spring. The spring stiffness has been estimated using USFOS.

The results are presented in chapter 6 and shows that the strength of the column decreases if the axial flexibility is taken into account. The effect is most evident for large column-deformations. The reduction in strength is also largest for the weakest columns since the column-deformation is largest in these cases. Hence, for the strongest columns, the effect of the axial flexibility is only important if one considers high-energy impacts. However, in order to be on the conservative side, it is recommended that the effect of the surrounding structure is taken into account when performing impact analyses of jacket platforms.

In table 6-1, the maximum spring force is compared against the axial tension capacity. The results show that the assumption of an elastic spring is valid.

Parameter Study of Column Dimensions

In chapter 7, a parameter analysis of the column dimensions has been performed. The column diameter and wall-thickness have been varied according to table 7-1.

The results have shown that if the total deformation of the columns is considered, a larger diameter is favourable. However, the total deformation is not enough to understand the true behaviour of the impact scenarios. One needs also to consider how the total deformation is divided between the global and local column deformation. A compact cross-section will have large global deformations and small local deformations. On the other hand, a less compact cross-section will be dominated by local deformations. This may be of importance with respect to global analyses of the damaged platform.

One interesting finding with respect to the column wall-thickness is that the increase in strength of the column is not proportional with the increase in wall-thickness. The results have shown that the strength of the column with diameter = 1.5 m increases significantly when the column thickness is increased from 40 mm to 50 mm. The same significant increase in resistance has been observed when the thickness is increased from 50 mm to 60 mm for the column with diameter = 2.0 m. The increase in strength is mainly a consequence of increasing resistance against local indentation and shows that a small variation of the structural configurations may have large beneficial effects on the structural integrity.

The different column-designs have been categorized according to the design-categories described in section 2.3. The results have shown that if strength design is aimed for, the wall-thickness has to be at least 70 mm for columns with diameter = 1.5 m and at least 60 mm for columns with diameter = 2.0 m. The column with diameter = 1.0 m was analysed with wall-thicknesses up to 60 mm, but strength design was not achieved in this case. Strength design for the columns with diameter = 1.0 m would probably require a wall-thickness above 70 mm.

Resistance against Local Indentation

The capacity of a platform-leg may be significantly weakened by local indentation. Accurate estimate of the resistance against local indentation are therefore very important. The normalised resistance against local indentation for the different column-configurations have been discussed and compared with resistance curves used in NORSOK N-004 [4].

The resistance curves presented in NORSOK N-004 have been developed based on experiments and theoretical calculations where the impacting ship is assumed perfectly rigid. This assumption is reasonable for the weakest column-configurations and NORSOK represents these columns quite well. However, as the column thickness increases, the assumption becomes less and less valid. The results show that NORSOK is fairly conservative in its representation of the stronger columns. An exception is the columns with diameter = 1.0 m. In this case, NORSOK is quite un-conservative in all cases.

Another important factor which is not taken into account by NORSOK is the gradual increasing contact area. When the contact is first initiated, the contact-area is close to zero. Then, the contact-area increases as the column and ship deforms leading to an increase in the resistance against local indentation. However, NORSOK evaluates the strength at constant $Contact - width/_{Column\ Diameter}$ - ratios. The increase in resistance from small to large contact-width is therefore not represented by NORSOK. I section 7.4.4, an empirical design-curve was developed that takes the increasing contact area into account. The design-curve is intended for columns which may be classified as ductile-designed, or as a conservative lower-estimate of the strength of other column-designs. Comparisons between the design-curve and the FEA results of the weakest columns show that the design-curve represents the strength of these columns quite well.

Based on the results and discussion in this thesis, is recommended that one use caution when applying the NORSOK-curves in a design-phase. If ductile design is aimed for, the NORSOK-curves may be used together with the design-curve that was developed in this thesis. If ductile design is not aimed for, accurate finite element analyses are recommended.

Simple Calculation Model

The FEA results have been compared with an ideal rigid plastic model that takes into account the increasing strength in the post-collapse range due to the development of membrane forces. Two load-cases have been considered for the simplified model: one case where the column is subjected to a point-load (see figure 3-8), and one case where the column is subjected to a partly-distributed load as shown in figure 7-30. For both impact scenarios, the model which assumes a distributed loading gives a better representation of the FEA results.

The results show that the columns with large local indentations have a significant reduction of the plastic collapse capacity compared with the ideal load. The capacity of the strongest columns almost reaches the ideal collapse load. The ideal rigid model is generally conservative for large deformations in the post-collapse range.

The results have also been compared against an ideal model that takes the reduction of the moment-capacity due to local indentations into account. The reduction has been calculated based on equations provided by NORSOK that depends on the size of the local indentation. However, NORSOK do not propose any design-values for the local-indentation size. Therefore, the local indentation values at the moment where the columns first start to buckle have been used when calculating the reduced capacity for the different column-configurations. The results show that the ideal model with reduced capacity predicts the buckling capacity quite well for the beam impacts, and that the buckling capacity of the columns subjected to stern impacts are underestimated by approximately 20-30 % . The ideal model with reduced capacity underestimates the strength in the post-collapse range for all column-configurations and impact scenarios. A linear relationship between the $w_d/_D$-ratio

and the D/t-ratio has been suggested as design-values for the local indentation size. However, the data show some scatter and should be verified by more analyses.

Based on the results, it may be concluded that the ideal rigid model may be used to estimate the buckling capacity of the columns if the following conditions are met:

- The simplified model should be as accurate as possible with respect to boundary conditions and loading.

- The reduction of the plastic collapse capacity due to local indentations should be taken into account.

If these conditions are met, the simplified model will generally yield conservative estimations of both the buckling load and post-collapse strength.

Beam vs. Stern Impact Scenario

In this thesis, beam and stern impacts of the platform leg-segment have been considered. The contact area of a typical supply vessel may be considerably smaller for stern impacts compared to beam impacts. This may be crucial to the platform response.

The force-deformation relationships show that the required force to produce a given displacement is generally smaller for both ship and platform when stern impacts are considered. The reduction in strength for the column is mainly due to a smaller contact-area for stern impacts compared to beam impacts. However, it has been seen that the columns subjected to stern impacts dissipates a smaller percentage of the total available strain energy than the columns subjected to beam impacts. Also, the column deformation at the moment where the total strain energy is dissipated is largest for the beam impacts. The only exception is the column with diameter = 30 mm which is worse when stern impacts are considered.

The reason for this behaviour is two-fold:

- The strength of the stern-model is lower than the strength of the more compact beam-model. This effect becomes more important as the column thickness is increased.

- The total available strain energy is smaller for the stern impacts due to a smaller hydrodynamic mass.

The columns subjected to beam impacts also have a larger overall deformation than the columns subjected to stern impacts.

All considered, the results show that the beam impacts are most critical with respect to the platform response. However, this might be different if the strength of the stern-model was larger. For example if the stern model was of an anchor-handling vessel with stern-rollers.

Effect of Stiffeners

The effects of ring-stiffeners applied in the collision zone have briefly been considered in chapter 9. However, the results showed that the effect is small. The maximum decrease in energy dissipated by the column was estimated to about 5% when stiffeners were applied. However, by increasing the column thickness to 60 mm, the energy dissipated by the column was decreased about 20%.

Therefore, it is not recommended that ring-stiffeners are used in order to increase the impact-resistance for jacket structures. However, longitudinal stiffeners applied alone or in combination with ring-stiffeners may have a better effect. Longitudinal stiffeners will increase both the resistance against local and global deformations.

11. Further Work

- Global analyses of the damaged platform should be performed in order to ensure that the platform has the necessary residual strength.

- A more comprehensive model for estimation of the resistance against local indentation than the current NORSOK version should be developed. The model should take the varying contact area into account. The effect of roll motions on the contact area should also be included.

- Improvement of the simplified methods for global deformations. Design values for the local indentation size should be developed.

- Evaluation of how sensitive the response is with respect to the spring stiffness applied for axial flexible boundary conditions. The assumption of an elastic spring could also be investigated further.

- The effect of stiffeners in the contact-zone should be investigated further. Especially the application of longitudinal stiffening.

- Analyses of Stern Impacts using a ship-model with increased strength compared to the model used in this thesis. A suggestion is to use a model with stern-rollers.

- Comparison between the results from beam and stern impacts against results from column subjected to bow and stern-corner impacts.

References

1. Henrik Raaholt, 2009, Analysis and Design of Columns in Offshore Structures subjected to Supply Vessel Beam Collisions, Master thesis, NTNU

2. Reny Watan, 2011, Analysis and Design of Columns in Offshore Structures subjected to Supply Vessel Collisions, Master thesis, NTNU

3. NORSOK, 1999, NORSOK standard N-003: ACTIONS AND ACTION EFFECTS, Norwegian Technology Standards Institution

4. NORSOK, 2004, NORSOK standard N-004: Design of steel structures, Norwegian Technology Standards Institution

5. Thore H. Søreide, 1985, Ultimate Load Analysis Of Marine Structures, TAPIR

6. M. Bill Wong, 2008, Plastic analysis and design of steel structures, Amsterdam, Elsevier

7. Skallerud & Amdahl, 2002, Nonlinear Analysis of Offshore Structures, England, Research Studies Press Ltd

8. Jørgen Amdahl, 1983, Energy Absorption in Ship-Platform Impacts, Trondheim, The Norwegian Institute of Technology

9. Martin Storheim, 2008, Analysis of Structural Damage of Tankers subjected to Collision, Master thesis, NTNU

10. Jørgen Amdahl, 1980, Impacts and Collisions Offshore, Det Norske Veritas, Oslo

11. Torgeir Moan, 2003, Finite Element Modeling and Analysis of Marine Structures, NTNU, Institutt for Marin Teknikk

12. Hagbart S. Alsos, 2008, Ship Grounding: Analysis of Ductile Fracture, Bottom Damage and Hull Girder Response. PhD Thesis, NTNU.

13. Kjetil H. Qvale, 2011, Analysis and Design of Columns in Offshore Structures subjected to Supply Vessel Beam Collision, Project Thesis, NTNU

14. Livermore Software Technology Corporation, (2006), LS DYNA Theory Manual. Livermore Software Technology Corporation

15. Jørgen Amdahl, Lecture note in TMR4195 “Design of Offshore Structures”, NTNU

16. Professor Jørgen Amdahl, Personal discourse, NTNU

17. PhD Candidate Martin Storheim, Personal discourse, NTNU

18. LSTC Inc and DYNAmore GmbH, 2012, [Internet], Available from < http://www.dynasupport.com/>

19. Tavakoli, Amdahl, Alsos & Klæbo, 2010, Analysis of Supply Vessel Stern Impacts with an FPSO, NTNU & SINTEF, Trondheim

Appendix A. Force-Deformation Relationships

A.1 Fixed vs. Axial Flexible Boundary Condition

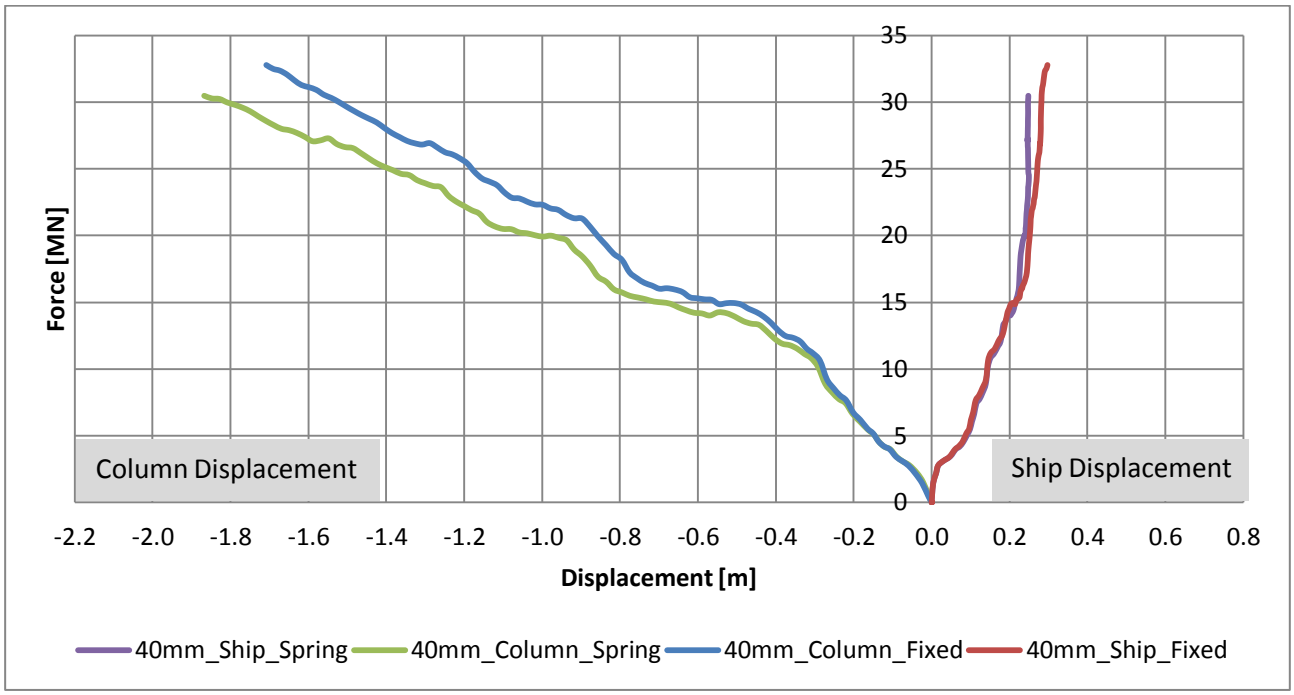

Figure A-1 - Force-Deformation – Spring vs. Fixed Boundary - 40mm Column

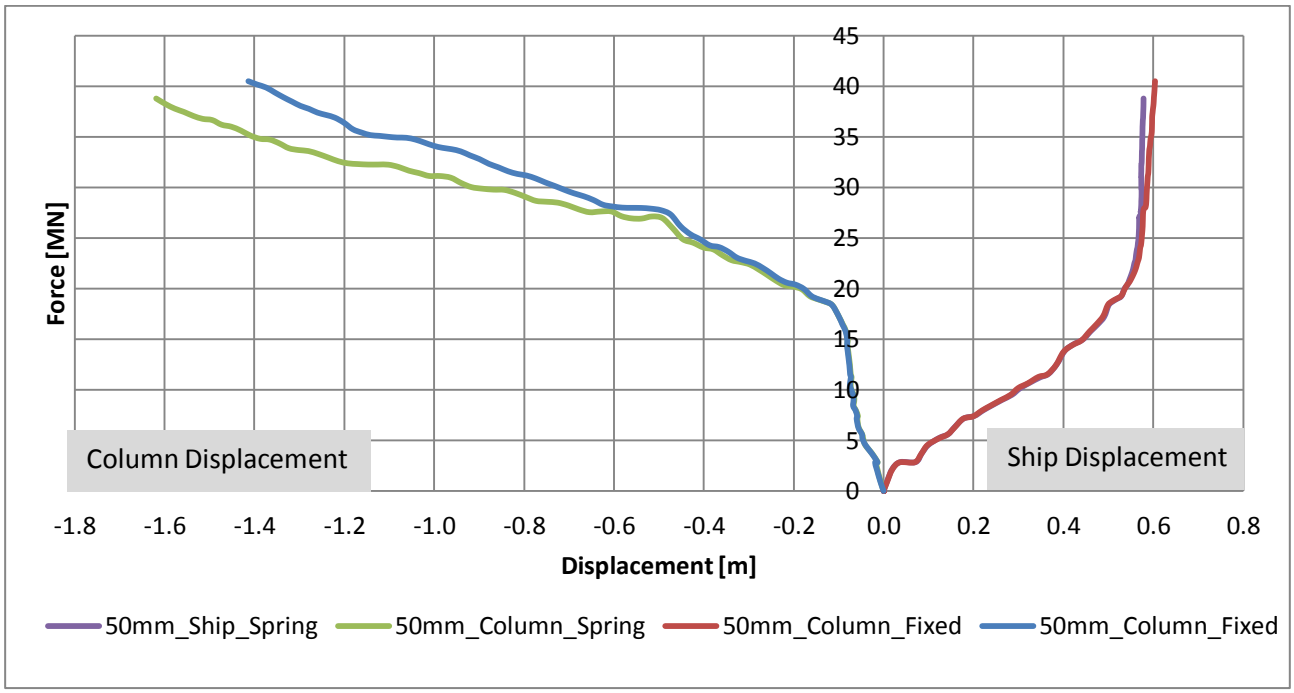

Figure A-2 – Force-Deformation – Spring vs. Fixed Boundary - 50mm Column

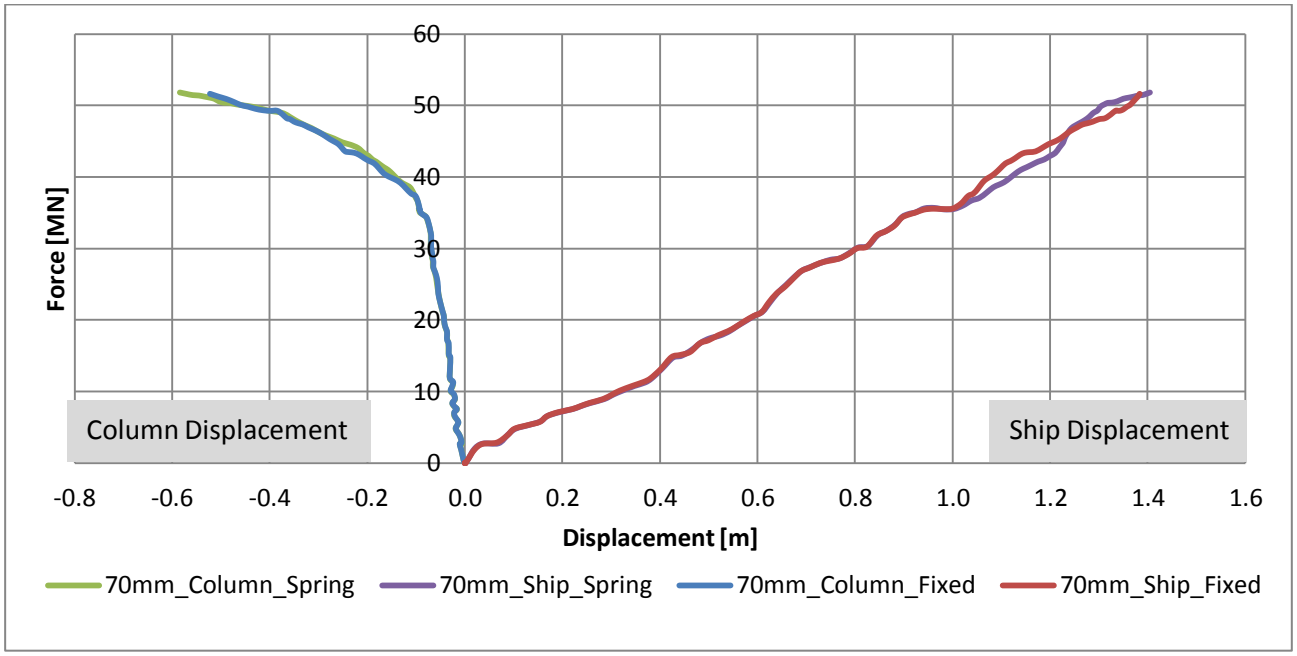

Figure A-3 – Force-Deformation – Spring vs. Fixed Boundary - 40mm Column

A.2 Column Diameter = 1.0 m

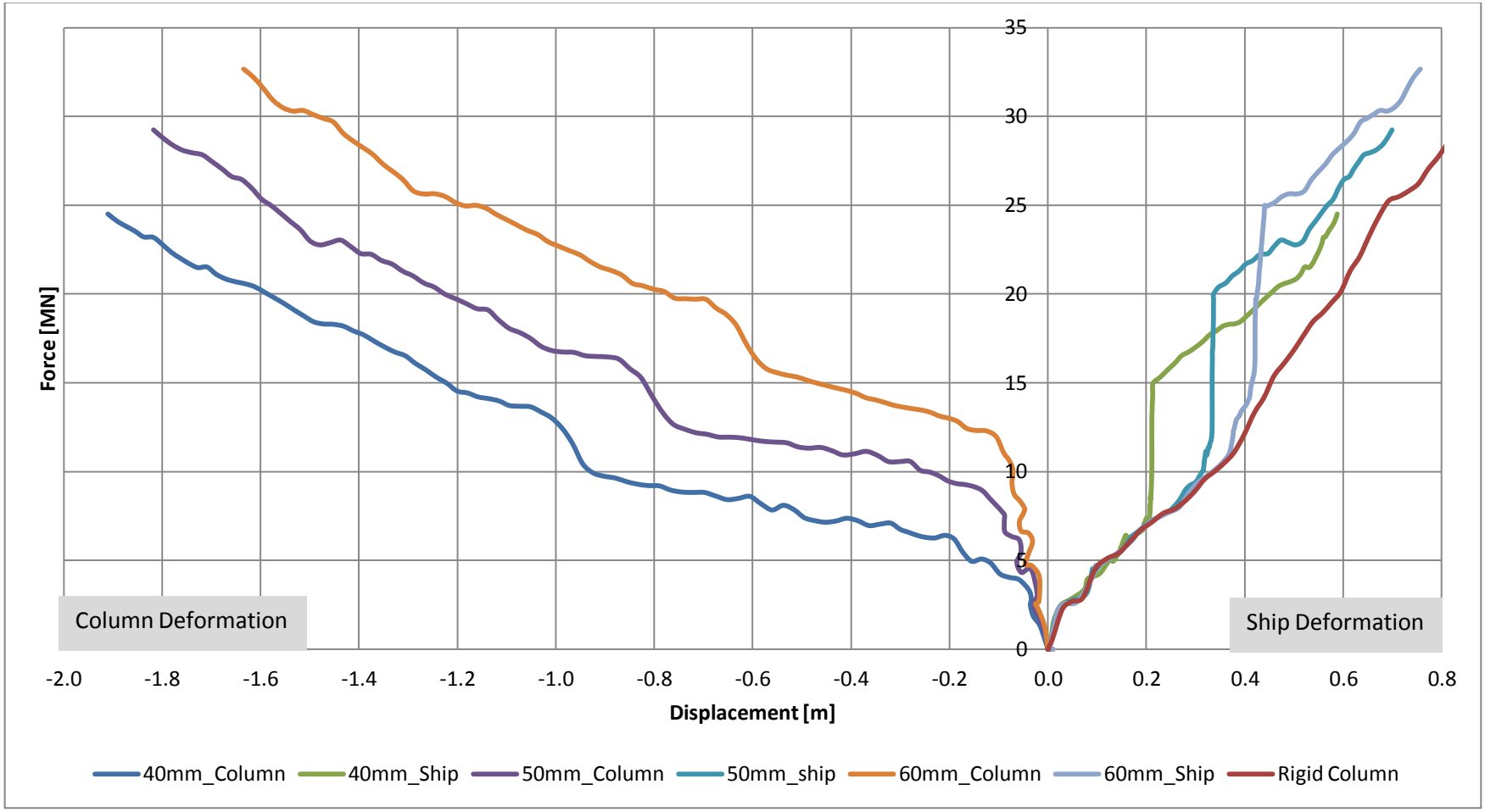

Figure A-4 – Force Deformation Relationship – Column Diameter = 1.0 m

A.3 Column Diameter = 2.0 m

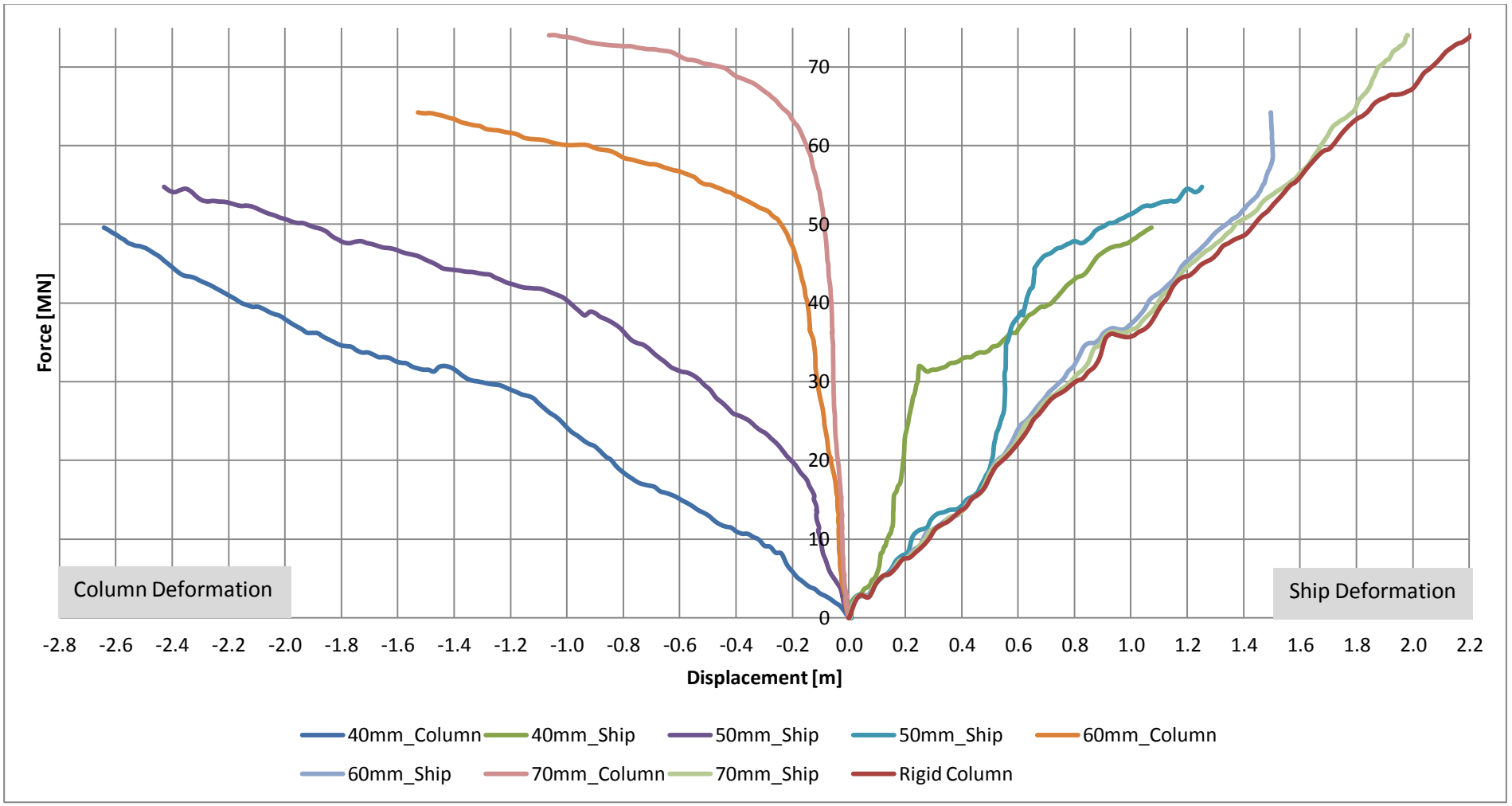

Figure A-5 – Force Deformation Relationship – Column Diameter = 1.0 m

Appendix B. Global and Local Column Deformation

B.1 Beam Impact

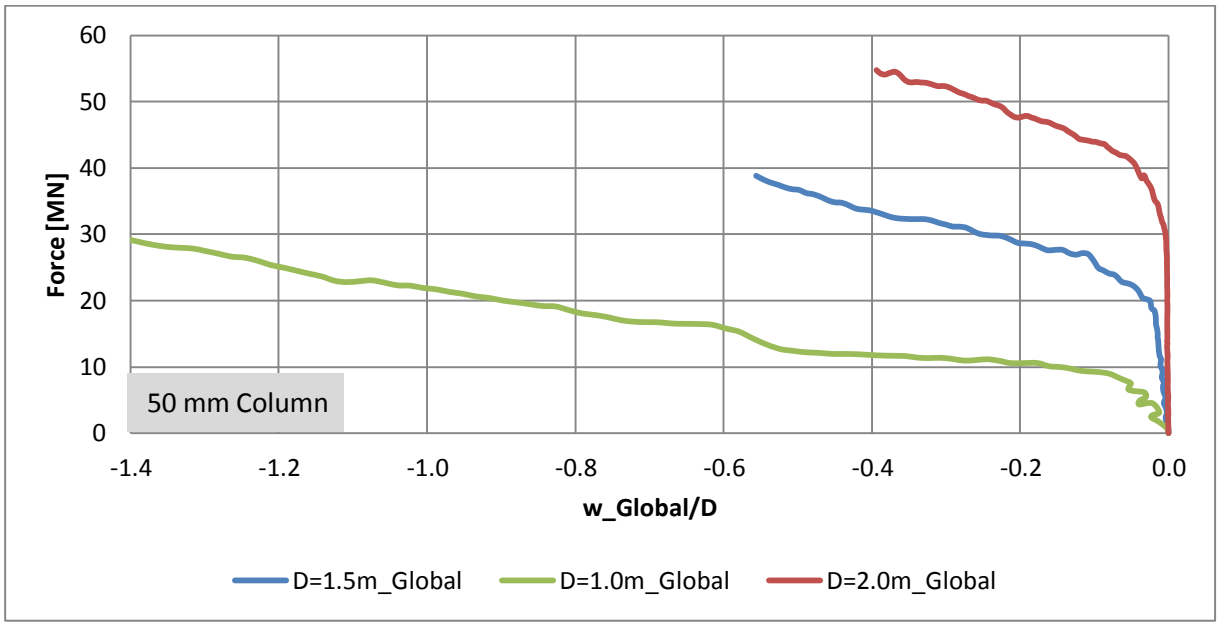

Figure B-1 – Global Column Deformation – 50 mm Column

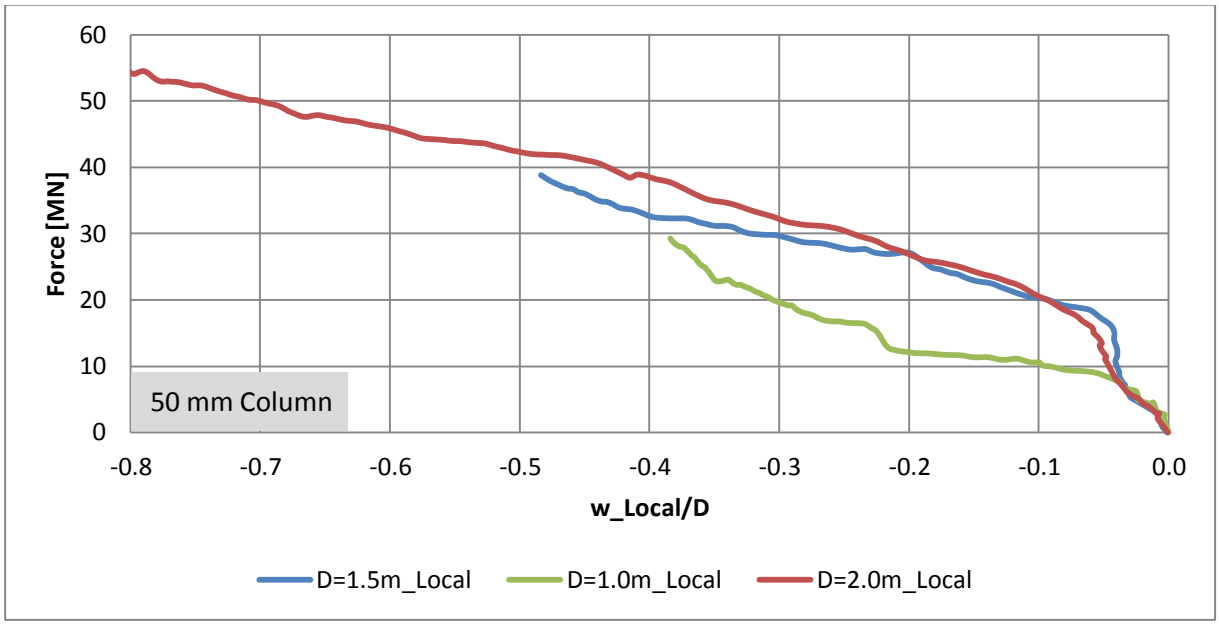

Figure B-2 – Local Column Deformation – 50 mm Column

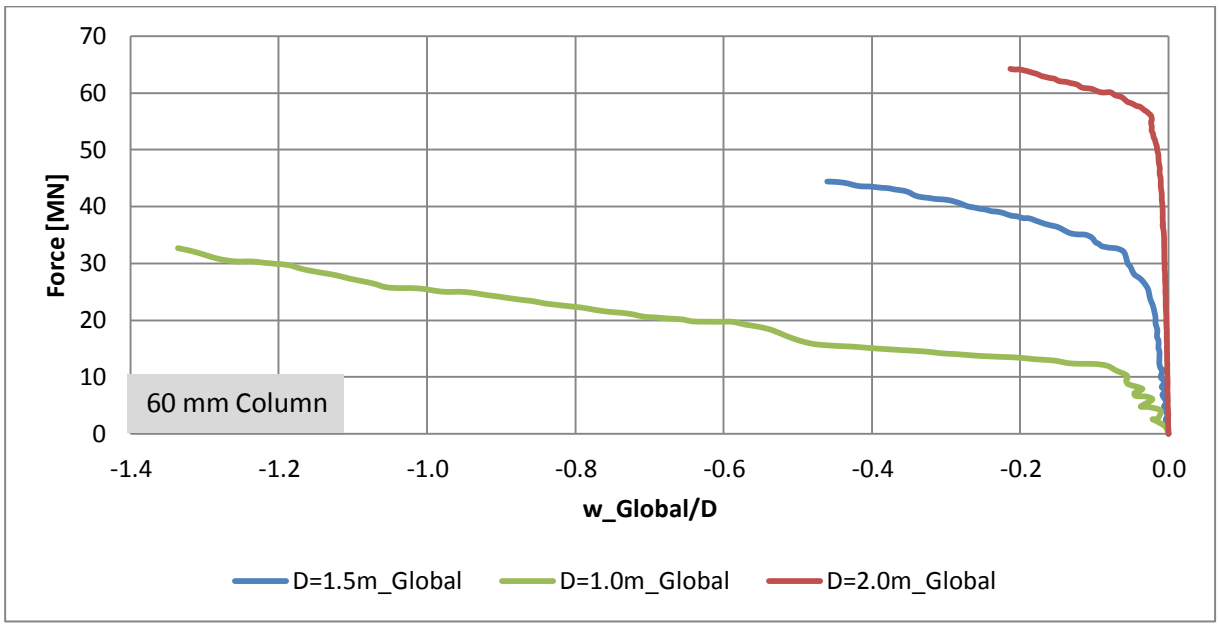

Figure B-3 – Global Column Deformation – 60 mm Column

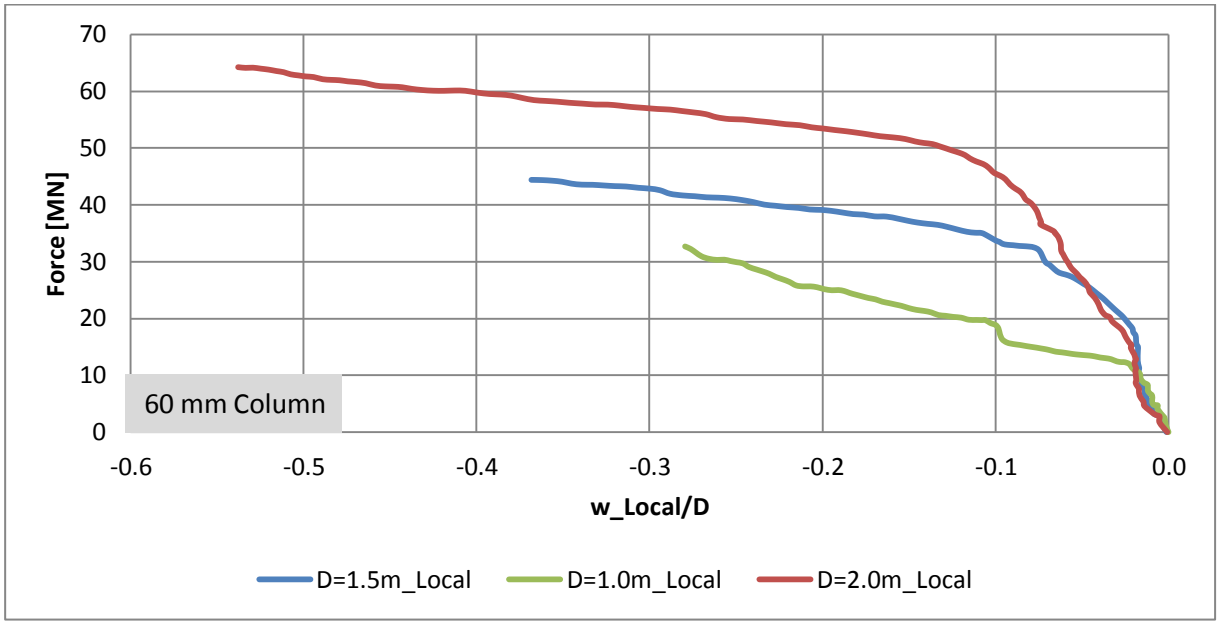

Figure B-4 – Local Column Deformation – 60 mm Column

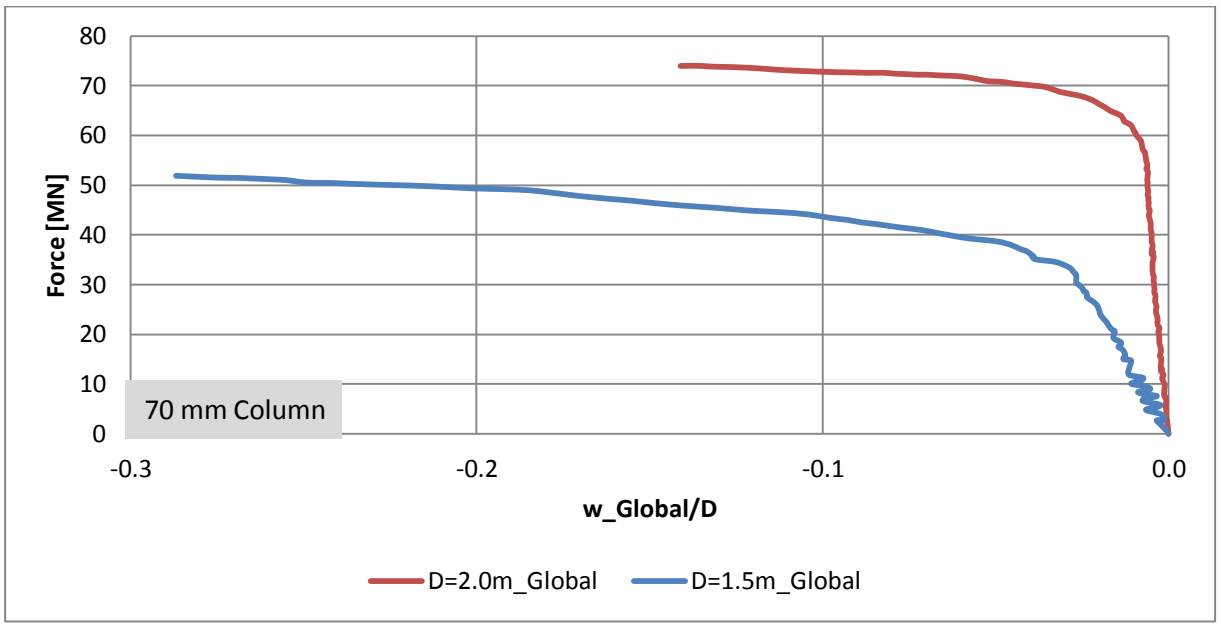

Figure B-5 – Global Column Deformation – 70 mm Column

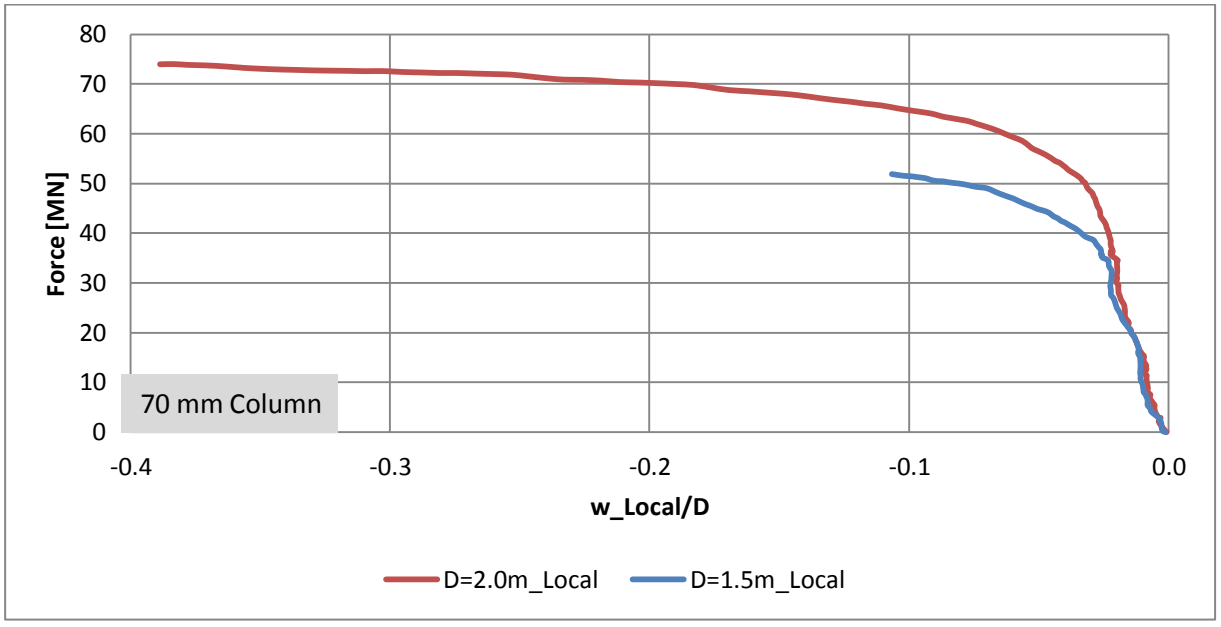

Figure B-6 – Local Column Deformation – 70 mm Column

B.2 Stern Impact

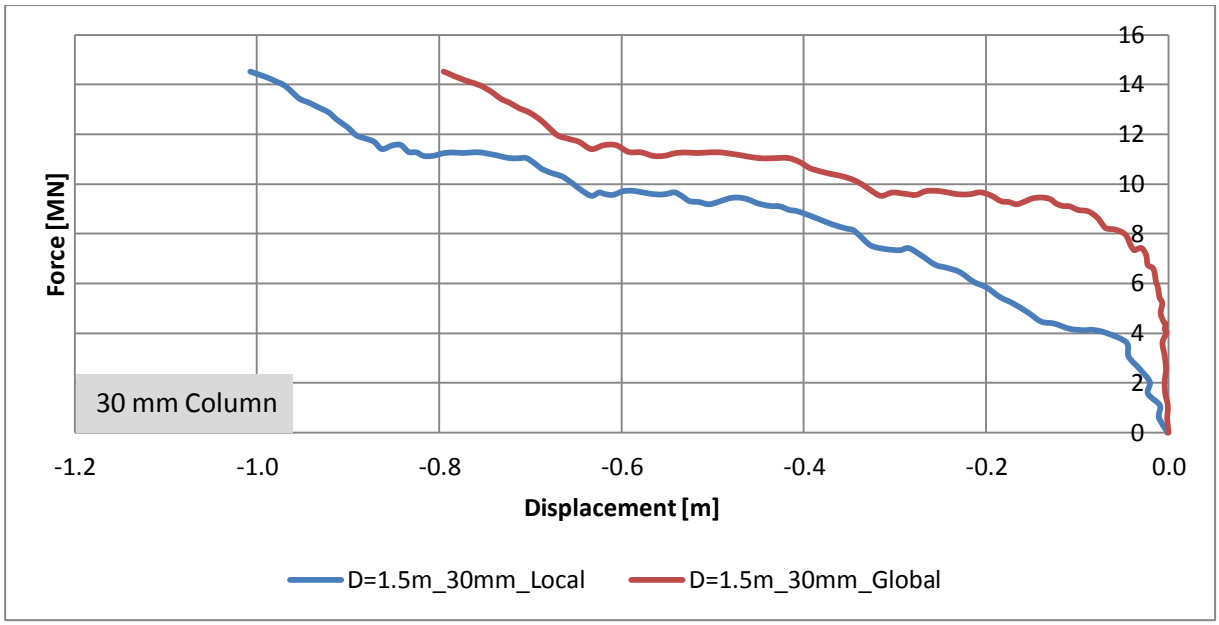

Figure B-7 – Global and Local Deformation – 30mm Column – Stern Impact

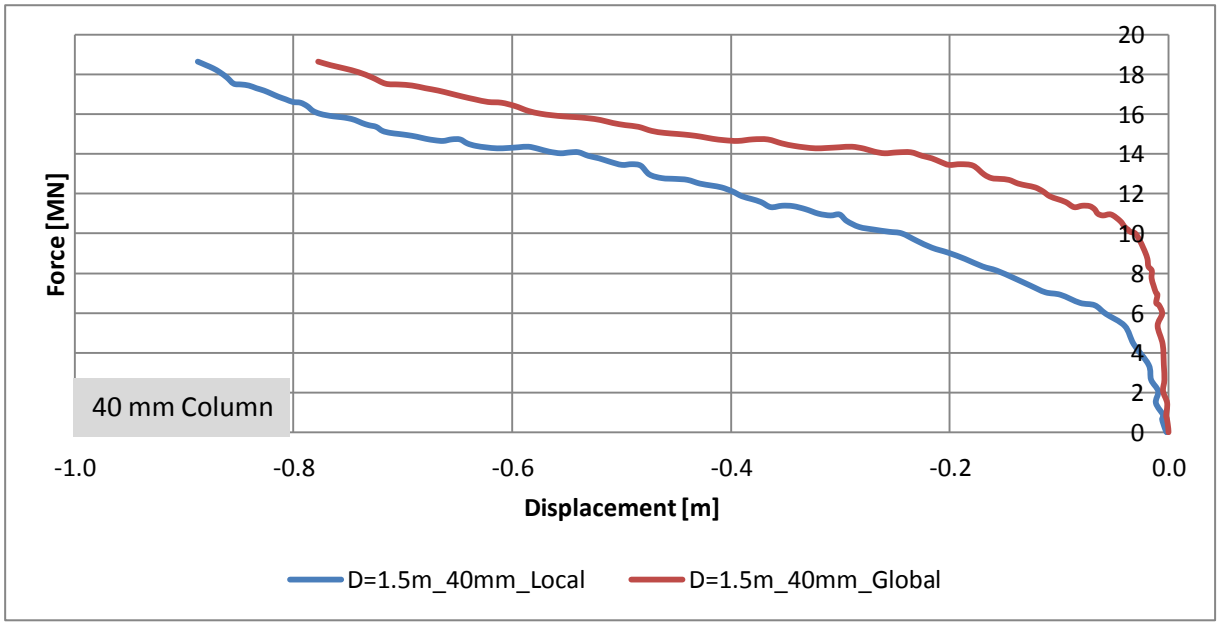

Figure B-8 – Global and Local Deformation – 40mm Column – Stern Impact

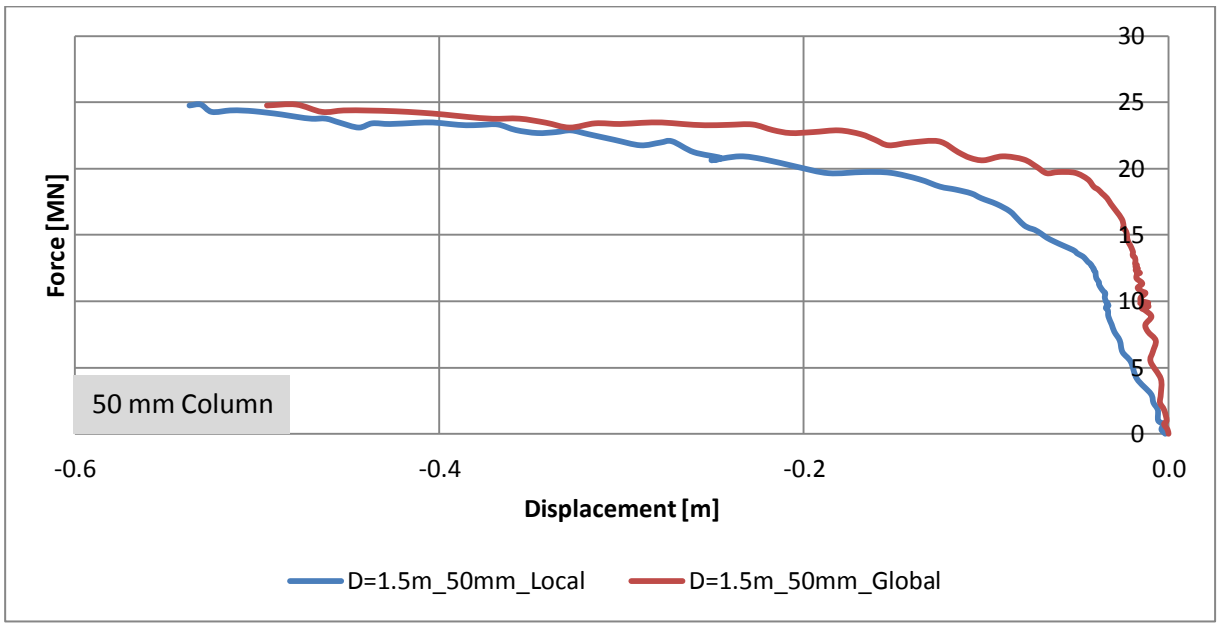

Figure B-9 – Global and Local Deformation – 50mm Column – Stern Impact

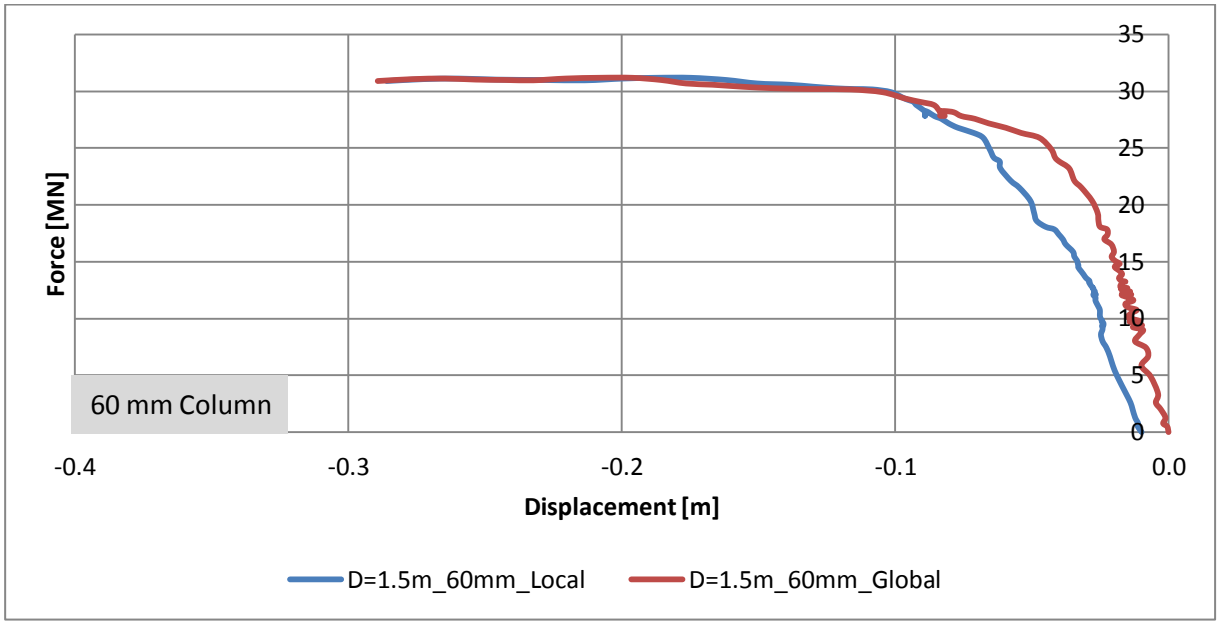

Figure B-10 – Global and Local Deformation – 60mm Column – Stern Impact

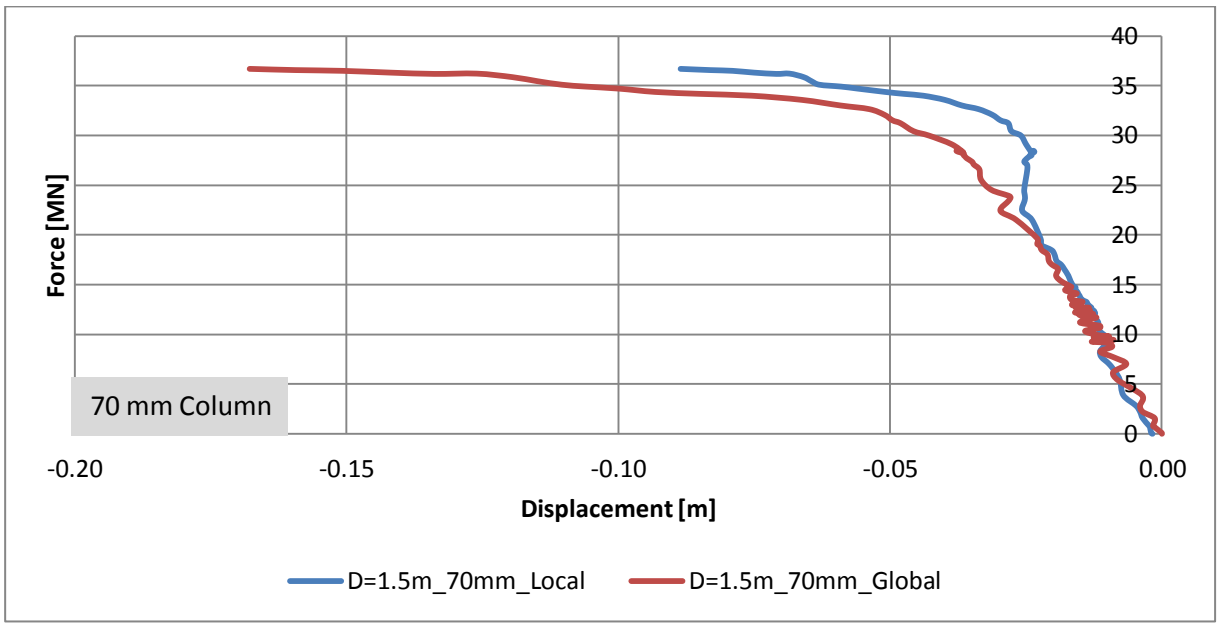

Figure B-11 – Global and Local Deformation – 70mm Column – Stern Impact

Appendix C. Resistance Against Local Indentation

C.1 Comparison with NORSOK – Beam Impacts

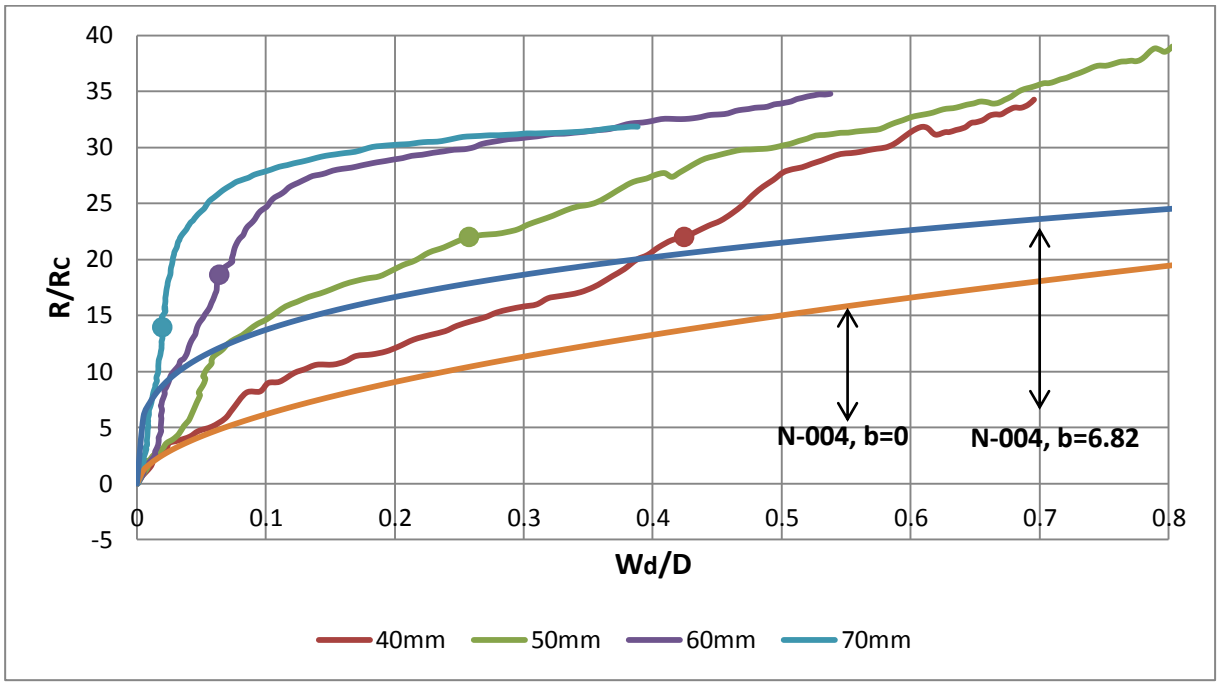

Figure C-1 – Resistance to Local Indentation – Diameter = 2.0 m

C.2 FEA Results vs. Design Curve for Ductile Design

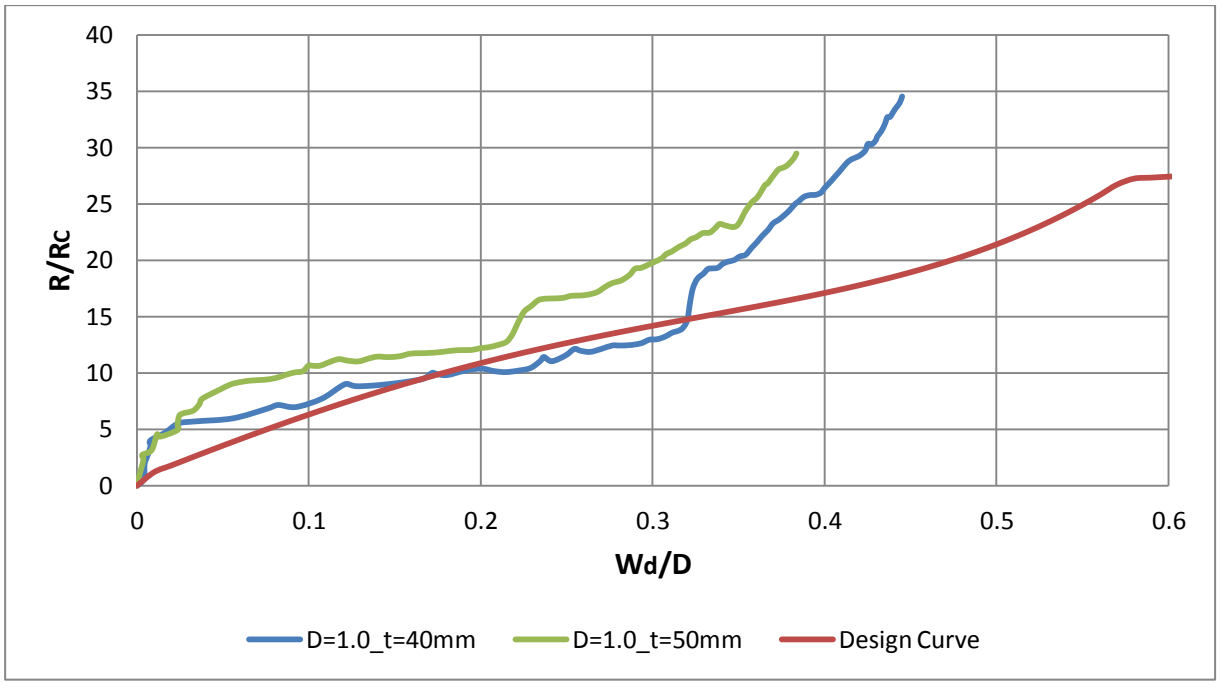

Figure C-2 – Comparison with Design Curve – Column Diameter =1.0 m – Beam Impact

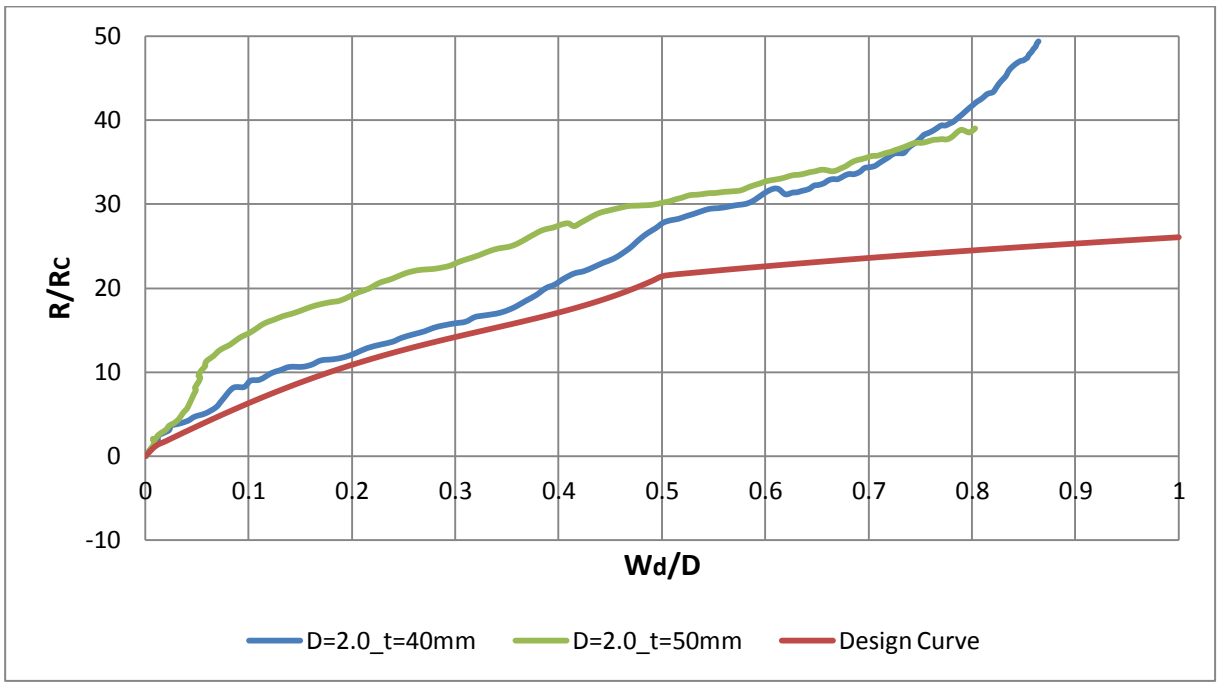

Figure C-3 – Comparison with Design Curve – Column Diameter =2.0 m – Beam Impact

Appendix D. FEA Results vs. Simplified Calculations

D.1 Point Load Model

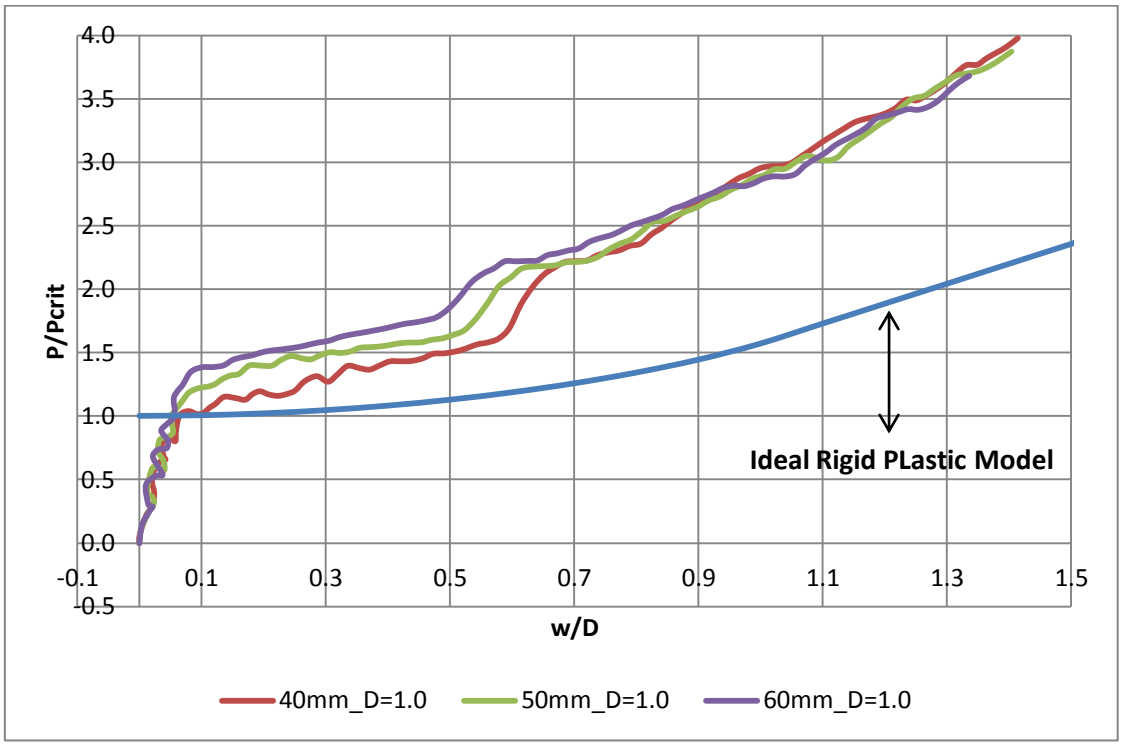

Figure D-1 – FEA Results vs. Point Loaded Model – Column Diameter = 1.0 m – Beam Impact

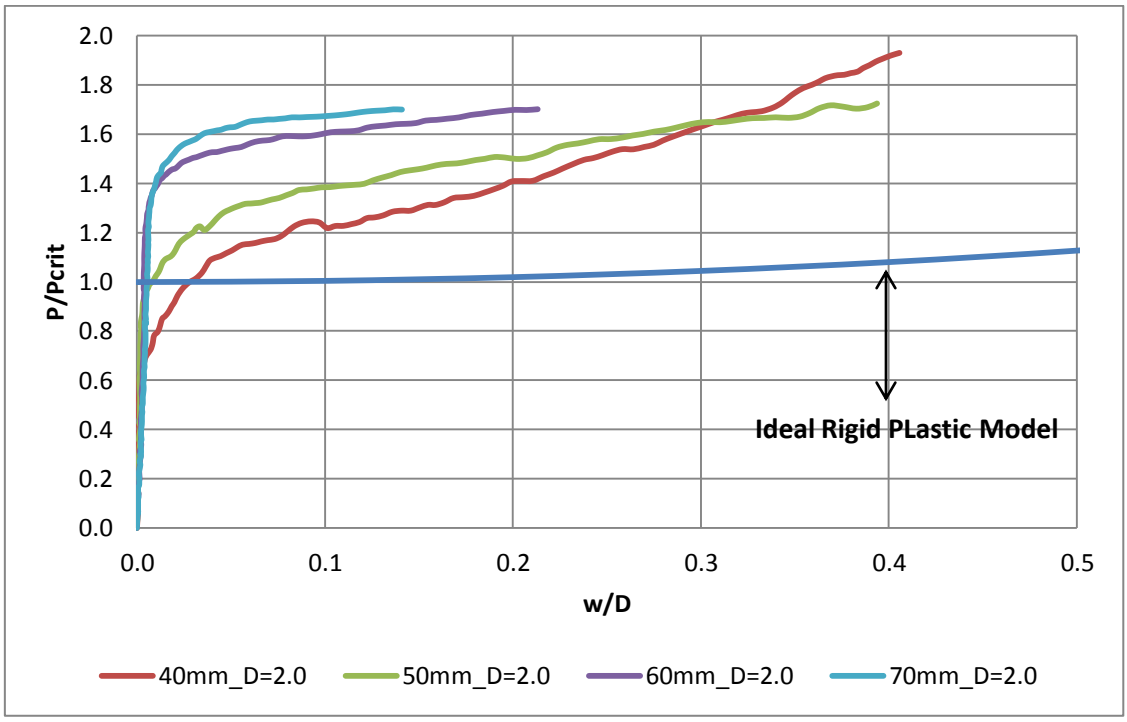

Figure D-2 – FEA Results vs. Point Loaded Model – Column Diameter = 2.0 m – Beam Impact

D.2 Distributed Load – Reduced Capacity

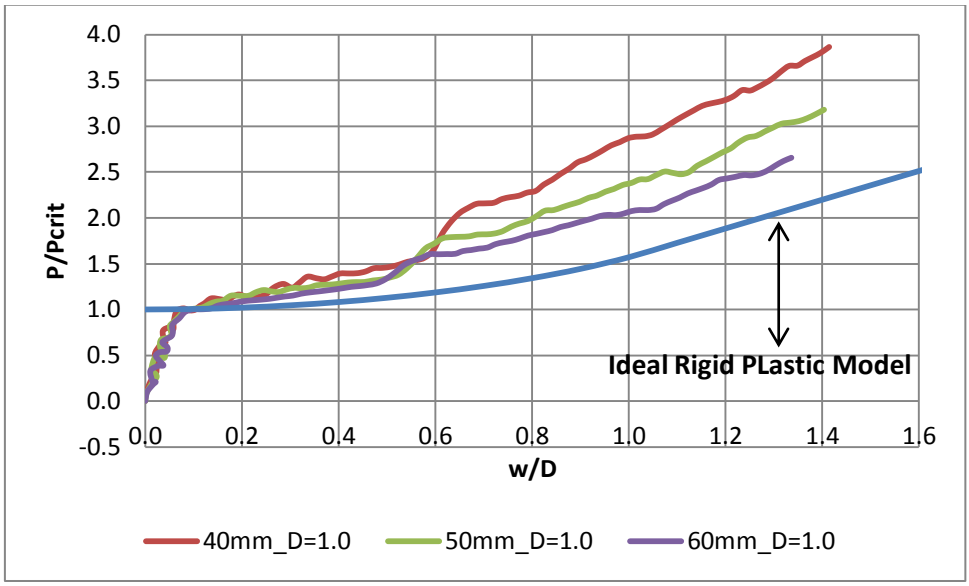

Figure D-3 – Simplified Model with Reduced Capacity – Column Diameter = 1.0 m – Beam Impact

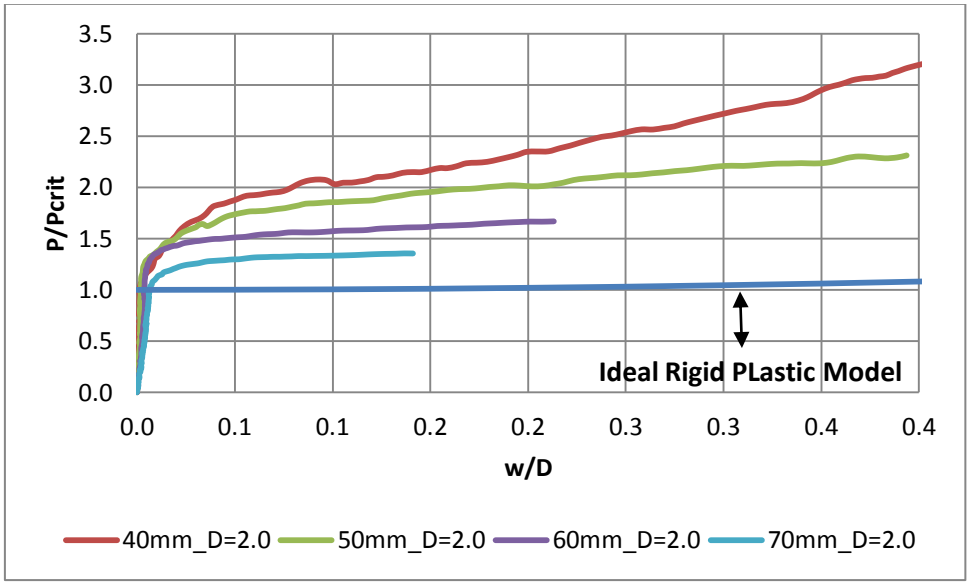

Figure D-4 – Simplified Model with Reduced Capacity – Column Diameter = 2.0 m – Beam Impact

Appendix E. Contact Area – Beam vs. Stern Impact

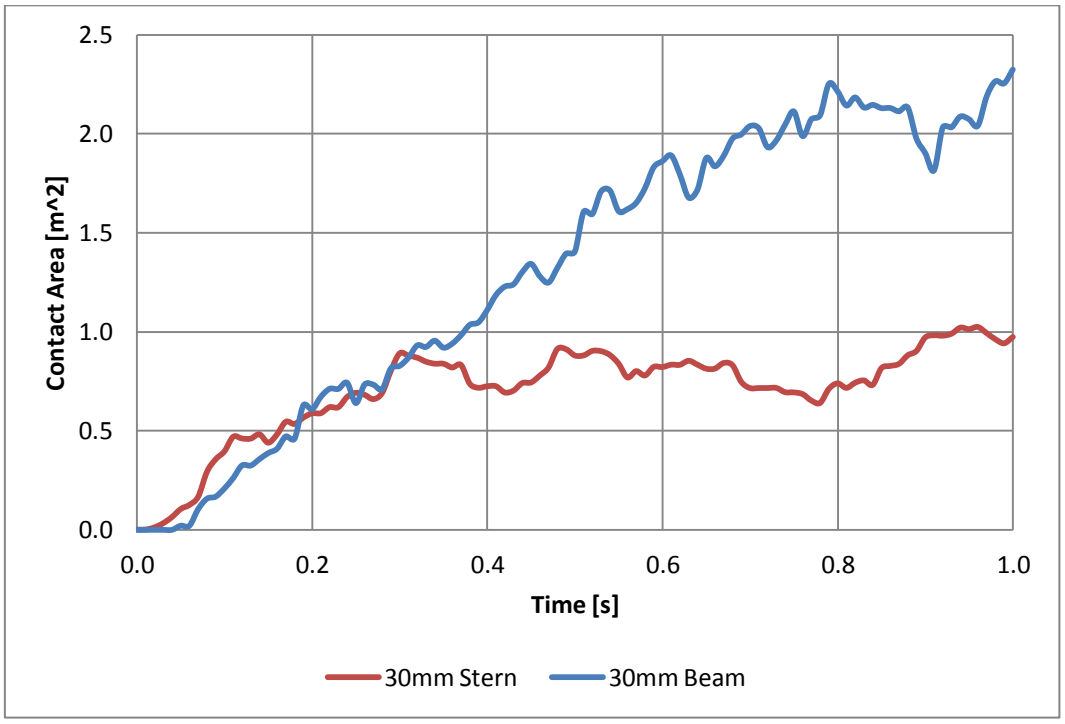

Figure E-1 – Contact Area – Stern vs. Beam Impacts – 30mm Column

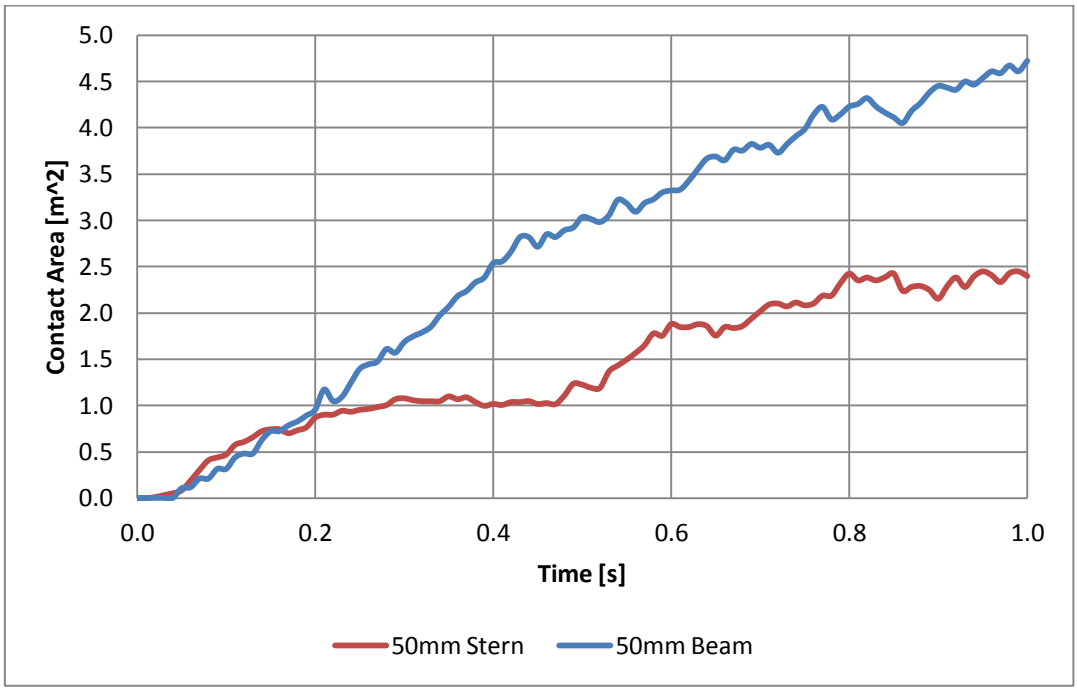

Figure E-2 – Contact Area – Stern vs. Beam Impacts – 50mm Column

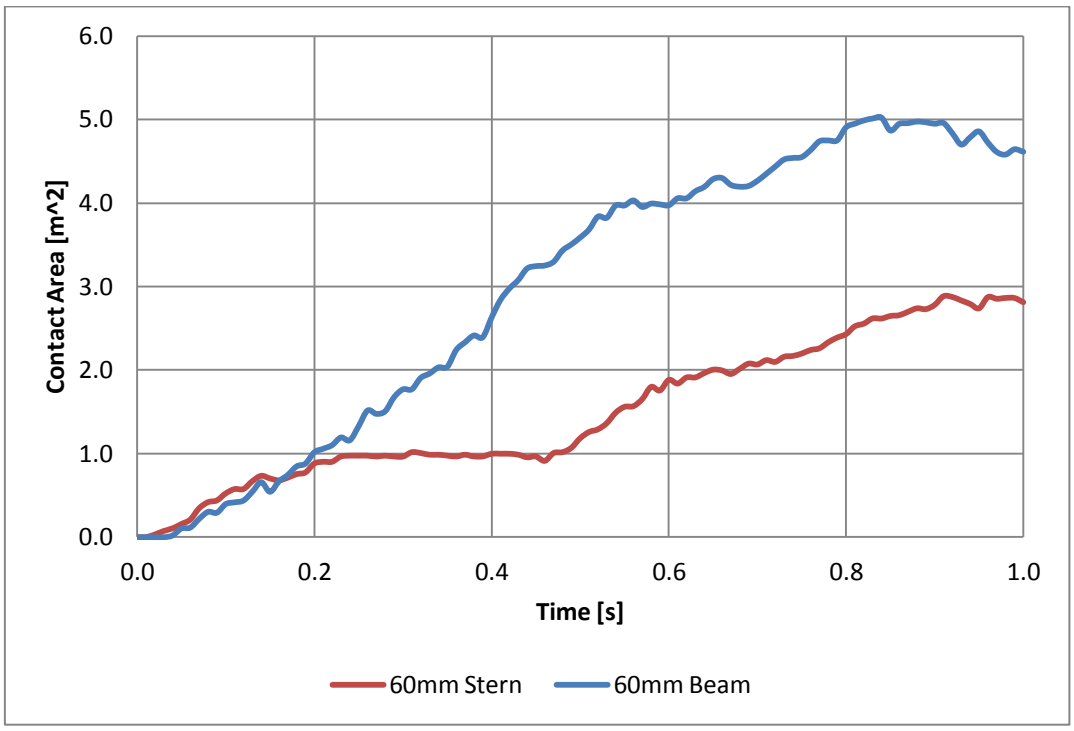

Figure E-3 – Contact Area – Stern vs. Beam Impacts – 60mm Column

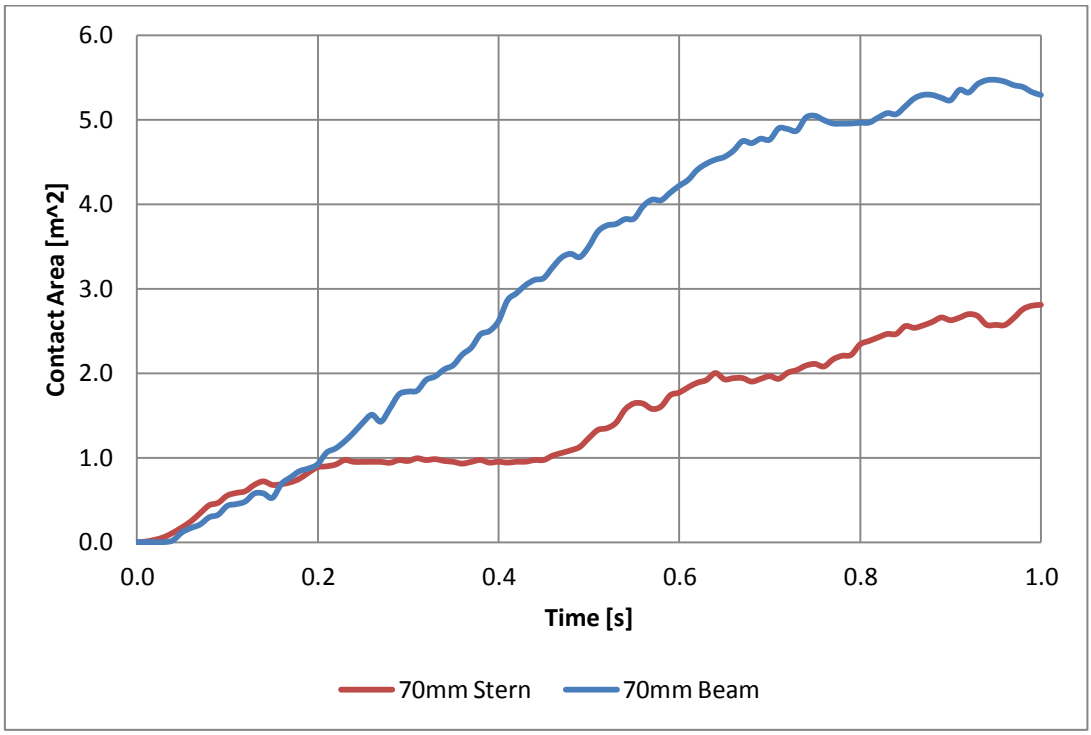

Figure E-4 – Contact Area – Stern vs. Beam Impacts – 70mm Column